Safety Case

For

"Proposed Novel Cementitious Leachate Barriers"

P A Claisse and E Ganjian Coventry University

A Atkinson and M Tyrer Imperial College

August 2004

CONTENTS **PAGE**

PREFACE

The purpose of this document is to establish the safety case for the construction of a novel cementitious barrier as a landfill liner. It is intended for submission to the Environment Agency and describes the work that has been carried out since 1998 to establish the safety of the barriers. It is anticipated that the document will evolve in discussion with the EA.

The safety case is developed on the basis of predictive models which are validated by site trials. These trials have taken place at the Risley landfill site in Cheshire. Three trial cells have been constructed containing a total of 70m^3 of concrete. The data used in the models has been derived from laboratory experiments with permeability (high pressure through flow) and diffusion tests.

The principal intended benefits of the new barrier are:

- Low permeability combined with high cation exchange capacity to give improved containment.
- Construction from waste materials which would otherwise go into landfills.
- A relatively hard concrete surface to permit operation of vehicles and to prevent damage from large items of waste compacted onto it.

DEFINITION OF TERMS

Aggregate. The component of a concrete mix which is does not hydrate.

Capacity factor. A measure of adsorption defined as the ratio of the total concentration per unit volume of solid to the solution concentration per unit volume of liquid.

Cementitious. The component of the concrete mix consisting of material or materials which hydrate to for a solid matrix.

Coefficient of permeability. This is also known as the hydraulic conductivity and is the ratio of the Darcy velocity to the gradient of hydraulic head.

Concrete. A mixture of a cementitious component and a fine and a coarse aggregate.

Diffusion Coefficient. In this document the intrinsic diffusion coefficient is used and this is defined as the ratio of the flux to the concentration gradient for an ion diffusing through a **liquid**.

Mortar. A mixture of a cementitious component and a fine (<5mm) aggregate.

PART 1 THE "TOOLKIT"

1 INTRODUCTION

1.1 Background

1.1.1 Previous research

During the 1980's a very large research programme was carried out in the UK to develop designs for repositories for nuclear waste [1-3]. Three of the present authors (Claisse Atkinson and Tyrer) worked on this programme. The design which was developed to the greatest extent was the repository for intermediate and low level waste. This repository was required to have a predictable performance in a deep saturated geological environment over a timescale of up to a million years. The design essentially involved placing the waste in concrete containers and placing these containers in an excavated underground cavern. This cavern was then to be backfilled with a relatively soft cementitious grout.

One of the achievements of the nuclear programme was to analyse and define the performance which was actually required of the concrete when used for this application. This performance requirement is quite different from the requirements for concrete in normal construction and lead to the development of some very unusual concrete mixes.

The barrier design uses conventional engineering materials but its method of operation is far from conventional for an engineering structure because it is essentially sacrificial [4]. The main function of the barrier is to condition the chemistry of the repository to high pH by dissolving alkalis in the groundwater. The alkalis are free sodium, potassium and lime and subsequently the calcium silicate hydrate which forms the structure of the hardened cement. At the high pH values the harmful species from the waste which are permeating through the barrier are adsorbed onto the cement matrix and immobilized. Clay based liners were considered for the nuclear repository but concrete was chosen as the best option for the UK. The nuclear programme was stalled in the 1990's by the refusal of planning permission for the test facility at Sellafield in Cumbria.

1.1.2. Containment

A barrier will physically inhibit the transport of leachate to the environment. There are numerous physical transport processes which could take place in the barrier, these include: Thermal migration, Electromigration, Osmosis, Electro-osmosis and Capillary suction. Initial analysis has, however, shown that these will not be significant and for the present work only advection and diffusion are considered.

By far the most effective containment mechanism will, however, be chemical containment. In the work reported here many harmful species are immobilised by the chemistry of the barrier. This process is simulated using linear adsorption isotherms in the initial modelling and by full modelling of the chemistry using PHREEQE in the more detailed study.

1.1.3 Limits on the performance of the barrier

Cracking

This is the obvious mode of physical failure which has been the reason why concrete barriers have not been common in the past. Cracking could be caused by drying or thermal effects or the imposed stresses on the barrier. The solution to this is to use composite systems of concrete and clay and their performance has been demonstrated experimentally in this work.

High pH "boulder" formation

A possible cause of premature chemical failure is the formation of impermeable "boulder-like" pieces with preferential flow paths for water around them. These boulders could develop impermeable surface layers through the formation of carbonates, chloroaluminates or magnesium compounds in a similar manner to that observed at the surface of existing concrete structures in hostile environments. If this occurred the alkaline buffering and sorption capacity of the interior of the boulders would be lost. In this way the total buffering and sorption capacity of the repository would be substantially reduced.

In the plans for nuclear waste it is envisaged that almost all of the cementitious material will be in the form of a soft grout. This material has been chosen to comply with various operational criteria including being readily pumpable into small spaces between the packages and having a

low strength. These requirements have the effect that the formation of hard impermeable boulders will be strongly inhibited. For non-nuclear waste the strength of the concrete will also be kept as low as possible.

Action of sulphates

Sulphates react with hardened concrete and cause expansion of the matrix which leads to significant loss of strength. This effect may be prevented by the use of sulphate resisting cement or Blastfurnace Slag cement. It is of note, however, that in a deep nuclear repository the effect is harmless because the expansion is contained by the surrounding rock. For non-nuclear applications the containment pressures should also be sufficient with typical waste emplacement depths greater than 20m and expansion would be harmless if it did take place.

1.1.4 Concept of the basic novel barrier designs

The concept is based on the theory that the pollution of soils and watercourses by the release of leachate may be prevented by adoption of a composite-barrier liner, which not only chemically conditions the waste, but is designed to be self-sealing through secondary mineralisation and will retain heavy metal ions through ion exchange, surface sorption, filtration and precipitation.

The design concept of the novel composite landfill liners is to emplace a number of different layers, each of which compliments and enhances the behaviour of the others. Each of the layers has different properties, so that any defects such as cracks, are likely to form at different locations in different layers, thus limiting the creation of connected pathways through the barrier. In the design considered in this work, three layers are envisaged as illustrated in figure 1.1. The clay-based hydraulic barrier is sandwiched between two layers of concrete.

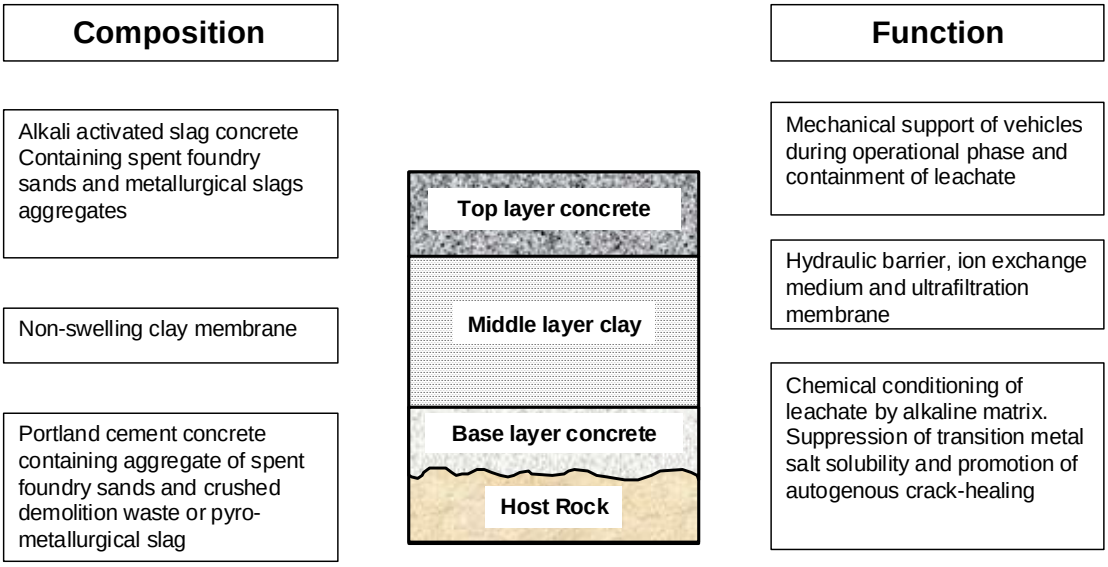

Figure 1.2: *The new composite landfill liner.*

1.2 The Landfill directive

In the Landfill Directive (Council Directive 1999/31/EC) specific requirements are made of the different layers of the barrier. In different applications different parts of the novel barrier might be assigned to the layers as defined in the directive.

The Geological Barrier.

For applications such as the proposed barrier on the Poplars site where only a single concrete layer is envisaged over existing clay the clay will form the geological barrier. Where no existing barrier is present the novel barrier will have three layers of which the lower two will be part of the geological barrier. The minimum thickness for artificial barriers is specified as 0.5m in the directive.

The Sealing Liner

No thickness is specified for this and for many applications the top layer of concrete in the novel system will be the sealing layer. In applications where an HDPE membrane is deemed to be necessary this will be placed **below** the top concrete for protection. Although the directive does not specify that the sealing layer has to be above the geological barrier this may be deemed

to be necessary. If this is not necessary the top concrete layer will be assumed to be part of the geological barrier when HDPE is used.

The Drainage Layer

Because the sealing liner will be protected any industrial waste (e.g. ferrosilicate slag or demolition hardcore) could be used for this. A minimum thickness of 0.5m is specified in the directive.

1.3 Other chapters in this document

In chapter 2 the materials and mix designs are described. Almost all of the materials are "wastes".

In chapter 3 the different computer models are described. All of the experiments and plans have been modelled using the "Coventry University" model and specific samples have been modelled using PHREEQE to show that the results are conservative.

Chapters 4 and 5 describe the experimental work in the lab and on site at Risely.

Chapters 6 discuss the stability of the proposed barriers and chapter 7 and 8 the quality assurance.

In chapter 9 current work in progress is described.

In part 2 (chapters 10 and 11) a proposed 2-layer barrier for the Poplars site is presented.

In part 3 and 4 (chapters 12 – 15) generic designs for a 3-layer barrier and a vertical barrier are developed.

2 MATERIALS AND MIX DESIGNS

2.1 Materials

2.1.1 Sources of materials

The various waste or by-product materials, which were supplied by the sponsors and used in the laboratory investigation, are listed below. Following screening tests, subsets of these were considered further as components in candidate mixes for both laboratory and site trials and subsequently, proposed for use at the Poplars site.

a) Sodium sulphate slag (Britannia Refined Metals Ltd.)
b) Spent borax slag (Britannia Refined Metals Ltd.)
c) Ferrosilicate slag (lumps from Britannia Refined Metals Ltd. sand size from Britannia Zinc Ltd.)
d) Ferrosilicate copper slag (IMI Refiners Ltd.)
e) Soda slag (Britannia Refined Metals Ltd.)
f) Chrome Alumina slag **(**London & Scandinavian Metallurgical Co. Ltd.)
g) Cement Kiln Dust ,CKD (Rugby Cement)
h) Run of station ash (Ash Resources Ltd.)
i) Lagoon ash (UK quality Ash Association)
j) PFA (Ash Resources Ltd.)
k) Granulated Blast Furnace Slag, GBS (Tarmac Quarry Products Ltd.)
l) Steel slag (Tarmac Quarry Products Ltd.)
m) Steel Slag Dust (Tarmac Quarry Products Ltd.)
n) Burnt Oil Shale (Tarmac Quarry Products Ltd.)
o) By-product Gypsum (Biffa Waste Services Ltd.)
p) Glass cullet (Mercury Recycling Ltd.)
q) GGBS (Ground granulated blastfurnace slag)
r) Limex70 (British Sugar Plc.)
s) Shell foundry sand (Bruhl UK Ltd., Hepworth Minerals & Chemicals Ltd.)
t) Green foundry sand (Castings Plc. And Bruhl UK Ltd.)
u) Fire kettle setting (Britannia Refined Metals Ltd.)
v) Fine rotary fascia bricks (Britannia Refined Metals Ltd.)
w) Sodium sulphate solution (Britannia Refined Metals Ltd.)

These waste materials which were used in this project can be divided in the three following categories:

- Those materials, which may be used as aggregates in the concrete or mortar layers, such as Spent foundry sands Residues from the castings industry. These materials are principally quartz sands with residues of thermally degraded binders such as clay minerals (green sand) and phenolic resins combined with carbon char (shell sand) and Semi-crystalline slags from the metals refining industry i.e. alkaline sulphates, ferrosilicates and heavy metal–bearing "soda" slags.
- Waste alkalis which may be suitable activators for cementitious ground granulated blast furnace slag (GGBS) or pulverised fuel ash (PFA) *i.e.* Liquid raffinates such as alkaline sodium sulphate solution produced during acid neutralisation of processing waste.
- Those waste materials which have inherent cementitious properties, like Spent borax, GGBS and Gypsum 'filter cake' recovered from acid neutralisation arising from pigment manufacture.

The bulk of the materials are wastes from the castings and metals refining industries such as metalliferous slags and spent foundry sands. Subsequent laboratory work has focussed on examining these materials as cementitious binders in their own right and as cement replacement materials or as chemical activators for other cementitious materials. This has allowed the solids to be grouped into those materials which have cementitious properties, those which are relative chemically inert and would be suitable for use as aggregates and to identify any materials which are not suitable for use as liner materials.

Before describing the individual materials in detail, some consideration should be given to their functions in the composite barrier such as those in the site trials and the properties which they must necessarily exhibit to fulfil their intended roles. The aggregate materials must be physically strong enough to support the intended loads, chemically unreactive towards the cementitious binders and dimensionally stable (for example not differentially shrink or swell with changes in temperature or water content). The binder materials need to develop their strength and permeability characteristics reasonably promptly (a period of days to weeks-slower hydration prejudicing their ease of use in construction). They must be unreactive towards the aggregates and only react slowly with the leachates. Lastly, the soluble alkalis

must be reactive towards cement replacement materials, such as blast furnace slag and fly ash, and be available in a state of purity which does not introduce mobile species which are either toxic or detrimental to the hydration of the cement components.

2.1.2 Binder materials

Conventional Portland cement comprises four main anhydrous phases; C_3S, C_2S C_3A and C_4AF. The clinker recovered from the cement kiln is interground with a few percent by mass of gypsum (added to control the otherwise rapid hydration of the aluminate phase) and is reduced to a fine powder. On hydration, the calcium silicates react with water to form both calcium hydroxide (portlandite) and poorly crystalline calcium silicate hydrate gel. Although the detailed hydration chemistry is somewhat complex (owing to the formation of a range of minor phases) to a first approximation, the hydration of the silicates may be summarised as follows:

$2C_3S + 6\,H \rightarrow C_3S_2H_3 + 3CH$ (fast)

$2C_2S + 4\,H \rightarrow C_3S_2H_3 + CH$ (slow)

Where $C_3S_2H_3$ is the calcium silicate hydrate gel, "CSH"

Structurally, this simplified view of cement hydration may be thought of as an extension of a "shrinking core" model of a reacting solid particle in which the clinker grains react with the water, forming CSH gel as a reaction product on their surfaces.

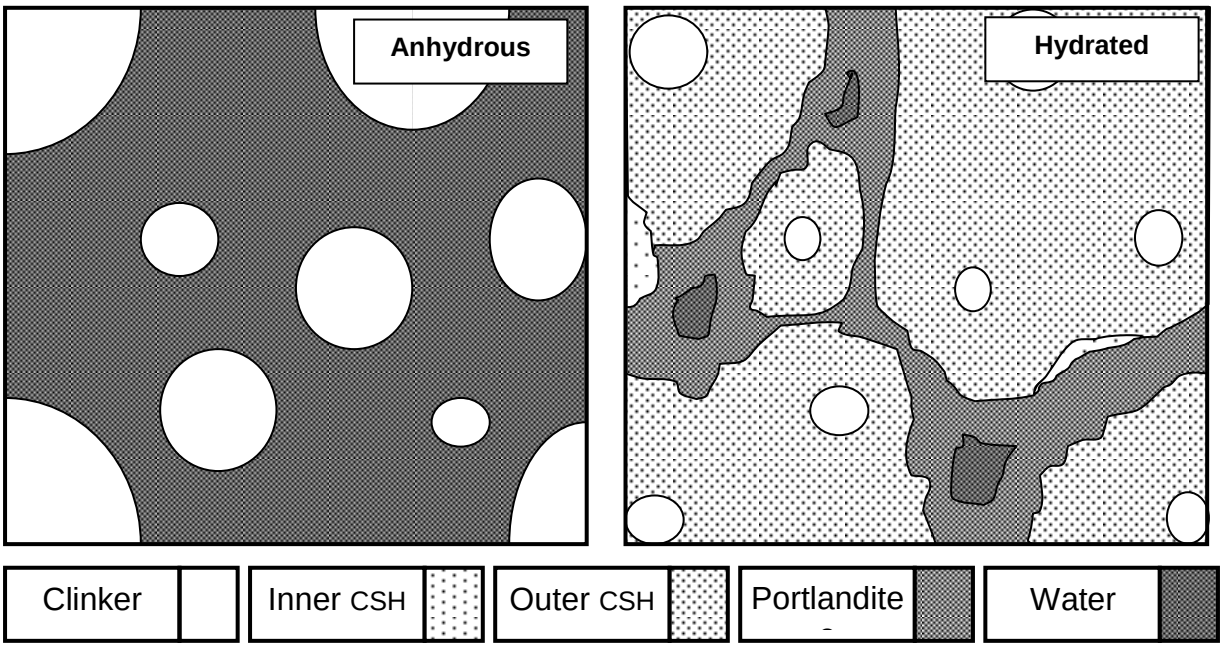

Figue 2.1 *Schematic diagram of the hydration of Ordinary Portland Cement (OPC)*

As hydration proceeds, nucleation of both gel and calcium hydroxide occurs in the intergranular spaces, ultimately bridging the gaps between the particle grains. The resulting microstructure comprises relict cores of anhydrous clinker surrounded by dense, inner CSH, surrounded by outer hydration products (CSH and portlandite). It is in this "outer" CSH that the bulk of the macro porosity is located in hydrated Portland cements.

After a few days of hydration, Portland cement shows the major phases expected in the fully hydrated product. A considerable amount of the clinker remains and is surrounded by inner CSH. These particles are bound together by outer CSH containing the macro porosity (dark - see figure 2.1) and some free Portlandite (marked "P"). Note that the large domains marked "A" are quartz sand aggregate.

In the presence of organic acids from landfill leachate, the portlandite will dissolve, increasing the porosity, whilst neutralising the organic acids. This will be accompanied by dissolution of the calcium-rich structural units of the CSH phase, further increasing the porosity and reducing the strength of the binder. In effect, there is a balance between the buffering capacity of the cement and its increase in porosity due to dissolution.

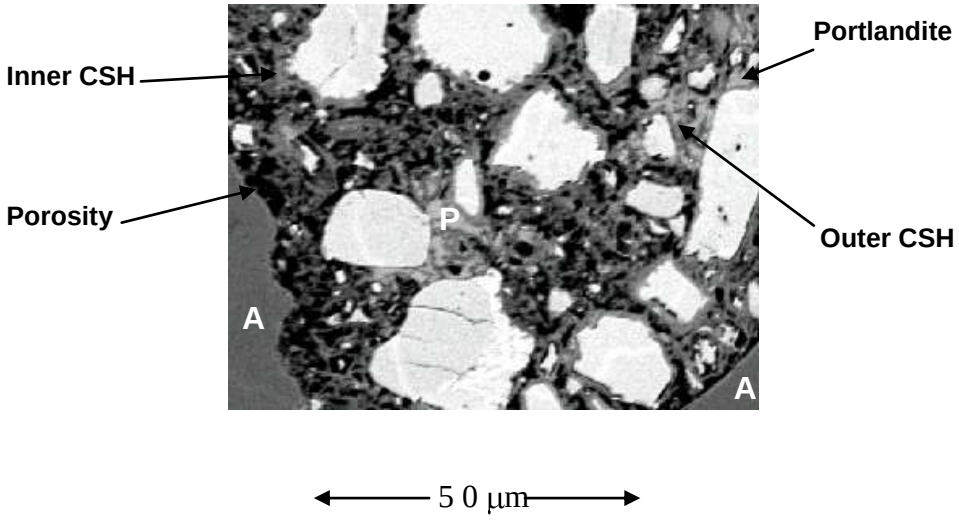

Figure 2.2 *Backscattered electron micrograph of Portland cement hydrated for 4 days*

In order to limit the rate of this reaction (and hence the mass transport through the barrier), alternative binders were sought with much lower porosities and higher resistance to organic acid attack. These materials contain cement replacement materials such as blast furnace slag and fly ash, which have latent hydraulic properties, released during hydration in the presence of soluble alkalis.

Cementitious blast furnace slag is a commercial by product of the iron industry. During production, addition of a limestone flux to the blast furnace charge to form "sinter cake", provides a means by which the aluminosilicate impurities may efficiently be separated from the iron after melting. The slag, which forms a siliceous layer floating on the molten iron, is periodically tapped and its subsequent use depends on the rate at which it is cooled from the furnace temperature (around 1500°C). If the material is air cooled over several days, the crystallites are able to grow forming a relatively stable solid, which has commercial value both as road stone and as construction, aggregate. Blast furnace slag cooled in this way does not show hydraulic properties and is therefore of no value as a cementitious binder. The figures below show the bulk chemistry of a range of cements and the relationships between the major crystalline phases, which may form in blast furnace slag.

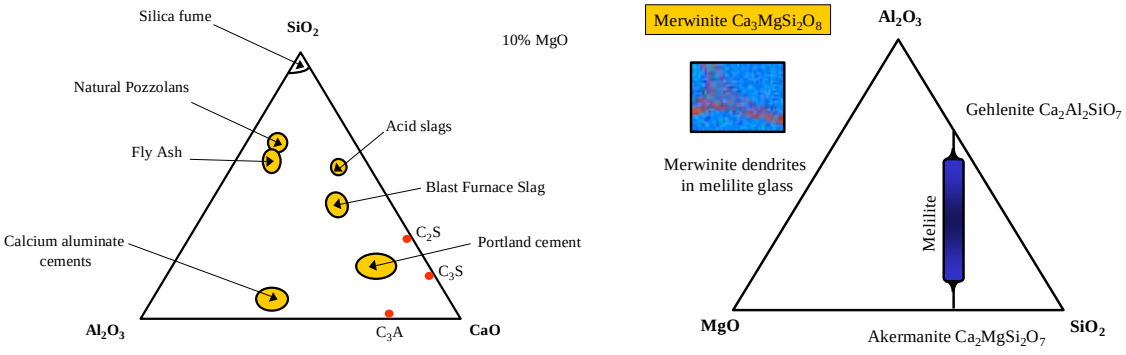

Figure 2.3 *Bulk composition of cements and slags (left) and phase chemistry of blast furnace slag (right)*

In order to make the slag chemically reactive, it must be chilled rapidly, freezing it to a glass, which greatly limits the rate of crystal growth. This is achieved by granulation; usually by passing the molten slag through a high pressure water jet, although dry granulation processes

are adopted by some manufacturers. This glassy slag has a higher residual free energy than its crystalline counterpart and it is this energy which may be released during hydration.

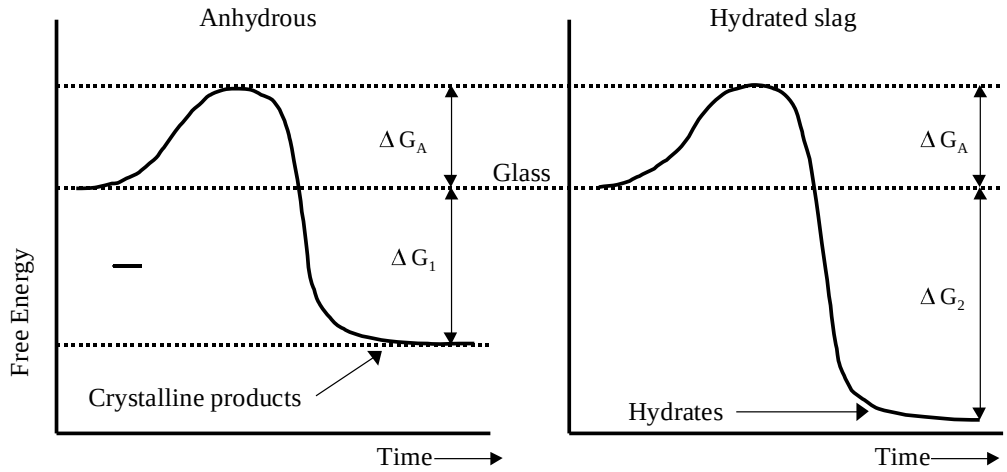

Figure 2.4 *Free energy changes in blast furnace slag on cooling (left) and during hydration (right). N.B. The same relationship also holds for other pozzolanic materials but it should be remembered the free energy change is often less than for BFS. Pulverised fuel ash, for example has a lower ΔG than does slag, hence the "driving force" for the hydration reaction is proportionally less, resulting in slow, often incomplete hydration.*

In order to form a hydraulic binder, the slag glass must dissolve and re-precipitate as interlocking mineral hydrates, as is the case for other cementitious binders. As the slag glass is siliceous, this is relatively rapid in an alkaline environment and this is conventionally maintained by blending BFS with Portland cement (OPC). In order to ensure that the two components in slag cement hydrate at the same rate, BFS is ground somewhat finer than OPC (about twice the specific surface area, typically 375 - 425 m^2kg^{-1}) in order to compensate for its relatively slow hydration kinetics. The hydrated binder therefore has a much finer porosity and hence lower permeability than that formed from pure OPC, which accounts (in part) for its high durability.

Of course, the greater the fraction of slag in a blended BFS-OPC binder, the lower might be its expected permeability on hydration. In practice, this effect is limited by the need for a supply of alkalinity (from OPC) with which to dissolve the slag glass and a typical

replacement ratio is seen in the Humber Bridge, which contains 70% BFS and 30% OPC in its cementitious binder.

If however, the alkalinity is supplied from the mix "water", rather than by dissolution of Portland cement, a very low permeability product might be produced. These materials are known as alkali activated slag cements (AAS) and, although they represent a relatively small fraction of the market, they offer extremely low permeability products. The "activation" (strictly reaction) of slags by soluble alkalis may be achieved by using alkaline solutions of Group I metal sulphates, hydroxides, carbonates or silicates although a range of other soluble alkalis has been investigated in recent years.

The use of AAS binders has been included in the present study for two principal reasons. First, as the permeability of the hydrated matrix is very low, it was though that the materials would perform well as barriers to pollution migration. Secondly, as the particle size of blast furnace slag is small in comparison to that of other cement types, the past-aggregate bond is especially well developed in AAS concretes, allowing use of so called "marginal aggregates"; those which do not bond especially well with OPC binders. The latter property allows inclusion in this project of aggregate materials, which have limited use in constructional concrete.

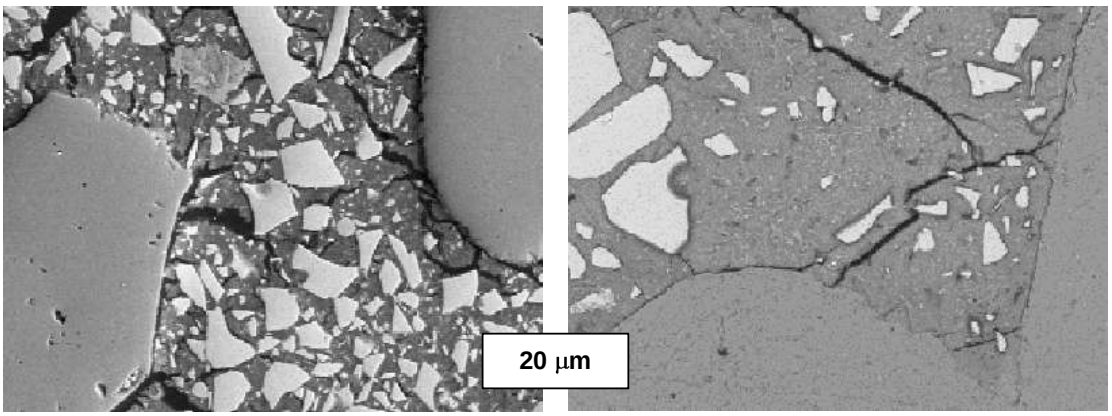

Figure 2.5 *Microstructures of alkali activated blast furnace slag cement mortars at early age (left; 3 days) and late age (right; 6months). The important feature is the dense and relatively low porosity hydration product formed by these materials.*

From the outset, considerable efforts have been made to identify potential sources of waste alkalis. Although many processes produce alkaline waste streams, it is common that the same process or plants produces a surplus of acidic waste, the two waste streams being used to neutralise each other. Consequently, relatively few processes produce a net surplus of waste alkalis and those that have been considered are as follows:

Papermaking: Paper pulp liquor is mildly alkaline, containing dissolved carbonates and sulphates. Preliminary investigations reveal that the paper industry's waste arisings are principally sludge, containing short paper fibres, filler minerals, de-inking residues and relatively low concentrations of extractable alkalis. A simple energy balance shows that the removal of the alkalis from paper mill sludge does not offer an economically viable source of alkaline solutions for AAS production.

Sodium sulphate slags are a product of pyrometallurgical metal refining, and it was thought that they may be leached in order to release residual sodium sulphate to recover an alkaline solution. Unfortunately, this proved not to be the case, the fraction of soluble sodium sulphate remaining in these slags proved too low to be of value. Figure 2.6 (below) shows the highly porous surface of the sodium sulphate slag. It has a considerable insoluble solids content which is largely siliceous. Initial experiments using this material as an aggregate in a range of different cent types showed that it was slightly reactive towards the cement and dimensionally unstable. The material was considered unsuitable for further study.

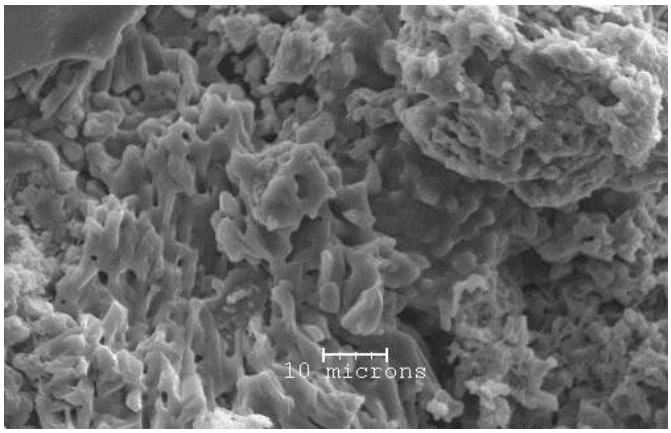

Figure 2.6 *Sodium sulphate slag from the secondary lead industry, Secondary electron SEM image of fracture surface.*

Soda slags: Non ferrous metal refining relies on the use of fluxes with which minor impurities may be removed from the melt. Pyrometallurgical processes were seen as a potential source of spent sodium carbonate slags, which may contain residual (and hence recoverable) alkalinity. A soda slag from the lead industry has been identifies as potentially fitting the requirements of this study as it contains a high residual sodium carbonate content. This material originates in the ISAMELT furnace and contains mixed heavy metals present as both oxides and sulphides in addition to the remaining sodium carbonate.

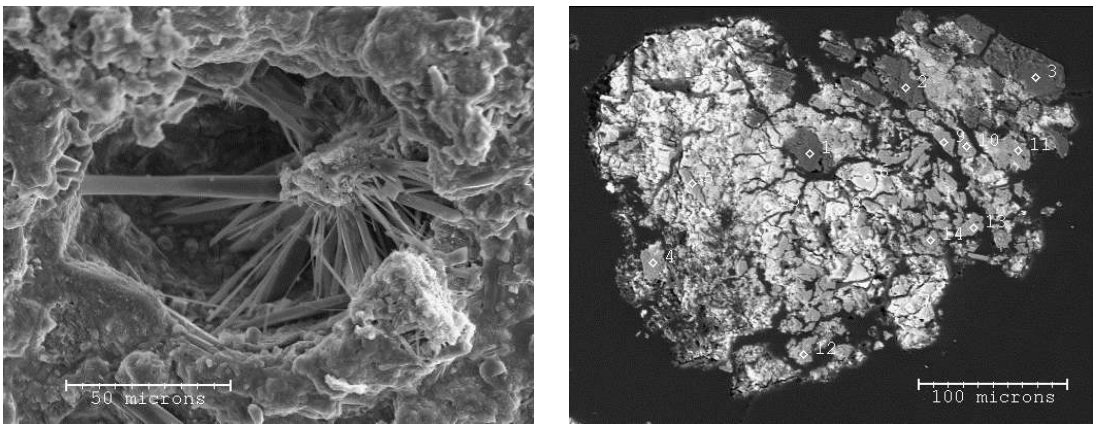

Figure 2.7 *Fresh (right) and aged (left) soda slag prior to leaching*

Above left shows one of the products formed when this material is open to the atmosphere. As the slag is hygroscopic, it absorbs moisture from the atmosphere allowing both dissolution and oxidation of its constituent phases. The crystals seen in the vug are smithsonite (zinc carbonate) and thought to be an artifact of atmospheric aging. Above right shows the complex structure of the slag, containing free lead prills, along with mixed sulphides and carbonates.

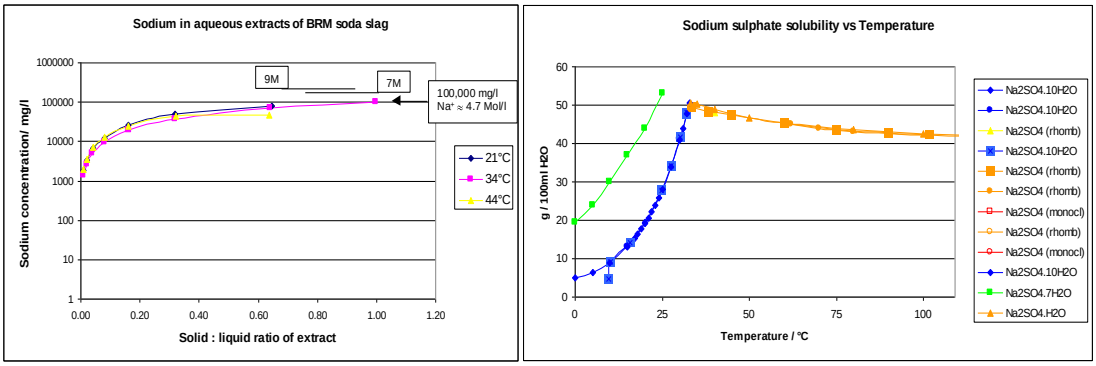

Figure 2.8 *Left: Sodium content of water-leached soda slag as a function of solid:liquid ratio. Right: Thermodynamic solubility of pure sodium sulphate solids (Data from PHRQPITZ)*

Preliminary leaching experiments show the slag to produce highly alkaline (pH >13) and strongly reducing solutions, the E_H being close to the stability limit of water (-0.5 volts). In order to estimate the quantity of soluble alkali recoverable from this material the sodium yield (and pH) were measured at a range of solid:liquid ratios and the results are compared with the thermodynamic solubility of sodium sulphate below:

These very encouraging results suggest that almost all the recoverable alkali content can be dissolved using equal quantities of water and slag, so a quantity of leachate was produced with which to react the blast furnace slag. Although the cement pastes made by this method developed a dense microstructure on setting, concern was raised about the residual arsenic content of the leachate, which ranges from a few μm to 95 μm in concentration. This can be accounted for by the relative stability of the sodium arsenate complexes as shown in the Pourbaix diagram below:

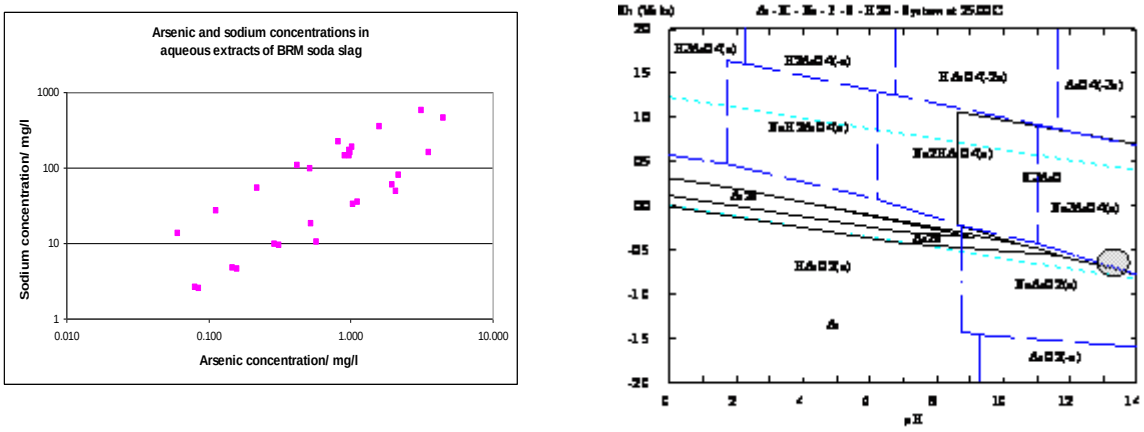

Figure 2.9 *Left: relationship between sodium content of the soda slag aqueous leachate and arsenic concentration. Right: Pourbaix diagram for the As-K-Na-P-S aqueous system, drawn for leachate chemistries associated with 50* μm *As solutions. The chemical environment of the leachates is shown by the grey circle at pH 13.5 and -0.5V* E_H.

Thermodynamic calculations show the range of leachates produced span the boundary between two sodium arsenates; Na_3AsO_4 and $NaAsO_2$. It was speculated that this may account for the two populations of arsenic concentrations seen with respect to aqueous sodium (above left). In fact, the different concentrations reflect different slag compositions, illustrating the inherent variability of waste materials.

At the same time, several kilograms of soda slag were ground to a fine powder and mixed with BFS and water in differing proportions. The water demand of the soda slag is quite high as the sufficient water must be available to dissolve the sodium carbonate/sulphate/thiosulphate phases in the slag and fully hydrate the ferric floc (largely $Fe(OH)_3$ and goethite [FeOOH]). Cement pastes made with this material show dense microstructures but low resistance to drying shrinkage. Whilst kept moist, these materials are dimensionally stable, but loose their structural integrity after a few wetting/drying cycles. This was shown to be largely due to the differential expansion of the ferric floc and the cementitious hydrates. The cement paste is susceptible to drying shrinkage, whilst the floc readily expands on re-wetting.

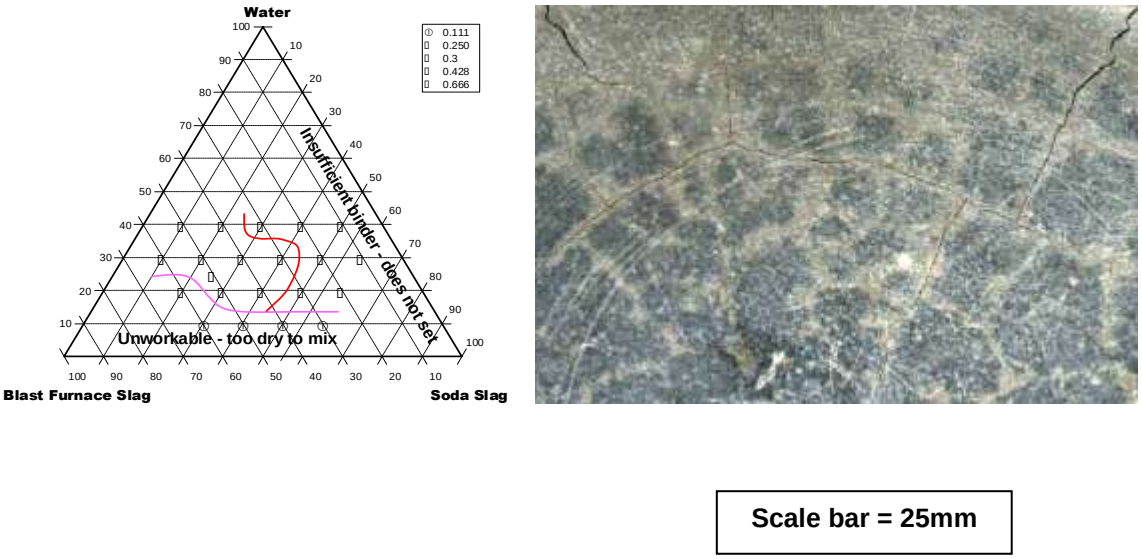

Figure 2.11 *Blast furnace slag cement paste incorporating solid soda slag*
Left: Water : Soda Slag : BFS ratios considered
Right: Cracking due to differential expansion of ferric floc and hydrated AAS paste

Aqueous sodium sulphate waste. The secondary lead process recycles a vast quantity of traction batteries, recovering lead, antimony (and minor non ferrous metals alloyed with the lead) polypropylene and other plastics materials, leaving only the spent electrolyte for disposal. This is presently neutralised by reaction with sodium hydroxide to produce a sodium sulphate liquor. Although not fully oxidised to sulphate, this alkaline solution is equivalent to around 11% Na_2SO_4 by mass and therefore is well suited for use as a slag activator. Preliminary experiments showed that reaction with both blast furnace slag and a range of pulverised fuel ashes proceeds rapidly to produce an alkali activated hydration product. This solution was therefore adopted as the most suitable activator for use in this project.

Borax Slag. One entirely new cementitious material was developed exclusively from this project, the spent borax slag. Initially, the material was considered as a potential source of soluble alkalis, with which to activate cement replacement materials such pozzolanic slags or ashes. Preliminary leaching experiments intended to determine the soluble alkali content, showed the material to be hydraulic in its own right, and hence possibly useful as a cementitious binder. It is a zinc oxide - containing, sodium tetraborate slag, (a by-product of silver refining) and its chemistry and microstructure are described more fully below. The

hydrated slag appears to have a high resistance to organic acid attack and was therefore screened as a potential binder material in the early stages of the project (7).

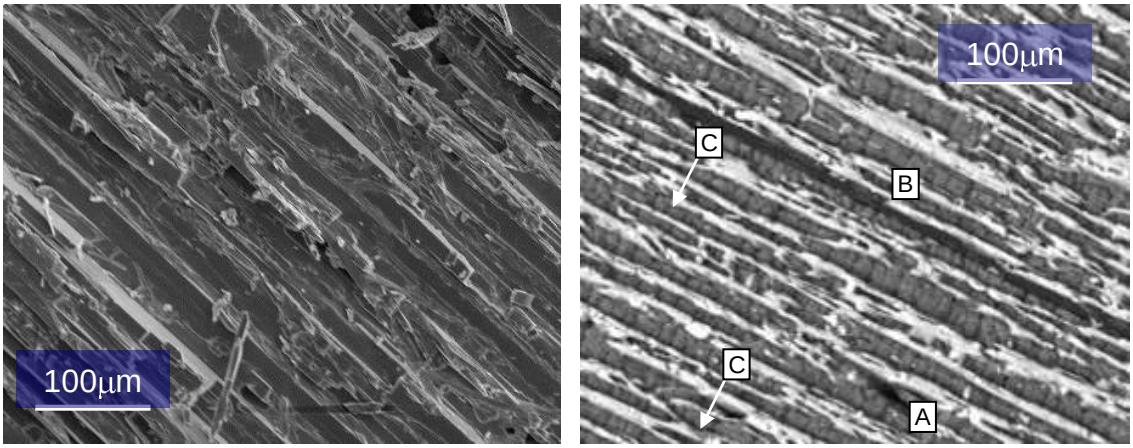

Figure 2.12 *Unhydrated borax slag*
Left: Fracture surface, secondary electron image
Right: Polished surface, back scattered electron image, showing constituent domains.

The borax slag generated as a by-product of lead refining. On cooling, the material forms acicular or sub-parallel bundles of crystals comprising three major phases. The borax, substituted with iron and zinc is a poorly crystalline phase and appears in a back scattered electron image as a dark grey matrix (A) with extensive cooling cracks perpendicular to its longest axis. This alternates with a relatively pure zinc oxide (bright phase, B) containing iron-rich domains (brightest phase, C). The major alternating domains occupy approximately equal volumes in the solid and are between 5 and 25 μm wide.

It was discovered early in the study that this material exhibits hydraulic properties and that its hydrated product shows a higher resistance to organic acids than conventional cements. Consequently, the top layer of the first experimental liner uses this material as a binder to allow the maximum length of time to investigate its chemical evolution. Laboratory examination of the slag – water system shows that it is bound by low-density phase of low crystallinity. Examination of the material by electron microscopy and x-ray diffraction does not reveal the nature of the hydration product and investigation of the material continues. Exposure of the hydrated binder to a range of organic acids suggests that although some

degree of reaction certainly occurs, the binder does not readily dissolve in weak acids as would be expected of a Portland cement.

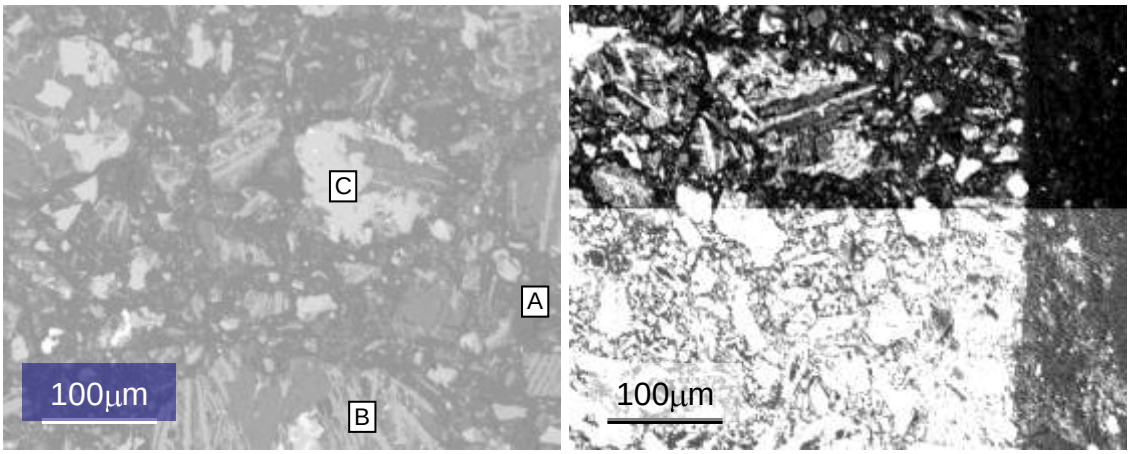

Figure 2.13 *Hydrated borax slag binder*
Left: Polished surface, back scattered electron image, showing dark hydration product (A) unhydarted slag fragments (B) and ferrosilicate aggregate particle (C).
Right: Polished surface, back scattered electron image. The sample has been leached by 0.1M acetic acid from the right. Above; high contrast showing detail of matrix, below, low contrast showing detail in the reaction product

There are two implications to this finding. First, the borax slag binder is likely to persist long into the service life of the liner, yet its contribution to the acid neutralisation capacity of the system is expected to be low. The nature of its acid reaction, like its hydration reaction, remains unclear. All that can be said with confidence at this stage is that the reaction products are gel-like in as much as they do not produce distinct x-ray diffraction patterns and that their electron density is lower than the unhydrated slag.

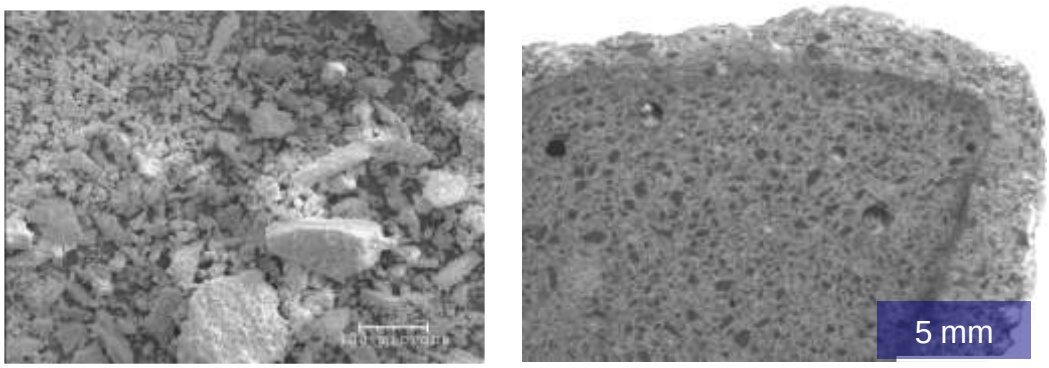

Figure 2.14 *Borax Slag Paste Left: Unhydrated, crushed slag*

Right: Microphotograph of polished section through a leached, hydrated sample of the borax slag binder. This sample was coarse-ground (<500 μm) to maximize the porosity and hence rate of leachant ingress. Three months exposure to 0.1M acetic acid at ~25°C.

The rate of leaching in aqueous acetic acid appears to decrease with time, suggesting that the reaction products occlude the sample from further ingress of the leachant. The presence of a low-density reaction product in the leached zone suggests a swelling gel may be formed which closes the connective porosity. As the product remains unidentified, it is not possible to predict whether the gel is likely to re-crystallise or to estimate the associated volume change should this occur. Preliminary investigations suggest that rapid reaction occurs over two or three millimetres within the first few days, after which the advancement of the reaction front is very slow over a period of three months at room temperature.

Ashes Two types of siliceous, pozzolanic ash have been examined in this project. Lagoon ash (UK Quality Ash Association) and Pulverised Fuel Ash (commercial PFA and an unclassified, run of station ash, both from Ash Resources Ltd). Chemically, these materials are similar in that they are relatively calcium poor, aluminosilicate glasses containing a variety of crystalline phases. The principal difference between them is that the unclassified ash contains a considerable quantity of carbon char, which would normally preclude it from use in structural concrete. Although the char makes up only a percent or so, of the ash composition by mass, its extremely low density makes its contribution to the volume fraction somewhat higher. As its strength is negligible, standards for cementitious ash limit its content in cementitious ashes. In addition, the high surface area of the carbon char particles, make it able to sorb ions form solution, which in a hydrating cement, may interfere with the hydration chemistry.

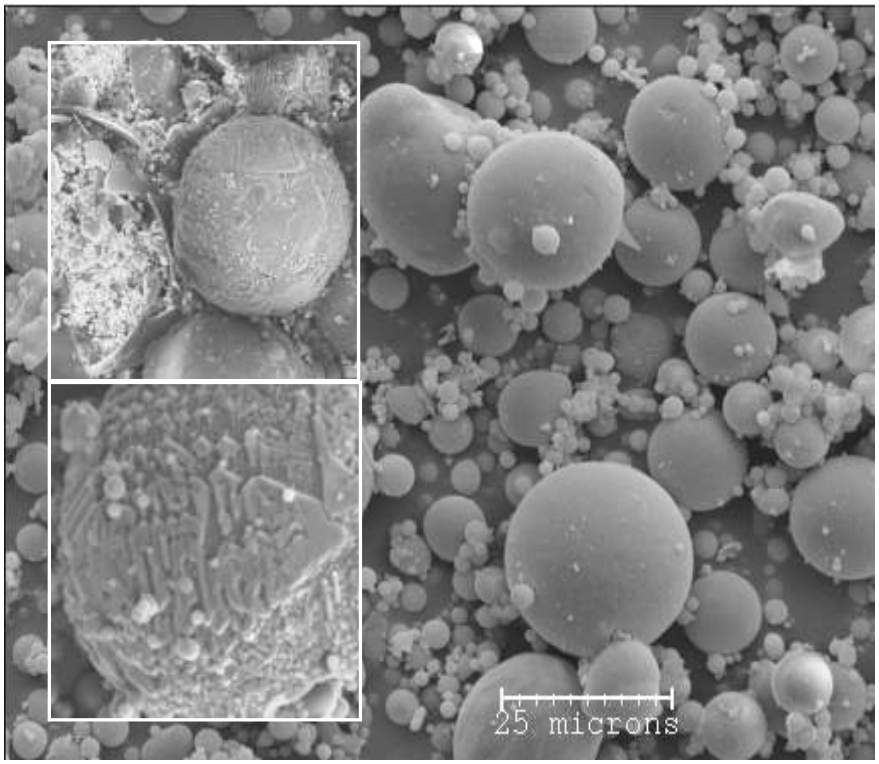

Figue 2.15 *Fly Ash. Inset: Cenospheres (above) Mullite (below)*

Figure 2.15 shows an interesting feature common in combustion products. During combustion, melting of the incombustible fraction produces molten droplets of material. The chemistry of some of these liquid drops is such that one or occasionally more phases will precipitate from the liquid. As this proceeds, crystal growth is constrained by the surface tension of the droplet, greatly modifying the habit of the forming crystal. In this case, the crystalline inclusion is mullite ($2Al_2O_3.3SiO_2$) which has a melting point of 1880°C.

Figures 2.16 and 2.17 compare the particles present in the two ash types and demonstrate that other than the char particles, the two materials are essentially similar, ranging from sub-micron sized particles to those several tens of microns diameter. Both contain some crystalline phases and glassy cenospheres.

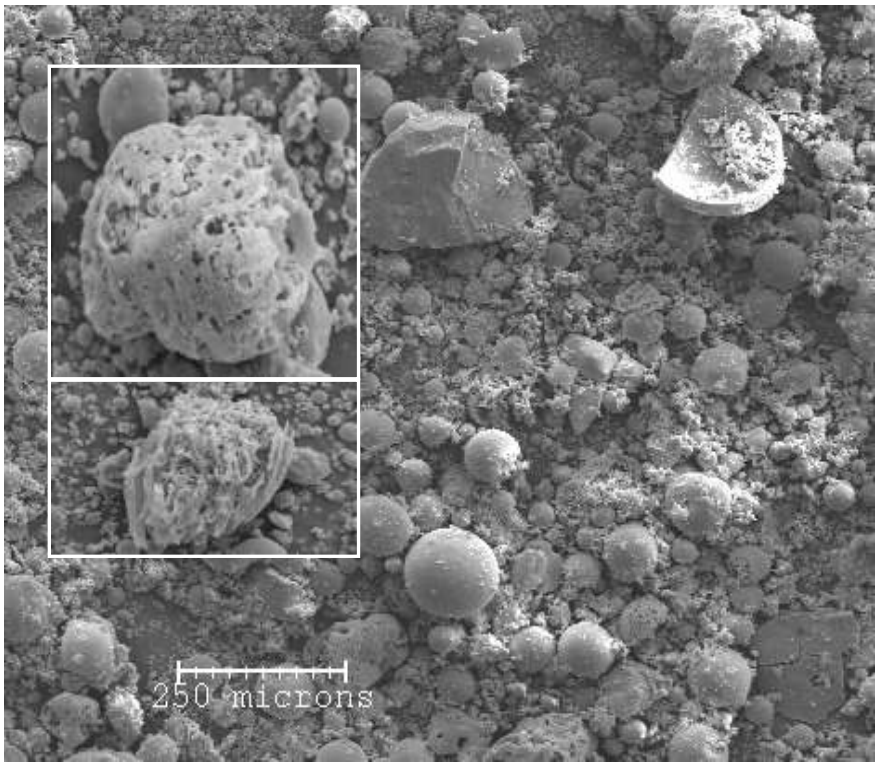

Figue 2.16 *Run of Station Ash. Inset: Carbon char particles*

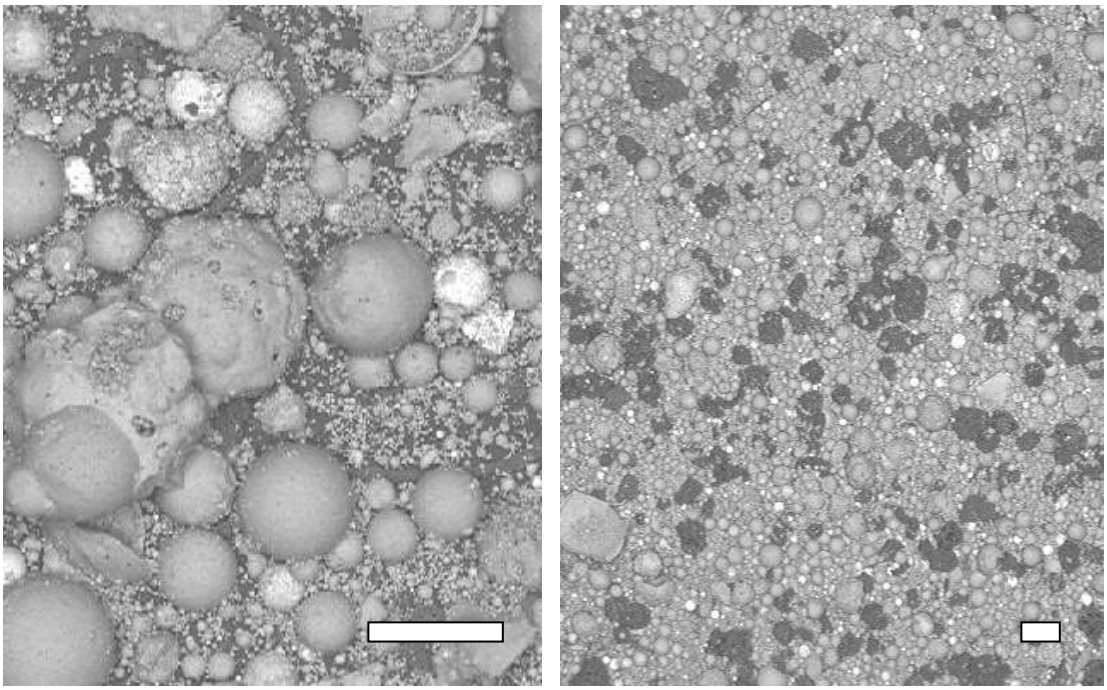

Figue 2.17 *Carbon char (dark particles) in PFA contributes significantly to the volume fraction, despite representing only a percent of the mass. (Scale bars = 25* μ *m)*

Cement kiln dust By comparison, the cement kiln dust is a relatively simple material. CKD is the primary waste product from the manufacture of Portland cement. This fine-grained material comprises partially reacted feed materials used in cement manufacture, including up to 50% calcium oxide, silica, alumina and up to 10 % potassium oxide, along with cement clinker mineral grains. There are strict composition limits imposed on Portland cement and, due to its high potassium oxide content, CKD cannot be reintroduced back into the cement manufacturing process. Currently much of the CKD generated in the UK is disposed to landfill. Figure 2.18 shows that the material used here ranges from small grains of a micron or two in diameter to grain clusters of a hundred microns or so. These samples are largely a mixture of partially calcined calcite with free calcium oxide, tricalcium silicate and larnite. A distorted glassy phase appears as shards of an alkaline glass (silica containing potassium ions).

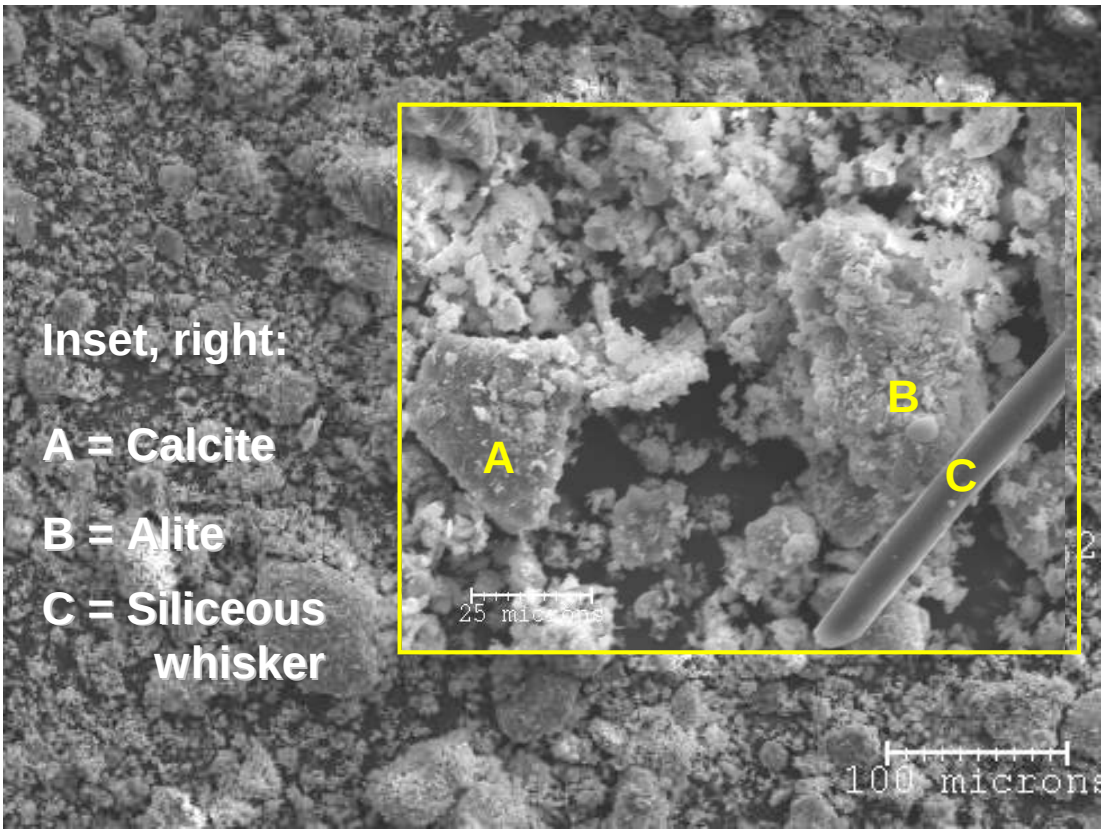

Figure 2.18 *Cement Kiln Dust (CKD) showing cleavage fragments of alite and calcite*

X-ray diffraction confirms that the major component in the CKD is calcite with minor amounts of free lime (calcium oxide), quartz, anhydrite and cement clinker minerals. Its relative oxide composition is shown in the table 2.1.

Oxide	% by mass
SiO_2	14.13
Al_2O_3	4.19
Fe_2O_3	3.25
CaO	58.26
MgO	2.30
SO_3	9.56
K_2O	4.70
Na_2O	1.48
P_2O_5	0.10
ClO	2.04

The loss on ignition is of the order 21% by mass, which we may reasonably assume is all due to loss of carbon dioxide on decomposition of calcite. This suggests that around 30% by mass of the CKD is calcium carbonate, the remaining calcium being partitioned between cement clinker grains and anhydrite.

Note the relatively high content of alkali metal oxides, which will be partitioned into the aqueous phase on mixing and available for reaction with glasses in the fly ash.

Table 2.1 *Relative oxide composition of CKD determined by energy dispersive spectroscopy on the SEM*

From the materials available in this study, it is possible to develop several binder types varying in composition, properties and cost. Figure 2.19 below summarises the binder formulations considered for screening in the experimental programme.

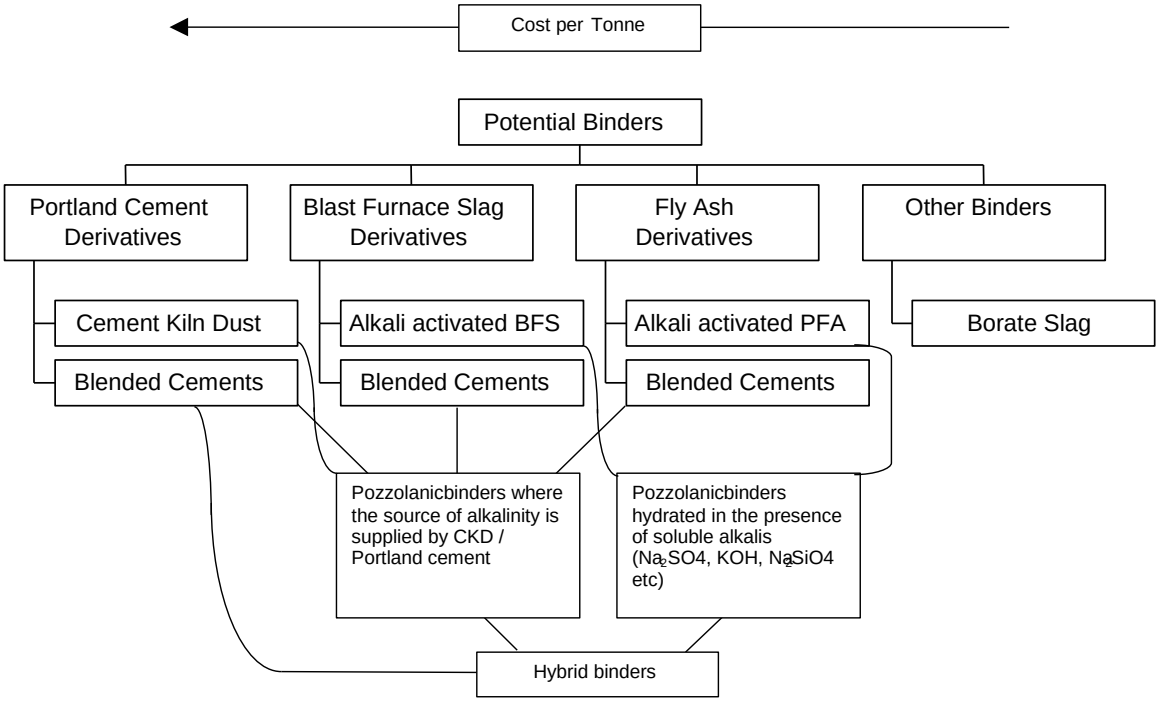

Figure 2.19 *The binder formulations considered for screening in the experimental programme*

2.1.3 Aggregate Materials

A wide range of industrial by-products have been considered as potential aggregates for concrete mixes in this project. They fall into two broad classifications: industrial slags and spent foundry sands.

Foundry sands are essentially pure quartz sands, with a surface coating of a binder. They are repeatedly recycled; sprue and casting debris being sieved from the sand after each casting operation. After several uses, the adhesive properties of the sand are reduced, as the binder is thermally degraded due to contact with the molten metal. This prevents them adopting the detail of the pattern and at that stage they are disposed of. They are not used as fine aggregates in structural concrete, owing to the presence of residual binder on their surfaces reducing the strength of the paste-aggregate bond. Foundry sands are typically of two types, those with a natural clay binder and those to which a synthetic binder must be added:

Greensand: Strictly, sands with a natural coating of glauconite, but the term is applied to casting sands coated with other clay minerals

Shell sand: Sands bound by a synthetic binder, such as phenolic resin.

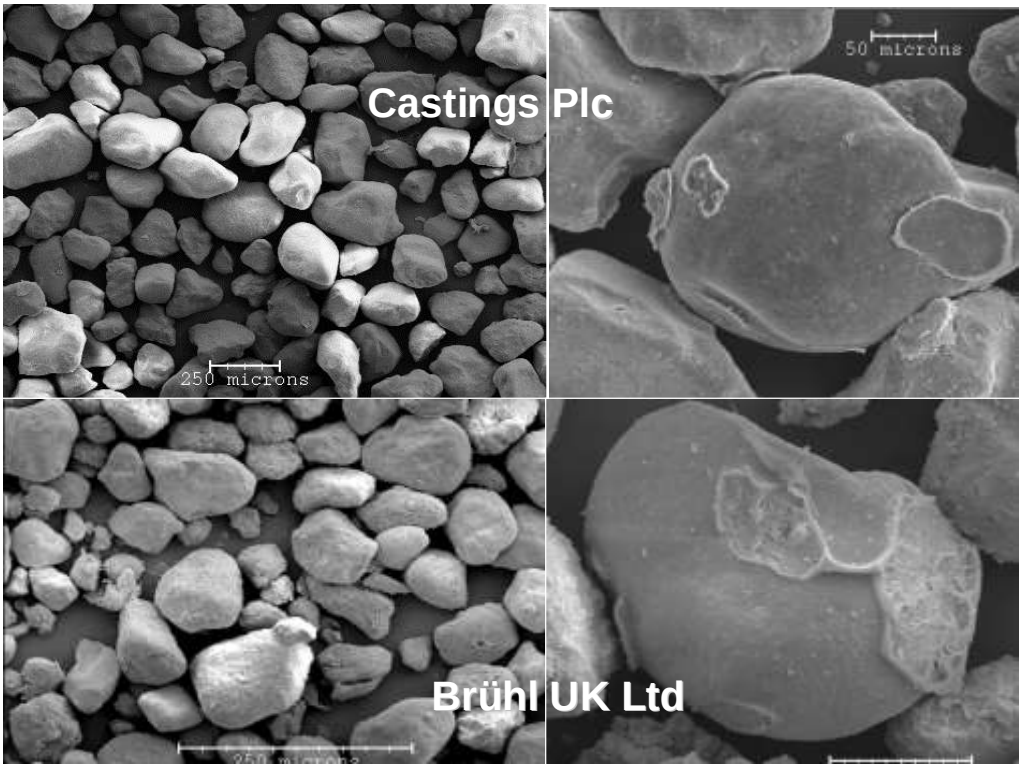

Figure 2.20 *Spent shell sands showing residual binders on the grain surfaces.*

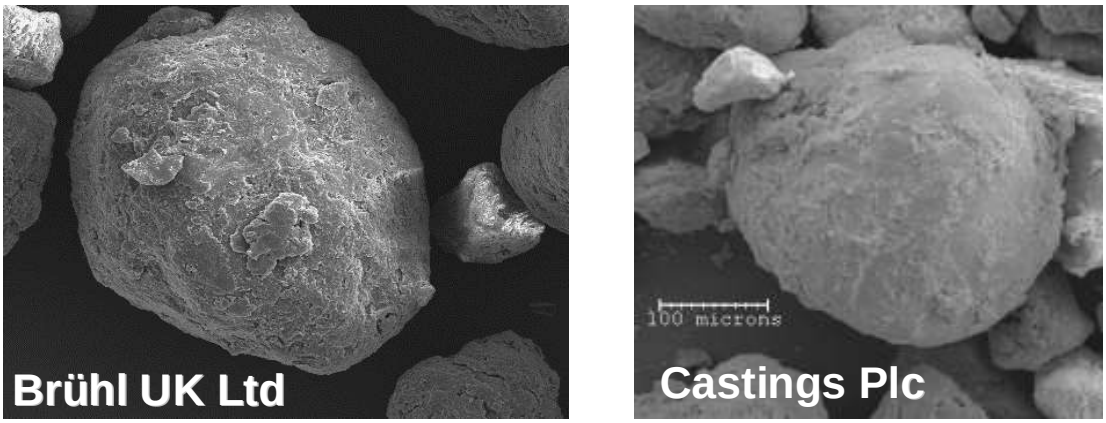

Figure 2.21 *Spent greensand showing fused clay mineral binder residue on the surface of the grains.*

Ferrosilicate slags are ubiquitous products of pyrometallurgy. They are derived from the siliceous gangue minerals present in the ores and are supplied either as chilled granules or fused lump. Both are very hard materials and the energy costs of crushing the fused lumps should be considered of the material is to be adopted for widespread use.

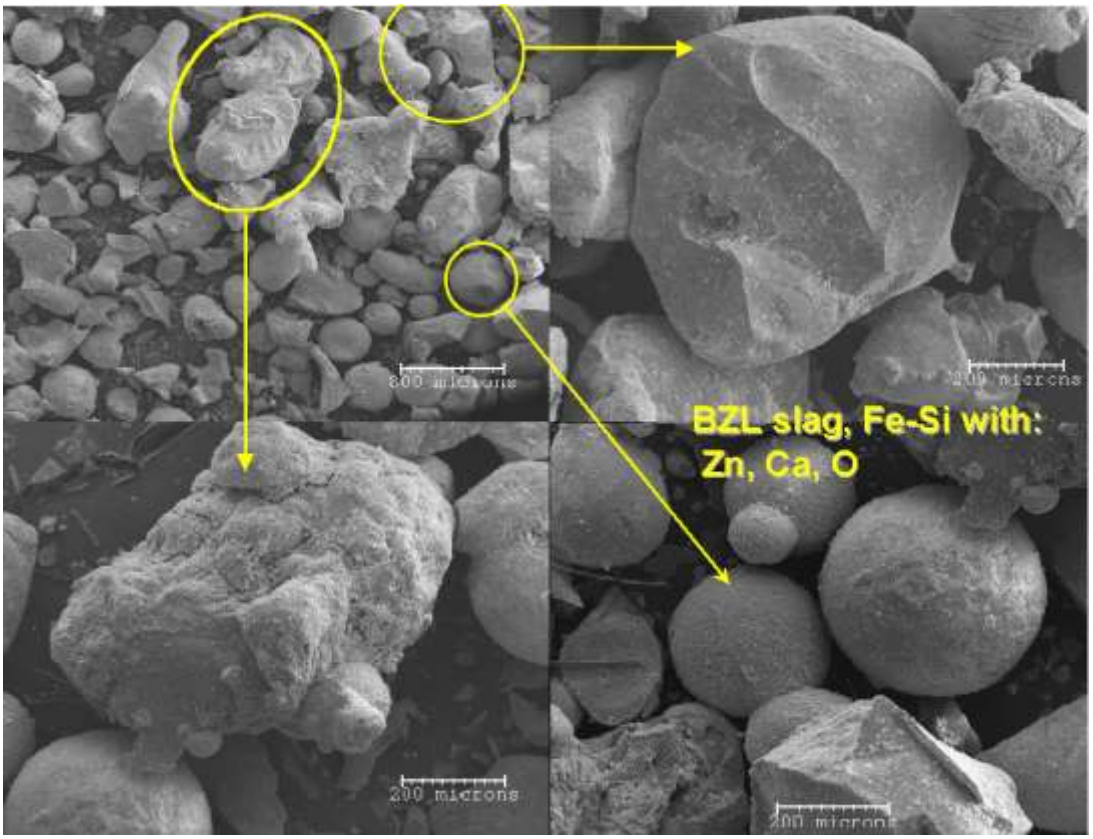

Figure 2.22 *Chilled ferrosilicate slag grains produced as a by-product of zinc refining.*

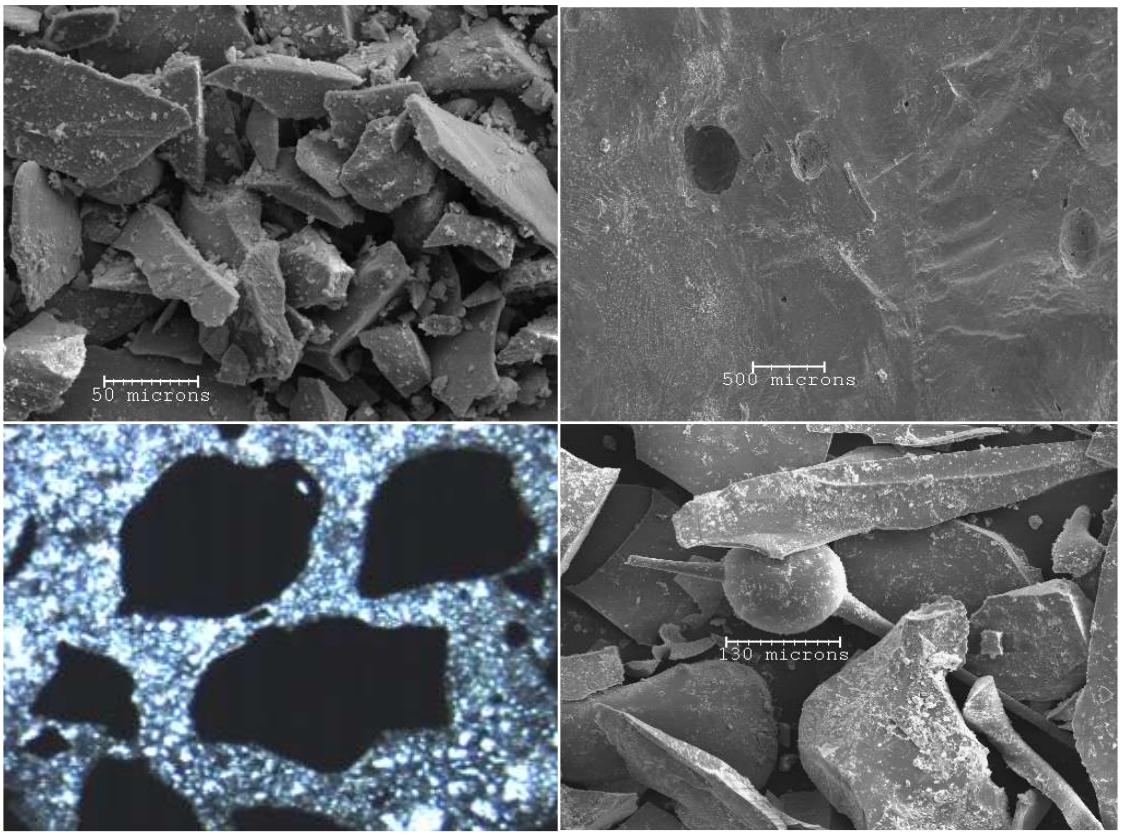

Figure 2.23 *Ferrosilicate slags. Top right, BRM slag (fused lump) Other images are IMI granulated slags, bottom left, as aggregate in AAS paste.*

Chrome alumina (London and Scandinavian Ltd) is a by-product of chromium manufacture and contains approximately 90% Al_2O_3 by mass with Cr_2O_3 and minor magnesium and transition metals. Within the largely glassy matrix are crystalline domains of substituted chromite. The material is supplied as very hard fused lumps.

Figure 2.24 *Chrome alumina slag in optical thin section showing characteristic purple body colour from* Cr^{3+} *in solution in the alumina matrix. Image width is 120* μ *m*

In optical this section, the slag shows repeated a lamellar structure of purple alumina glass alternating with substituted chromite layers.

At higher magnification, the chromite layers are seen to comprise many smaller strongly birefringent crystallites of characteristic trapezoidal cross section.

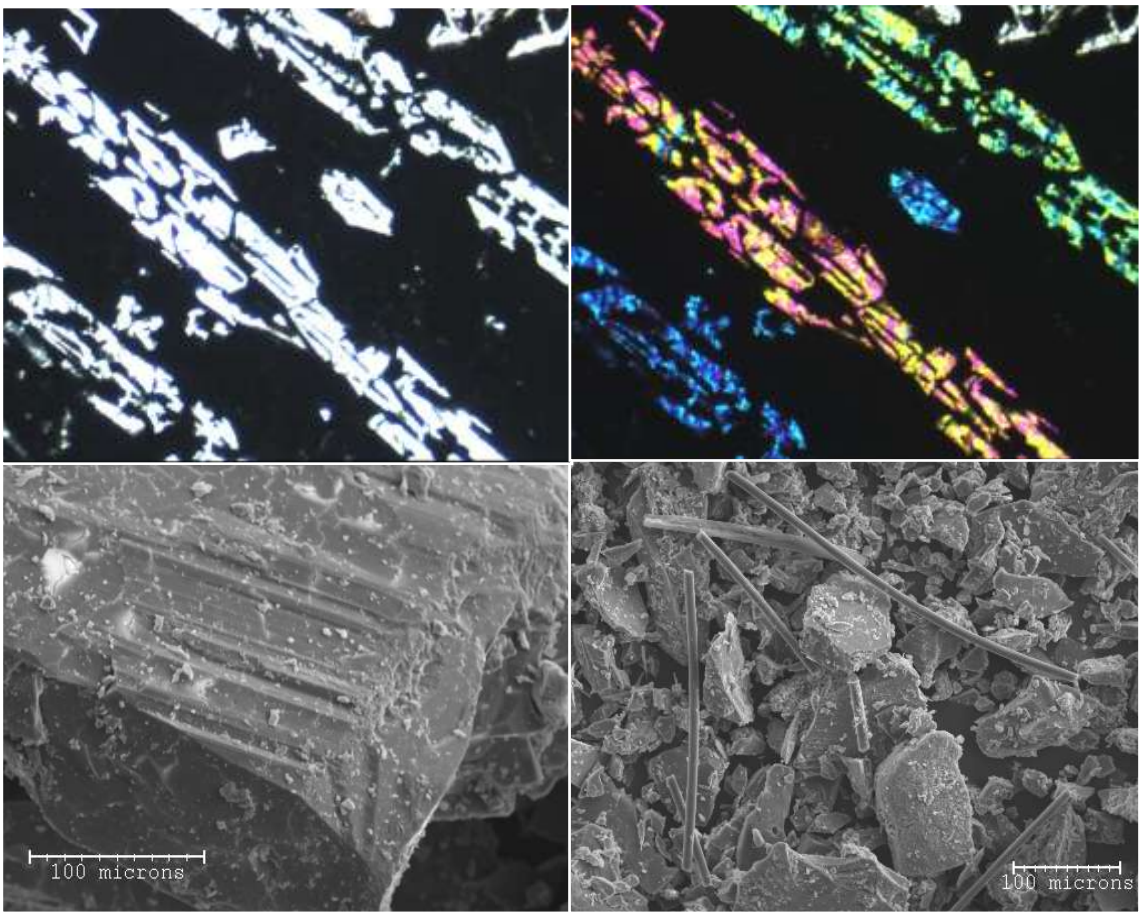

Figure 2.25 *Chrome alumina slag. Above, in optical sections, below, as secondary electron images showing whiskers which appear to be a magnesium silicate.*

To summarise, this study considers two groups of relatively inert aggregates: spent foundry sands and non-ferrous metallurgical slags. The former are fine quartz sands partially covered with either fused clay minerals or burned organic resins. The slags are all partially glassy; either ferrosilicate or chrome alumina. Of these, two are supplied as fused lumps which will require crushing to reduce their particle size. In addition to these relatively inert materials, consideration has been given to a group of potentially reactive aggregates and these will be discussed next.

Steel converter slags. The conversion of iron into steel is dominated by two technologies, by far the largest of which is the Basic Oxygen Process in which iron is refined into steel by selective oxidation of its impurities. The Electric Arc Furnace (EAF) is important in regions where electricity is relatively cheap and in some operations where scrap steel dominates the feed stock. The Basic Oxygen Steelmaking process differs from the EAF in that it is autogenous, or self-sufficient in energy. The primary raw materials for the BOP are 70-80% liquid hot metal from the blast furnace and the balance is steel scrap. These are charged into the Basic Oxygen Furnace (BOF) vessel. Oxygen (>99.5% pure) is "blown" into the BOF at very high rates.

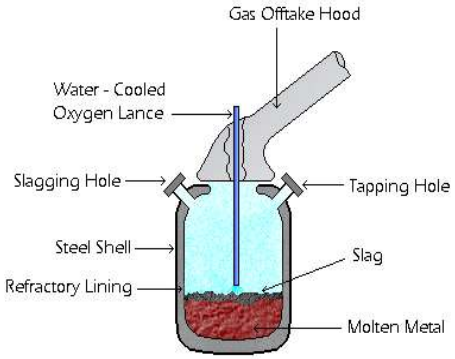

Figure 2.26 *Schematic representation of basic oxygen converter vessel*

This oxidises the carbon and silicon contained in the hot metal liberating great quantities of heat which melts the scrap. There are lesser energy contributions from the oxidation of iron, manganese, and phosphorus. The subsequent combustion of carbon monoxide as it exits the vessel, also transmits heat back to the bath.

The commercial product of the BOS process is molten steel at 1450°C-1660°C with a specified chemical composition. From here, it may undergo secondary refining or be sent directly to the continuous caster where it is solidified into billets prior to forming processes such as rolling or forging.

In order to control the metallurgy of the steel, various additions are made to the charge in the form of fluxes, commonly limestone or fluorite (CaF_2). The increased activity of calcium in the melt, scavenges silicon, phosphorous and sulphur from the metal as these elements preferentially partition into the flux. The term *Basic* refers to the magnesia (MgO) refractory lining which degrades, through contact with hot, basic slags. Although steel converter slags are dominated by the oxides of Ca, Si, P, Fe and Mn, the elemental ratios, phase chemistry and minor components are extremely variable. This reflects both the chemistry of the charge (iron and gangue minerals) and the alloying components added to the vessel to produce a steel of particular composition. To add further complexity to the slag, it is tapped (removed from the

vessel) before complete reaction, so the cooled slag may be far from thermodynamic equilibrium. Its phases are largely solid solutions of non-stoichiometric composition, so certain approximations are appropriate to its description. For example, consider figure 2.27 which show the range of major phases and their size distributions.

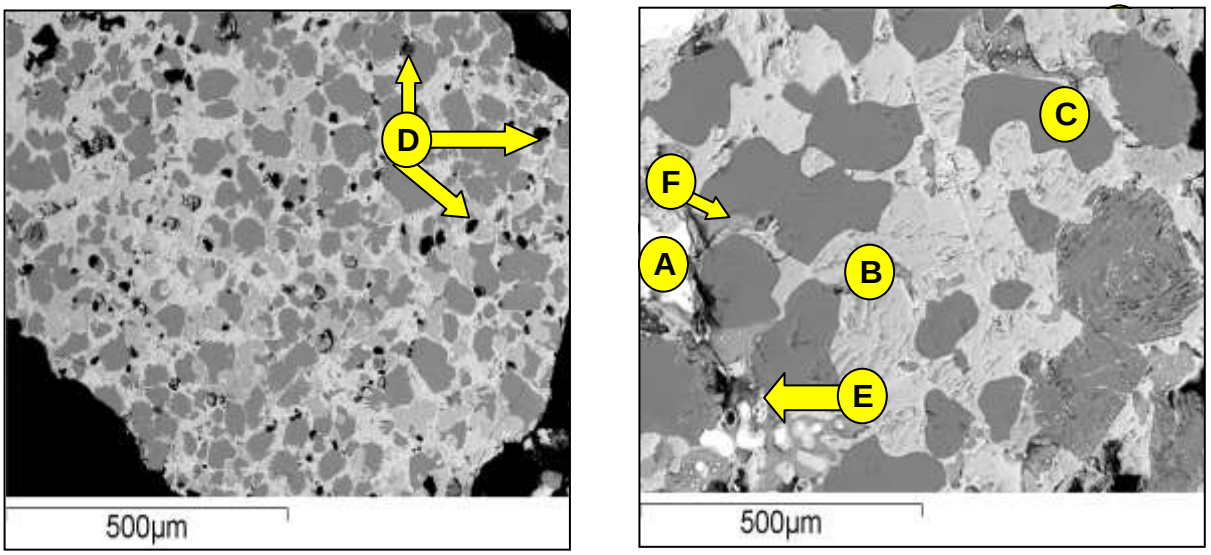

Figure 2.27 *Backscattered electron micrograph of polished section through basic oxygen slag*
Phase "A" is an iron-rich inclusion, "B" is a calcium-iron-manganese-magnesium oxide, phase "C" is a calcium silicate, approximating to impure wollastonite and "D" is porosity. The inclusions marked "E" are free lime and those shown as "F" are periclase (MgO)

The material supplied for this study exhibits two major porosity types. The discontinuous porosity shown in figure 2.27, originated as gas bubbles, trapped as vesicles on cooling. The second type is fracture porosity (figure 2.28) presumably results from cooling cracks and mechanical damage during processing. The steel slag undergoes a net volume expansion as it cools below about 630°C, where dicalcium silicate undergoes a re-crystallisation from the αC_2S to $\tilde{\alpha}C_2S$ forms. This phase transformation results in an increase in volume of around 10% and this is thought to be the energy source creating much of the fracture porosity. Figure 2.28 illustrates this second type of porosity, which is continuous throughout the grains.

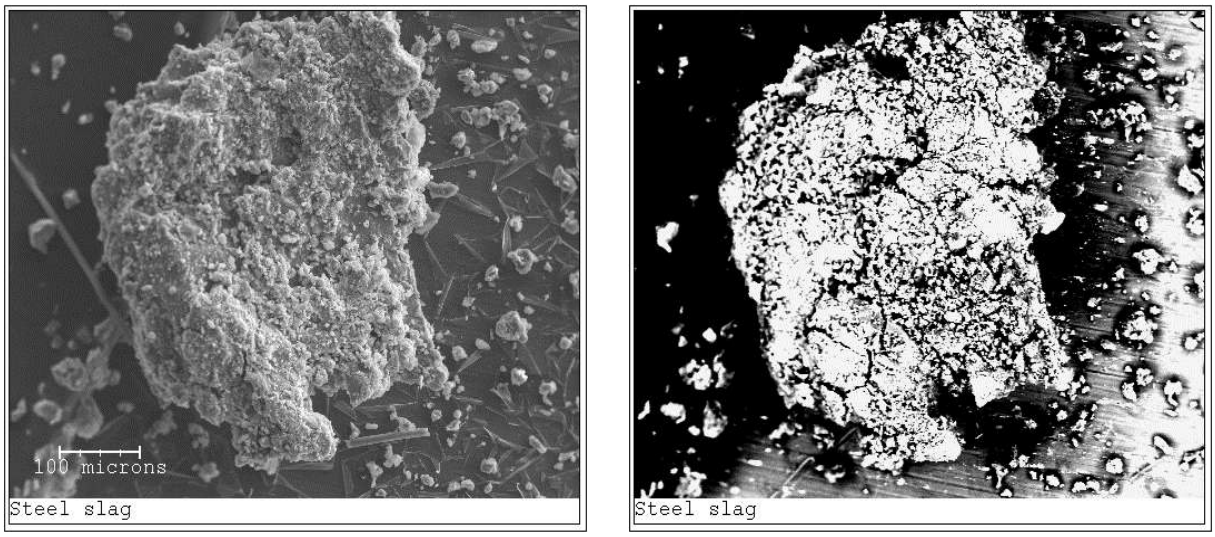

Figure 2.28 *Basic oxygen slag grain. Left: Secondary electron image showing surface morphology, right, backscattered electron image showing fracture porosity within the grain. As the efficiency of electron backscattering is a function of the average atomic number of the target, the technique reveals the internal fractures within the slag grain.*

Figure 2.29 shows the morphologies and range of grain sizes typical of the steel slag used in this study. Although a number of particles exceed two millimetres in diameter, the majority of the particles are angular fragments ranging from a few microns to a few hundred microns in size. The larger particles are polycrystalline, but many grains in the micron size range are monomineralic. Few well developed cleavage surfaces are seen at any scale, suggesting that the extent of crystal growth is limited. As the slag contains occluded domains of free lime, often connected by continuous fracture porosity, the use of the slag as a coarse aggregate in concrete is limited, owing to the risk of lime hydration after setting. Ingress of pore solution will slake the free lime to form calcium hydroxide, with a corresponding increase in molar volume. This reaction limits the use of these slags as aggregates in many construction applications, as the requirement is for a large aggregate particle, some millimetres across. In the applications considered here, the steel slag is used as a fine dust, where the particle size is little larger than that of the crystalline domains in the slag. It is reasonable to expect that hydration of the free lime will largely occur during mixing.

It is reasonable to assume that the grain size of basic oxygen slag is of critical importance to its suitability and long-term stability in cementitious materials. If the size of the grains is little bigger than the size of the phase domains it contains, hydration of calcium oxide to its hydroxide is likely to be rapid. As the particle size of the slag increases, so too does the time

taken for pore solutions to migrate through the fracture network in order to hydrate the free lime. If this hydration step can be achieved before setting of the mix, any volume changes will be accommodated whilst the material is in its plastic state. For brittle materials such as concrete, which have little strength in tension, an expansive reaction may be catastrophic. By comparison, controlled low strength materials are likely to be more compliant than conventional concrete and through careful selection of the particle size of (in this case the slag) components, such concerns may be overcome at the design stage.

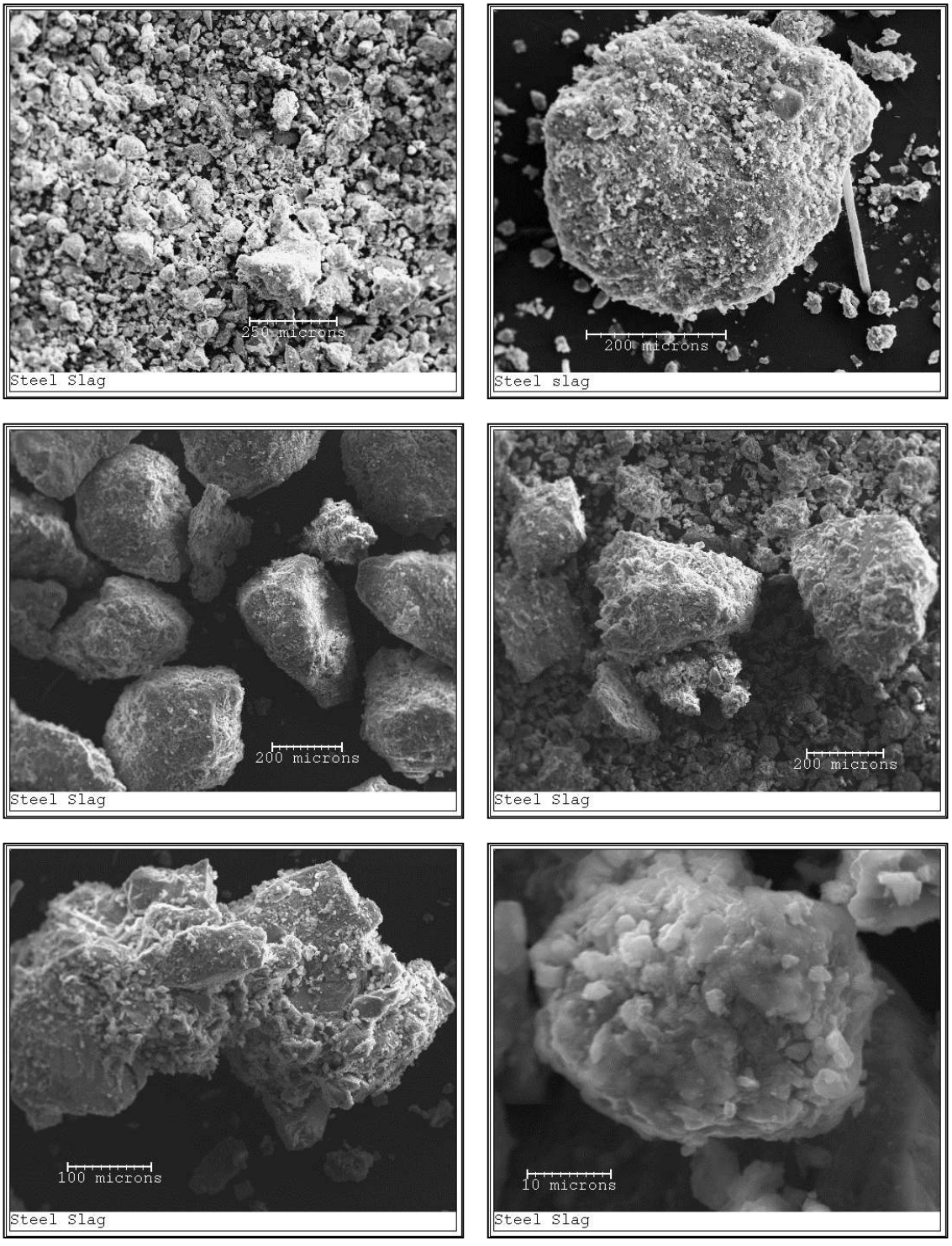

Figure 2.29 *Basic oxygen slag grains, secondary electron images. Each particle is a polycrystalline grain containing more than one distinct phase. That shown on the lower left is a polycrystalline grain, but of a single composition: free lime (CaO)*

One feature of the basic oxygen slag was surprising; the occasional presence of siliceous whiskers. These are presumably drawn out when the hot, mostly solid slag is moved after tapping. These whiskers, shown in figure 2.30, are approximately 20 μ m in diameter and are largely silica with some sodium and potassium and a little calcium in their composition.

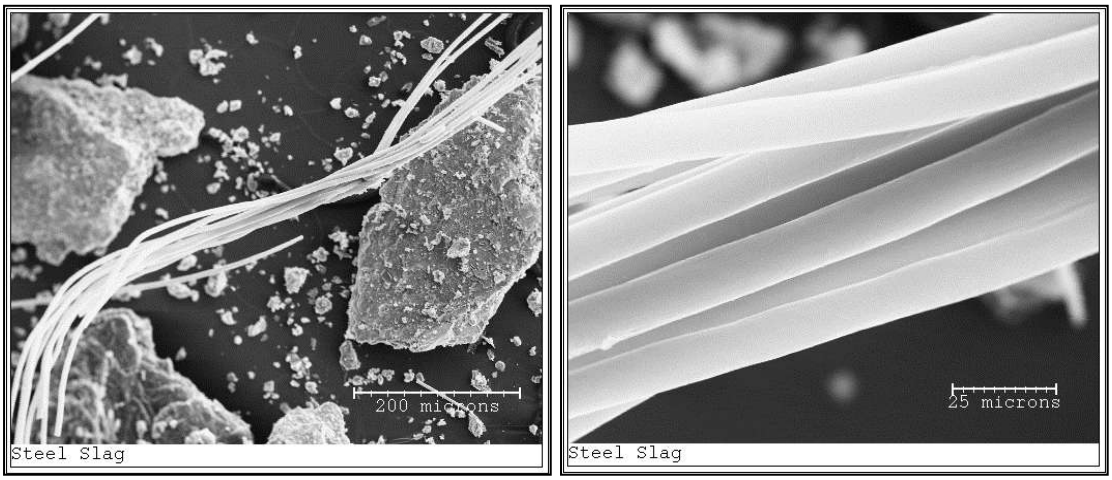

Figure 2.30 *Siliceous whiskers present in the basic oxygen slag. Secondary electron images*

Considering the composition of these steel slags, examination by x-ray diffraction reveals little about their phase chemistry. Figure 2.31 shows (for two samples of BOF slag) that the x-ray diffractogram is very complex, with few dominant, strong reflections.

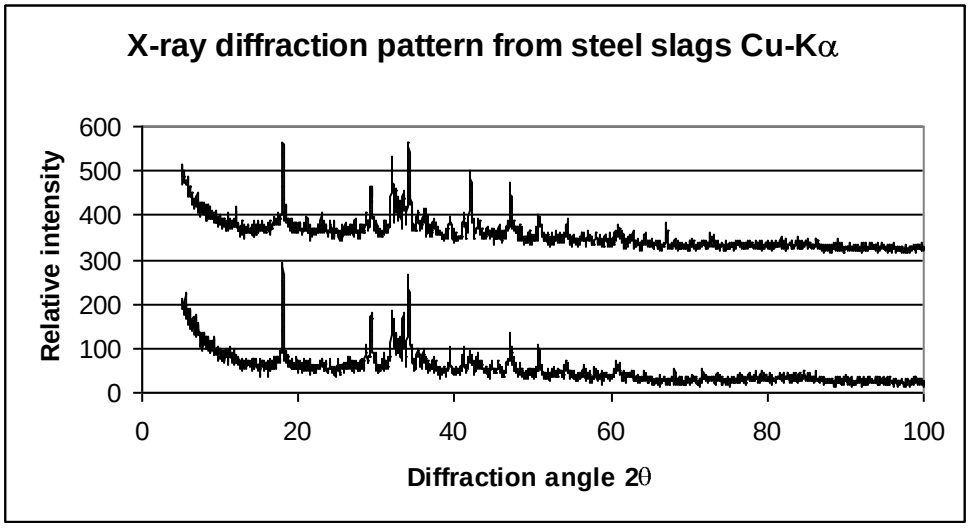

Figure 2.31 *X-ray diffraction pattern of the steel slag. Principle reflections correspond to larnite, Ca_2SiO_4 and Portlandite, $Ca(OH)_2$ suggesting that the slag has been in contact with water.*

Moreover, although the major peaks may be assigned to impure α-C_2S, if this is the case, the lattice is considerably strained. Identification is further complicated by the superposition of x-ray peaks on top of one another. The only other major phase which can be identified by x-ray diffraction is portlandite, suggesting that most of the calcium oxide has hydrated to calcium hydroxide during storage. This is not surprising, as finely divided free lime is highly hygroscopic and will readily hydrate if left open to the air. The complexity of the

diffractogram and the disordered and non-stoichiomentric nature of the slag, precludes further use of this technique for identification of anything other than qualitative identification of major phases. Nontheless, the major peaks present in the slag suggest that following minerals are probably present in the slag:

C_3S	[= $3CaO.SiO_2$]
α-C_2S	[= $2CaO.SiO_2$]
$54CaO{\cdot}MgO{\cdot}Al_2O_3{\cdot}16SiO_2$	
$11CaO{\cdot}7Al_2O_3{\cdot}CaF_2$	
α-C_2S *Major crystalline component*	[=$2CaO.SiO_2$]
$3CaO{\cdot}MgO{\cdot}3SiO_2$	
$CaMg(CO_3)_2$	[dolomite]
CaF_2	[fluorite]
$Ca(OH)_2$.	[portlandite]

Table 2.2 *Major phases identified in basic oxygen slag*

In light of the reactive nature of the free lime in these slags, a simple experiment was conducted to estimate the quantity of free lime available. Ten grams of powdered slag (sieved < 100 μ m) was dispersed in 100ml water and shaken every ten minutes for an hour in a sealed glass flask. The liquid was filtered and titrated against standard nitric acid to pH 7, using bromo-thymol blue as an indicator. Three replicates suggested that the mass fraction of calcium oxide in the slag was: 0.8% , 1.3% and 0.7% giving an average of 0.9% free CaO by mass. Although this is not a rigorous determination (it assumes all the soluble alkali is $Ca(OH)_2$) it serves as a first approximation and shows the alkaline nature of the pore solution. The solution pH was measured at 12.0±0.2 whereas the equilibrium pH of $Ca(OH)_2$ is 12.45 at 25°C.

Figures 2.32 and 2.33 show the phase distribution in the basic oxygen slags using backcsattered electron images of polished surfaces.

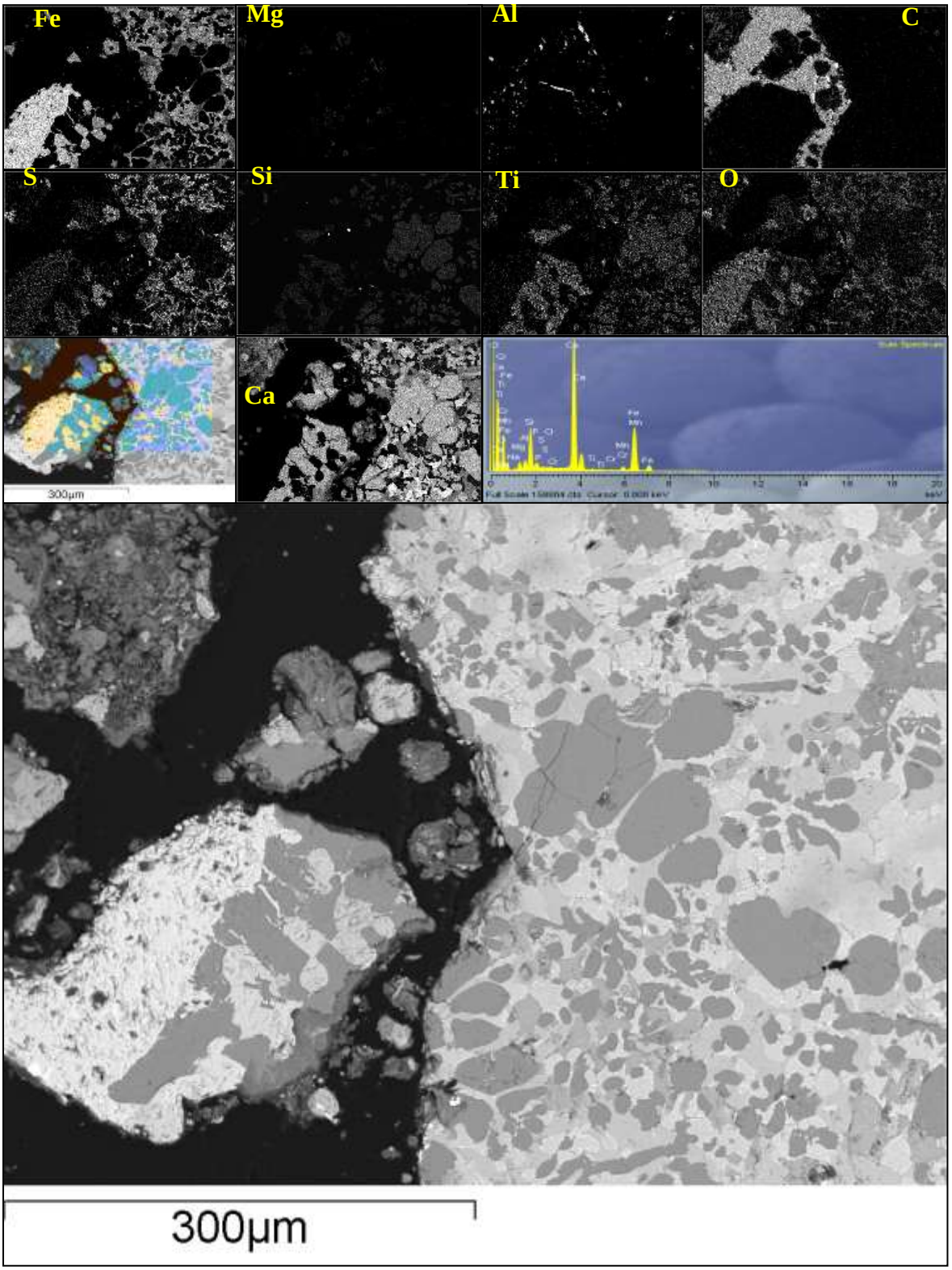

Figure 2.32 *X-ray maps and backscattered electron micrograph of polished basic oxygen slag showing element associations in the non-stoichiometric phases*

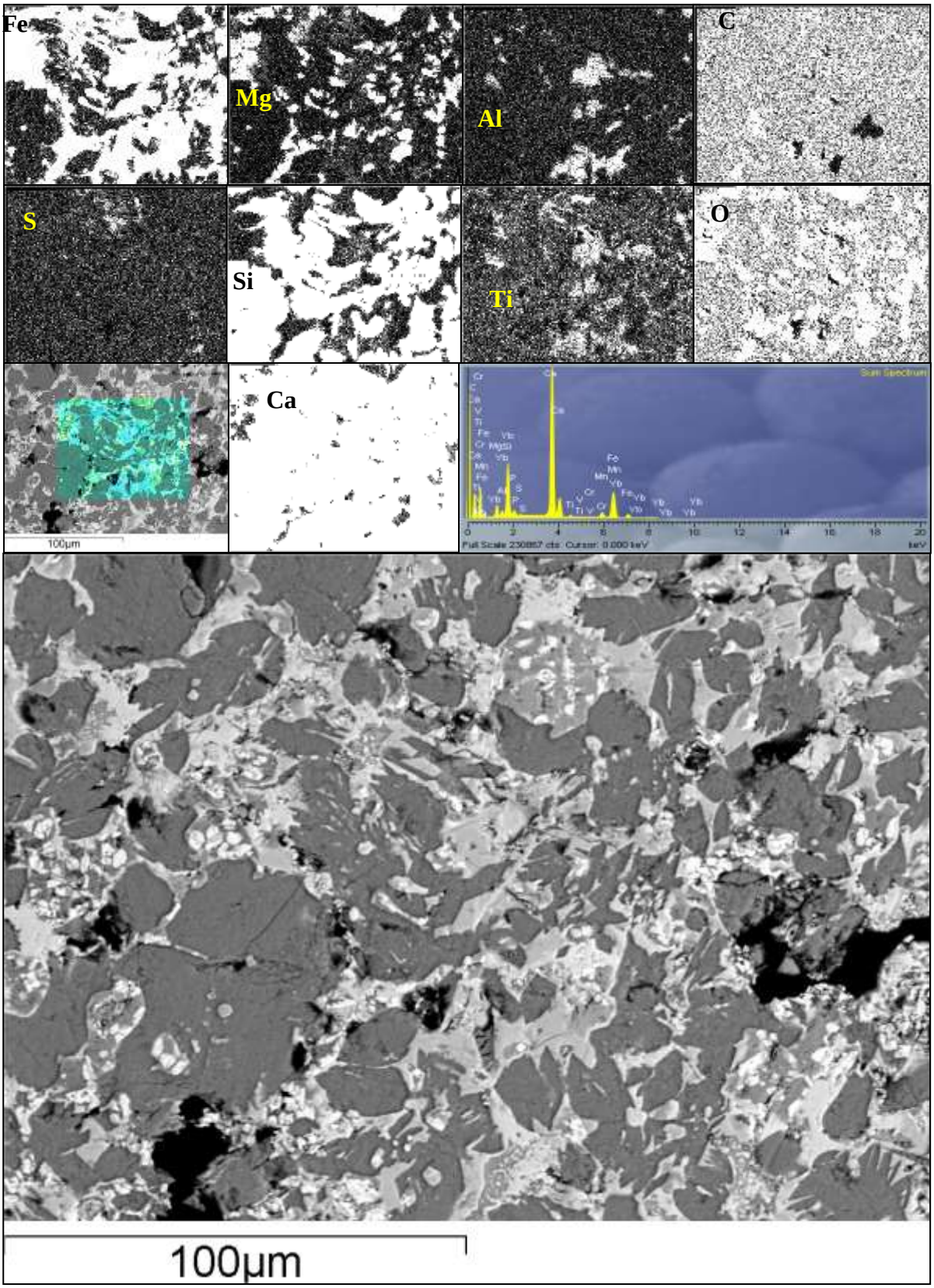

Figure 2.33 *X-ray maps and backscattered electron micrograph of polished basic oxygen slag showing element associations in the non-stoichiometric phases*

Each sample was examined by energy dispersive x-ray spectroscopy and, by image analysis to estimate the volume fraction assigned to each phase, along with an estimate of internal porosity in the slag.

Six distinct phase domains can be distinguished: The darkest region is porosity, largely in-filled with mounting resin whilst the brightest are free iron or steel inclusions. A Ca-Fe-Mg-Mn phase is continuous and contains an impure calcium silicate (α-C_2S). In addition, impure free lime (CaO) and impure periclase (MgO) can be seen.

Elemental composition of the slags was estimated using energy dispersive x-ray spectroscopy during examination under the electron microscope. This gives a first approximation to the relative oxide composition, but it must be borne in mind that the material is not fully oxidised; some of the iron is present in it's metallic state.

Oxide	**% by mass**
SiO_2	25.22
Al_2O_3	4.25
Fe_2O_3	6.35
CaO	52.71
MgO	8.60
SO_3	1.54
MnO	0.72
TiO_2	0.32
ZrO_2	0.29

Relative oxide composition of basic oxygen slag used in this study. Average of five determinations by EDS. Note that the elements determined as present at less than 0.1 % by mass are excluded and the residual normalised to 100%.

The confidence associated with these determinations is ± 5% at best.

Table 2.3 Relative oxide composition of basic oxygen slags as determined by SEM/EDS

In conclusion, basic oxygen slags are highly complex, polyphase materials containing few cementitious phases. Of those identified, only C_3S, α-C_2S and $54CaO.MgO.Al_2O_3.16SiO_2$ are known to be cementitious and these phases if present at all, comprise a very small fraction of

the slag. The thermal history of the slag is such that any free periclase (MgO) present is likely to be unreactive to water ("dead -burned"), leaving CaO to be the major phase which will undergo hydration.

In conclusion, there are three groups of materials which are suitable for use as aggregates in these applications; two (spent foundry sands and some non-ferrous slags) are relatively inert in an aqueous environment, whilst the third (steel converter slag) contains a phase which is relatively soluble in water. Figure 2.34 summarises these materials.

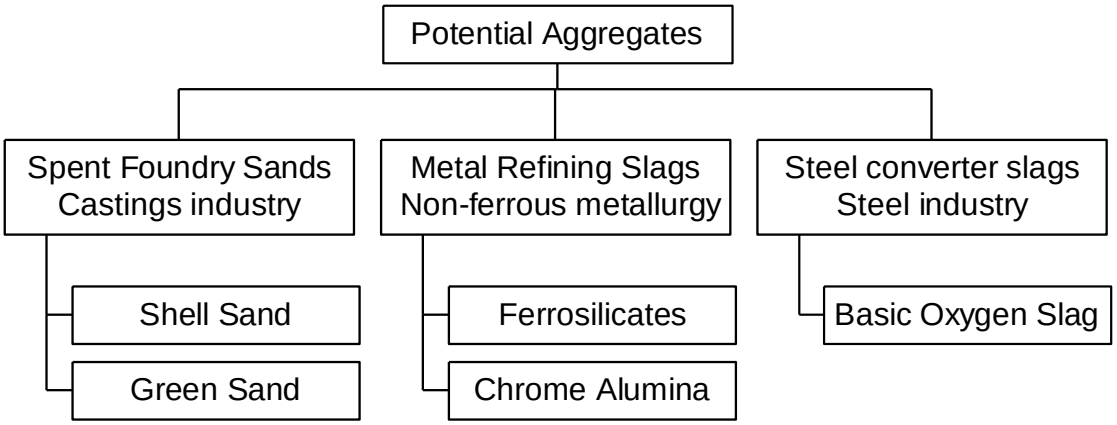

Figure 2.34 *Materials suitable for use as concrete aggegates*

2.2 Mix designs

2.2.1 Introduction

In order to establish the safety case a range of different mixes have been tested. These are categorised according to their specific use below but the results, and the methods used to obtain them, are intended to have more general application.

2.2.2 Mixes used in trial cells at Risley.

The materials and mix compositions used for the concrete and mortar layers in the three site trial cells at Risley are given in table 2.4 and their corresponding characteristics are given in table 2.5. The mix compositions of these mixes were chosen to contain high alkaline contents and give permeability of less than 10^{-9} ms^{-1} and compressive strengths of 5 MPa or slightly more.

2.2.3 Mix designs for laboratory tests.

The mix compositions of these mixes were designed to represent a typical site cell mix used (mix 3) and also to verify the effect of high strength conventional mortar. The materials and mix designs of the three mortar mixes used in the validation check of the high pressure tests are given in table 2.6.

2.2.4 Mix designs of the candidate mixes for the Poplars site.

The materials and compositions of the candidate mixes intended for the Poplars site are given in table 2.7. From the material available for Poplars site, mixes were designed to have high alkali content and satisfy the physical requirements given in section 2.2.2 above.

	Proportions Used	
	kg/m^3	% By mass
Composition of top layer concrete for cell No.1:		
Spent Borax	450	18.5
Ferrosilicate sand	895	36.8
20mm Limestone	1085	44.7
Water	210	
Composition of top layer mortar for cell No.2:		
Ferrosilicate slag sand (< 5mm)	1575	65.9
Cement Kiln Dust – 60%	490	20.5
Lagoon Ash – 40%	325	13.6
Water	200	
Composition of top layer concrete for cell No.3:		
Ferrosilicate slag (< 150mm to dust)	0	
Limestone (<20mm)	715	29.8
Ferrosilicate slag sand (< 5mm)	1105	46
Cement Kiln Dust – 60%	340	14.2
Lagoon Ash – 40%	240	10
Water	220	
Composition of lower layer concrete for cell No.1:		
Ground Granulated Blastfurnace Slag	180	7.6
Ordinary Portland Cement	20	0.9
Chrome Alumina Slag (40mm)	1515	64.2
Green Sand (ex-casting)	645	27.3
Na_2SO_4 solution	295	
Composition of lower layer concrete for cell No.2:		
Chrome Alumina Slag (< 40mm)	1175	49.6
Chrome Alumina Slag (< 5mm)	720	30.4
Green sand	100	4.2
Cement Kiln Dust – 60%	165	7
T1Sodium sulphate Solution (lt)	165	
Composition of lower layer concrete for cell No.3:		
Chrome Alumina Slag (< 40mm)	1175	50.3
Chrome Alumina Slag (< 5mm)	720	30.8
Green sand	110	4.7
Portland Cement – 5.2%	25	1.1
Cement Kiln Dust – 69.8%	185	7.9
Lagoon Ash – 25%	120	5.2
Water	240	

Table 2.4: *Composition of mixes used in the three trial cells at Risley.*

	7 days strength (MPa)	28 days strength (MPa)	Intrinsic permeability to water @ 28 days (m/s)	Intrinsic permeability to leachate @ 28 days (m/s)	Thro' pH water#	Through pH leachate#
Cell 1 top	5	4.5	1.5×10^{-8}	4.0×10^{-8}	10	_
Cell 1 base	11	13	No flow	2×10^{-12}	_	8.5
Cell 2 top	1.1	1.7	4.5×10^{-9}	5×10^{-9}	11.8	12.3
Cell 2 base	4.4	6.9	2.3×10^{-9}	4.5×10^{-9}	10.1	9.9
Cell 3 top	0.9	1.3	1.2×10^{-8}	7.5×10^{-9}	12.2	12.1
Cell 3 base	2.8	6	1.2×10^{-8}	6.2×10^{-9}	8.5	7.6

***** Initial pH of leachate: 5.1 - 5.4

The 'through pH' is the pH of the outflow from the permeability test (see chapter 4)

Table 2.5: *Characteristics of the mixes used in the site trial cells at Risley.*

Mortar mix	Cementitous material	% by mass	Pozzo-lanic ash	% by mass	Fine aggregate (<5mm)	% by mass	W/C	28 days Str. (Mpa)	Leachate permeability (m/s)
Cement/ Quartz	OPC	11.8	_	_	Quartz	88.2	0.92	15	1.7E-09
Cement/ Quartz	OPC	16.7	_	_	Quartz	83.3	0.75	20	2.2E-10
Top layer of cell2	CKD	20.7	Lagoon ash	13.6	Ferrosilicate slag	65.9	0.39	5	2.2E-09

Table 2.6: *Characteristics of the mortar mixes used for validation of the high-pressure permeability test.*

Mix. No.	Mat. 1	% By Mass	Mat. 2	% By Mass	Mat. 3	% By Mass	Mat. 4	% By Mass	L/S	28 days Str. MPa	28 days K M/s
1	SSD	75	ROSA	25	_	_	_	_	0.16	5.5	4.3E-08
2	CKD	50	ROSA	50	_	_	_	_	0.37	8.5	1.3E-10
3	CKD	42.5	ROSA	42.5	G S	15	_	_	0.34	6.0	5.0E-09
4	CKD	50	SSD	50	_	_	_	_	0.27	8.5	2.3E-09
5	CKD	50	ROSA	30	SSD	10	RG	10	0.36	10.0	8.2E-11

Table 2.7: *Characteristics of the candidate mixes intended for the Poplars site*
(Designed from the materials available to CU by end of June 2003)

SSD = Steel Slag Dust, a by-product from steel manufacturers, supplied from Scunthorpe works, Tarmac Ltd.
ROSA = Dry Run Of Station Ash, Unclassified ash from west burton, Rugby ash Ltd.
CKD = Cement Kiln Dust from Ribblesdale, Castle cement.
RG = Red Gypsum waste from Huntsman Tioxide.
GS = Green Foundry Sand, casting sands coated with other clay minerals, from WBB Minerals Ltd.

3 COMPUTER MODELS

3.1 Introduction

The first stage modelling of the barrier has been carried out with a computer model which has been written for the purpose at Coventry University. This model is based on physical transport processes with linear adsorption and uses the following assumptions.

1. The following mechanisms are assumed not to be significant: Thermal migration, Electromigration, Osmosis, Electro-osmosis, Capillary suction (saturation assumed – see below)

2. The barrier is assumed to be saturated when the leachate first comes into contact with it.

3. The layers of the barrier are assumed to be homogeneous. In particular "boulders" are assumed not to form. These would be regions surrounded by impermeable layers of carbonates, chloroaluminates or magnesium compounds which do not contribute to the transport or adsorption.

4. The properties of the barrier are assumed not to change with time or the amount of transport that has taken place through it other than the gain or loss of ions due to the transport processes.

5. The adsorption processes are assumed to reach equilibrium within each time step.

In order to confirm that these limitations lead to a conservative result a far more complex coupled chemical transport simulation has been carried out using PHREEQE on a limited number of situations.

Finally the output from the barrier into the environment has been modelled with Landsim.

3.2 The Coventry model

3.2.1 The Transport Processes

Advection

In this process the pressure of the leachate head causes water flow which carries dissolved ions through the barrier. The rate of transport through the barrier will be determined by the coefficient of permeability k which has the units of m/s and is defined from [3.1]:

$$V = \frac{k\,(h_1 - h_2)}{x} \quad m/s \qquad [3.1]$$

where V is the Darcy velocity of the fluid flowing through a thickness x (m) with pressure heads h_1 and h_2 (m) on each side.

Diffusion

In this process the dissolved ions move through the water at a rate determined by the concentration gradient. The flow per second per unit cross sectional area of a porous solid (the Flux, F) is given by [3.2].

$$F = \varepsilon D \frac{dC_l}{dx} \quad kg/m^2/s \qquad [3.2]$$

where ε is the porosity, D is the intrinsic diffusion coefficient and C_l is the ionic concentration in the pore fluid.

Adsorption

The physical transport processes are restricted, in part, by adsorption in which a linear isotherm is assumed, *i.e.* a fixed proportion of the ions in any part of the barrier are adsorbed onto the matrix and will not move. To describe these processes two different ionic concentrations must be defined:

C_l kg/m^3 is the concentration of ions per unit volume of liquid in the pores. These ions will pass through the barrier under the influence of the physical transport processes. The concentration per unit volume of the solid will be εC_l where ε is the porosity.

C_s kg/m^3 is the total concentration (including adsorbed ions) per unit volume of the solid. The ions which are adsorbed onto the solid will not move. The capacity factor is defined as [3.3]

$$\alpha = \frac{C_s}{C_l} \qquad [3.3]$$

Note that we may calculate $k = \dfrac{Concentration\ in\ solid}{Concentration\ in\ liquid} = \dfrac{Cs - \varepsilon Cl}{Cl} = \alpha - \varepsilon$ [3.4]

3.2.2 Basis Of The Calculations:

Output from Calculations

The purpose of the model is to calculate the transport of material through a barrier. The same code runs in four different modes to model:

The high pressure through-flow test
The diffusion test
The site trial cells at Risley
The barrier to be built at Poplars

In each mode the calculations are identical. The only differences are in the exact output given and the length of time that a run simulates.

Input data

The barrier is constructed with up to three layers. (Note that for the Poplars site only one or two layers are used) Each layer is characterised with the following parameters:

For layer j

Layer Thickness = x_j
Capacity factor = α_j

Permeability = k_j

Intrinsic Diffusion coefficient = D_j

Porosity = ε_j

Within the programme each layer is divided vertically into a large number of cells.

3.2.3 Methods Of Calculation:

Darcy Velocity

This is calculated as follows:

$$V = \frac{k \times (H + x_1 + x_2 + x_3)}{x_1 + \left(\frac{x_2 \times k_1}{k_2}\right) + \left(\frac{x_3 \times k_1}{k_3}\right)} \quad \ldots[3.5]$$

Where H is the head of leachate in m above the barrier.

Steady state conditions.

The transport by advection alone reaches a steady stated when the concentration throughout the barrier Cs_i = the concentration above it Cs_0.

Thus $F = V \times Cs_0$ …[3.6]

The transport by diffusion alone reaches a steady state when there is a linear concentration gradient through the barrier.

The flux is given by:

$$F = \frac{Cl_0}{\left(\frac{x_1}{D_1 \times \varepsilon_1}\right) + \left(\frac{x_2}{D_2 \times \varepsilon_2}\right) + \left(\frac{x_3}{D_3 \times \varepsilon_3}\right)} \quad \ldots[3.7]$$

These values are calculated at the start of the programme.

Time step

The time step dt for the programme is set to an estimated value and the time to breakthrough is calculated. The time step is then halved and the process is repeated. A change of less than 5% in the breakthrough time is taken to indicate stability.

The relationship between the time step and the cell size is initially determined by the advection calculation. This can mean that if the diffusion flux is high the concentration in the cell can change substantially during a single time step (it is assumed to remain approximately constant). This is checked and if the resulting change in concentration in the cell exceeds 25% of the concentration the time step is reduced.

Advection calculation

The advection from cell i to cell i+1 during a single time step dt is calculated as:

$$F \times dt = Ct_i \times \varepsilon_i \times Cl_i = dt \times V \times Cl_i \qquad \ldots[3.8]$$

where the cell thickness = Ct_i

Diffusion calculation.

The diffusion from cell i to cell i+1 during a single time step dt is calculated as:

$$F = \frac{\varepsilon_i \times \left(\frac{D_i + D_{i+1}}{2} \right) \times (Cl_i - Cl_{i+1})}{Ct_i} \qquad \ldots[3.9]$$

For the upper and lower cells (numbers 1 and n) the diffusion is doubled because the diffusion path to the centre of the cell only runs through half the distance of solid.

Definition of breakthrough.

Breakthrough is calculated for the modelling of the site trials and Risley site and is defined as the time obtained by extrapolating the linear part of the breakthrough curve to zero concentration.

Optimisation.

The programme is used for a single run when calculating the performance of a landfill cell but when calculating the properties of a sample (diffusion coefficient and capacity factor) from experimental results it can carry out repeated runs and optimise. For each run the root mean square error between the model results and the experiment is calculated and the sample properties are then adjusted to get the lowest error.

Treatment of tolerances.

The input data for the modelling of the full-scale barriers (e.g. layer thickness) is assumed to be normally distributed. For the purpose of modelling it is divided into three outcomes, an expected outcome and one high and one low. Studying the normal probability function shows that to give each outcome equal probability the expected outcome must include all results within 0.43 standard deviations of the population mean. The mean of the high and low outcomes have been calculated to be 1.1 standard deviations above and below the sample mean. The standard deviation has been estimated as a coefficient of variation V = standard deviation/mean. Thus 3 outcomes are modelled:

Outcome	**Mean value**	**Probability**
high	sample mean * (1 + 1.1 V)	0.33
expected	sample mean	0.33
low	sample mean * (1 - 1.1 V)	0.33

For the diffusion coefficient and the permeability the treatment is slightly more complex in that the distribution of results form a highly skewed distribution when measured on a linear scale. On a logarithmic scale they are, however, more normally distributed and the three

different outcomes have therefore been obtained by dividing up the distribution of the log of the parameter. In this case the three outcomes become:

Outcome	**Mean value**	**Probability**
high	sample mean ^ (1 - 1.1 V)	0.33
expected	sample mean	0.33
low	sample mean ^ (1 + 1.1 V)	0.33

Where V is the coefficient of variation of the sample on a logarithmic scale.

Typical values are as follows:

Parameter	Typical Value	Scale	Coefficient of variation %	Low value	High value
Capacity factor	5	Linear	50	2.25	7.75
Permeability	1E-9	Logarithmic	2	6.4E-10	1.6E-09
Diffusion Coefficient	1E-12	Logarithmic	5	2.2E-13	4.6E-12
Layer thickness	300	Linear	15	250.5	349.5

From this it may be seen that although V for permeability appears low at 2% it represents a range of +60% and –36% on a linear scale. The 5% for diffusion gives an increase of 460% on a linear scale.

Because the populations are skewed on a linear scale the mean outcome from this analysis is not the outcome with the highest probability (as would by expected from a normal distribution).

Each of these outcomes has been modelled for each input parameter for which there is significant uncertainty. Thus, for example, where four different input parameters have significant uncertainty 81 simulations have been carried out and the 10^{th} and 90^{th} percentiles

of the resulting population have been used to calculate the degree of uncertainty of the model predictions.

The coefficients of variation for the input data obtained in the laboratory work have been obtained by studying several series of replicate samples and also analysing the optimisation of the data from the through diffusion tests.

Some variables, such as layer thickness in multi-layer barriers, are in sets in which varying each one will have a similar effect. Reducing the thickness of one layer by 20mm will have a similar effect to reducing another layer. In there situations only the variation of one of the variables has been modelled.

3.2.4 Model Code Validation

The model code has been validated as follows:

The steady state values can be checked by hand calculation and for a number of different configurations the programme has been run for long enough to reach an effective steady state and the output checked for agreement.

For a single layer the model has been checked for agreement with the PHREEQE transport code for a single element.

3.3 Modelling with PHREEQE

3.3.1 Normative modelling of cement hydrate compositions

Of the range of materials studied in this project, a number readily lend themselves to deterministic modelling using equilibrium thermodynamics. Binder types based on blended Portland cements (with replacement by fly ash, blast furnace slag and limestone flour) react relatively quickly to produce a stable assemblage of mineral hydrates with predictable stoichiometric compositions.

In order to simulate the behaviour of these blended materials, the normative model "CEMCHEM" was used to estimate the likely phase composition of each cement type from the relative oxide compositions of the unhydrated components. At integral blending ratios, a simple normative calculation is performed, to estimate the relative molar oxide composition of the mixture at each blending ratio. CEMCHEM1, considers the hydration of two blending components hydrated at 25°C and initially, assigns all the magnesium in the system to hydrotalcite (M_4AH_{10}) and all the sulphur to ettringite (AFt-SO_4, $C_6A\underline{S}_3H_{32}$), along with stoichiometric quantities of aluminium and calcium. The remaining components are re-normalised to 100% and the calcium : silicon : aluminium ratio calculated, in order to assign the mixture to one of six mineral assemblages spanning the CSH -$Ca(OH)_2$ - hydrogarnet fields of the hydrous Ca-Si-Al system. The aluminium content of the remainder is used to determine the hydrogarnet portion of the hydrate mixture and the unassigned calcium and silicate are apportioned into the CSH. A similar treatment is made of systems of high calcium content, assigning a portion of this element to free calcium hydroxide (portlandite) such as would be expected in a pure Portland cement. The calculations are repeated at the ninety eight integral compositions between the two end members and in the case of limestone-containing mixtures, the calcite is treated as a simple diluent, whilst impurity elements are partitioned between the hydrates.

CEMCHEM1 (25°C model) does not consider highly siliceous systems such as blends containing a relatively high proportion of fly ash, the code containing error traps which prevent misleading predictions being made under such conditions. CEMCHEM2, by comparison, treats two blending components hydrated at elevated temperature (85°C) and assigns the integral compositions to a more complex set of mineral assemblages than CEMCHEM1. This model includes the zeolite phase Ca-P, similar to the gismondine-phillipsite type zeolites found in fly ash cements, which allows predictions to be made in siliceous systems. Additionally, gehlenite hydrate (strätlingite; C_2ASH_8) is estimated. The latter however, presents a problem in that the simplification of the system to relatively few components, often violates the Gibbs phase rule, preventing subsequent thermodynamic calculations from converging. As gehlenite hydrate is only sparingly soluble, it contributes little to the chemistry of the cement pore solution and can be safely removed from thermodynamic equilibrium calculations with correspondingly little effect on the chemistry of the aqueous phase.

Whilst the compositions considered in this study, are relatively siliceous, they are at the compositional limit (low Ca:Si ratio) at which CEMCHEM1 is appropriate. This has the advantage that the complexities of zeolite formation are avoided; fly ash hydrate assemblages often take many years to evolve fully.

Table 3.1 shows the relative oxide compositions of the unhydrated materials and table 3.2 shows the relative proportions of cement mineral hydrates which may reasonably expected to form on complete hydration of the cements at 25°C.

Relative mass of oxides	CKD	ROSA	SSD
CaO	58.26	3.70	3.70
MgO	2.30	1.24	1.24
SiO_2	14.13	60.00	60.00
Al_2O_3	4.19	23.00	23.0
SO_3	9.56	0.85	0.85
Na_2O	1.48		0.37
K_2O	4.70		1.30
Fe_2O_3	3.30		5.60
TiO_2			1.20

Table 3.1 *Relative oxide composition by mass of starting materials*

For the purposes of modelling this material, we must make certain assumptions about the partitioning of elements between the solid phases. Considering first, the cement kiln dust, analysis shows that the loss on ignition is around 21% of the dry mass. Assuming that this loss can be attributed exclusively to decomposition of calcite into free lime and carbon dioxide, it is possible to estimate the calcite content of the solid from the relative atomic masses:

CaCO3	→	CaO	+	CO2 (g)	
100.089	→	56.079	+	44.010	Formula mass
100	→	55.584	+	44.416	Mass fraction

This suggests that the CKD is 47.7 % calcite. Of the initial 58.26% CaO in the material, 27.8% remains to be partitioned between anhydryte and the cement clinker. It is further assumed that all the sulphur (9.56%) reported as SO_3, will be present only as the mineral anhydrite. Similarly:

CaSO4	→	CaO	+	SO_3	
136.18	→	56.079	+	80.058	Formula mass
100	→	41.19	+	58.81	Mass fraction

This suggests that 5.62% of the remaining calcium is present as anhydrite, leaving a mass fraction of 22.18% CaO incorporated in the cement clinker minerals. The remaining oxides may be normalised to 100% and used in a conventional CEMCHEM calculation.

On mixing, it is assumed that the anhydrite will spontaneously re-hydrate to form gypsum, so a corresponding quantity of gypsum must be added to the hydrate assemblage:

$CaSO_4$	+	$2H_2O$	→	$CaSO_4.2H_2O$
Anhydrite	+	Water	→	Gypsum
136.138	+	18.015	→	154.153= 13.2% mass increase on hydration

The remaining oxides suggest the following mineral hydrate assemblage shown in table 3.2.

Phase	Mole fraction	Mass fraction	Molar ratio
CSH (C:S = 1.7)	41.01	45.94	18.84
Portlandite	52.22		23.99
C_3AH_6	2.81		1.29
M_4AH_{10}	1.84		0.85
AF_t	2.12		0.97
Gypsum		6.36	21.28
Calcite		54.06	32.78

Table 3.2 *Hydrate assemblage predicted for the CKD component*

Naturally, the high solubility of gypsum, with respect to ettringite, means that this assemblage will simplify during hydration and as the addition of fly ash lowers the total Ca:Si ratio, a correspondingly lower quantity of free portlandite would be expected to form.

The second assumption to consider, is the composition of the pore solution of this assemblage. Although it will be calculated by equilibrium of the solids with their mix water, we must account for the alkali metals present in the CKD. By mass, sodium represents 1.48% whilst potassium comprises 4.70%. It is reasonable to assume that these ions will be rapidly partitioned into the aqueous phase.

The third assumptions concern the steel slag. To a first approximation, its reactivity is low, except for the free lime content. As the slag comprises 0.9% by mass free CaO and the material is finely ground, it is reasonable to assume that, it will immediately hydrate on contact with water. Let us assume that the 0.9% CaO by mass, corresponds to 1.19% $Ca(OH)_2$ and that the remaining components in the slag remain insoluble.

The final assumptions to consider, before establishing the hydrate assemblage present in the concrete are the ash compositions. It should be recognised that this normative approach has an obvious limitation in simulating these systems, in that it invokes a model of complete hydration. Over the first few of service, complete hydration is unlikely to be approached in the case of fly ashes. Moreover, some components of the ash (i.e. mullite) are unreactive to cement pore solutions. Nonetheless, we must consider the ash hydrates in the same way as

those of the other blending components, in order to establish a long-term assemblage of mineral hydrates. The consequence of this is that relatively high confidence may be assigned to predictions of the mineral hydrate assemblage, but a lower confidence should be associated with the absolute *quantities* of materials predicted. This introduces an uncertainty in proportion to the quantity of ash in the blend.

As it is unrealistic to consider ash hydration in isolation, its hydrate composition is determined during the final CEMCHEM calculation. The complete process is one of estimating the relative oxide compositions of the proposed mixture, from which the ash hydrates may be predicted:

Material	**Volume fraction** $Kg.m^{-3}$	**Mass fraction** **%**
Cement Kiln Dust	150	8.8
Steel slag dust	700	41.2
Conditioned fly ash	150	8.8
Shell sand	700	41.2

Table 3.3 *Components used in the concete mix proposed for use at the Poplars site*

Of these components, the shell sand is considered inert and of the steel slag, only 1.19% (mass of calcium hydroxide) is reactive. The hydraulic binder therefore comprises 18.09 % by mass of the solid components in the concrete.

This binder assemblage is appropriate for use in several of the mix formulations considered here. That proposed for use at the Poplars site, the top layers of the site trial cells 2 & 3 and the bottom layer of cell 3.

From this stage we can readily calculate the volume fraction which will accommodate the 9 to 11% porosity (as appropriate) to accommodate the pore solution. Reversing the sequence of

calculations and by simple scaling, it is possible to calculate the number of moles of each solid, which will be equilibrated with one litre (strictly dm^3) of pore solution. This is done as the equilibrium code PHREEQC makes all calculations with respect to a fixed volume of solution, reporting concentrations and amounts of reaction in terms of molal quantities.

Using a similar approach, a prediction of the phase assemblage likely to prevail in the mix used for the bottom layer of cell 3 in the site trial. The binder composition is more complex, containing OPC (5.2%) in addition to CKD (69.8%) and fly ash (25%). This gives a more siliceous mixture, resulting in the following predicted phase assemblage:

	Oxide	**Cell 3, top of cell 2 & Poplars**	**Bottom of cell 2**
		Oxide mass fraction	
	CaO	58.66	39.39
	MgO	3.01	9.37
	SiO2	23.49	35.56
	Al2O3	6.4	13.08
	SO3	2.37	0.15
Hydrate	**Formula**	**Number of moles fraction in contact with 1dm-3 of solution**	
Hydrotalcite	4MgO.Al2O3.10H2O	1.67	7.54
CSH 1.7	Ca 0.8 SiO5 H4.4	34.79	
CSH 1.07			67.41
Ettringite	3CaO.Al2O3.3CaSO4.32H2O	0.88	0.084
Hydrogarnet	3CaO.Al2O3.6H2O	3.02	
Gehlenite hydrate	3CaO.Al2O3.SiO2.8H2O		
Portlandite	Ca(OH)2	19.63	1.78
Calcite	CaCO3	13.95	13.95
Gypsum	CaSO4.2H2O	2.13	2.13

Table 3.4 *Phase assemblages used in the equilibrium models*

3.3.2 Equilibrium modelling using PHREEQC-I

At this stage it is possible to perform the first equilibrium calculations in the concrete barrier. The initial solution contains only sodium and potassium from the CKD, which buffer the solution to pH 12.766, as {Na} = 2.323e-2M and {K} = 4.854e-2M.

Equilibrating the cement hydrate assemblage with this alkaline solution establishes a realistic pore solution used in subsequent calculations. Phreeqc-I invokes and ion pairing model in which the free energy of the system is iteratively minimised to simulate chemical equilibrium. Mass is partitioned between the aqueous species and solid phases described in an external database. Following a reaction, the saturation state of the solution with respect to listed solid phases is reported and the user must choose which, if any of those solids, to bring to simulated equilibrium in subsequent calculations. In this way, a realistic chemical evolution of the system is built up, allowing some phases to remain at disequilibrium, should, for example, the user believe them to be kinetically unflavoured.

Solid Phase mineral hydrate assemblage		
Phase	**Phase quantity / moles**	
	Initial	Final
Calcite	1.40E+01	1.40E+01
CSH(1.8)	3.48E+01	3.48E+01
Ettringite	8.80E-01	8.80E-01
Gypsum	2.13E+00	2.11E+00
M4AH10	1.67E+00	1.67E+00
Portlandite	1.94E+01	1.94E+01

Solution Composition	
Element	**Molality**
Al	1.34E-10
C	7.86E-06
Ca	3.05E-02
K	4.85E-02
Mg	2.94E-06
Na	2.32E-02
S	1.60E-02
Si	6.42E-06
pH	12.3

Table 3.5 *Equilibration of hydrates with group I metals in the pore solution for Cell2, top of cell 3 and Poplars mixes*

Solid Phase mineral hydrate assemblage				Solution Composition	
Phase	**Phase quantity / moles**			**Element**	**Molality**
	Initial	Final		Al	2.57E-04
C2ASH8	8.29E+00	7.58E+00		C	1.89E-05
Calcite	1.40E+01	1.40E+01		Ca	2.54E-03
CSH(1.1)	6.74E+01	6.81E+01		K	5.89E-02
Ettringite	8.40E-02	7.94E-01		Mg	2.11E-10
Gypsum	2.13E+00			Na	2.82E-02
M4AH10	7.54E+00	7.54E+00		S	2.30E-05
Portlandite	1.93e+01	1.93e+001		Si	2.89E-05
				pH	12.859

Table 3.6 *Equilibration of hydrates with group I metals in the pore solution for bottom layer mix, cell 3*

Note that the gypsum in the latter assemblage has completely dissolved to re-precipitate as ettringite. In doing so, some gehlenite hydrate has also dissolved, its calcium going to form ettringite, whilst the other elements are incorporated in the CSH.

Having established both the solid and liquid phase chemistries for the binders of greatest importance in this work, attention can now be turned to reactive modelling of their evolution. First to be simulated are the earliest reactions of the barrier materials with the young, acetogenic leachates. Initial reaction between the cements and solution, results in a rapid reaction to establish both the most stable phase assemblage and equilibrium pore solution. Experiments show (section 4.4) that after some months, the rate of diffusive transport is slow and experience from landfill operators confirms that the acetogenic stage is relatively short lived; a small number of years. Considering the most extremely reactive case, that mass transfer is maintained at 10mm per year, around 50mm of our barrier may be degraded by reaction with the leachate. In order to assess the impact of this, attention must be given to reactions of the mineral hydrates with the leachate.

Using the synthetic leachate described previously, the cement minerals are equilibrated with the leachate shown in table 4.1. The initial exchange of pore solutions results in dissolution of calcium from the CSH, leaving a more siliceous solid remaining. At the same time, dissolution of portlandite neutralises the acid in solution, buffering the system to pH 12.3 whilst the minor phases, ettringite and the AFm phases precipitate. Gypsum and hydrogarnet dissolve completely and a new hydrate assemblage is established as shown in table 3.7.

	Moles of solid		
	Initial	**1 volume**	**2 volumes**
Ca-Monochloroaluminate		2.75E-02	5.41E-02
Ca-Monocarboaluminate		4.29E+00	4.26E+00
M4AH10	1.67E+00	1.67E+00	1.67E+00
Gypsum	2.11E+00		
C3AH6	5.03E+00		
Ettringite	8.80E+00	9.51E+00	9.52E+00
Calcite	1.40E+01	9.65E+00	9.68E+00
Portlandite	1.94E+01	4.37E+01	4.37E+01
CSH(1.1)		3.48E+01	3.48E+01
CSH(1.8)	3.48E+01		

Table 3.7 *Molar quantities of hydrates following reaction with acetogenic leachate. Binder type is CKD-PFA as used in cells 2 & 3 and proposed for Poplars site*

Extending this simulation for many pore solution exchanges demonstrates that CSH, calcite and especially portlandite contribute almost all the acid neutralisation capacity in these materials and that a pH in excess of 12 will be maintained for many years. Repeated batch calculations show that 1090 pore solution exchanges will be required before the alkaline reserve in this top layer concrete will be exhausted. Assuming it takes 16 years to exchange one sample volume of pore solution for a material of permeability 1E-9 m/s. It would seem reasonable to state that the acetogenic phase of leachate evolution will be long passed. It would also seem reasonable to speculate that as both the hydration reaction (consumption of

gypsum) and reactions with sulphate in the leachate produce ettringite in the surface layer, that the reaction is self-limiting. As ettringite has a high molar volume, it will close porosity in the reaction zone due, reducing the rate of leachate ingress.

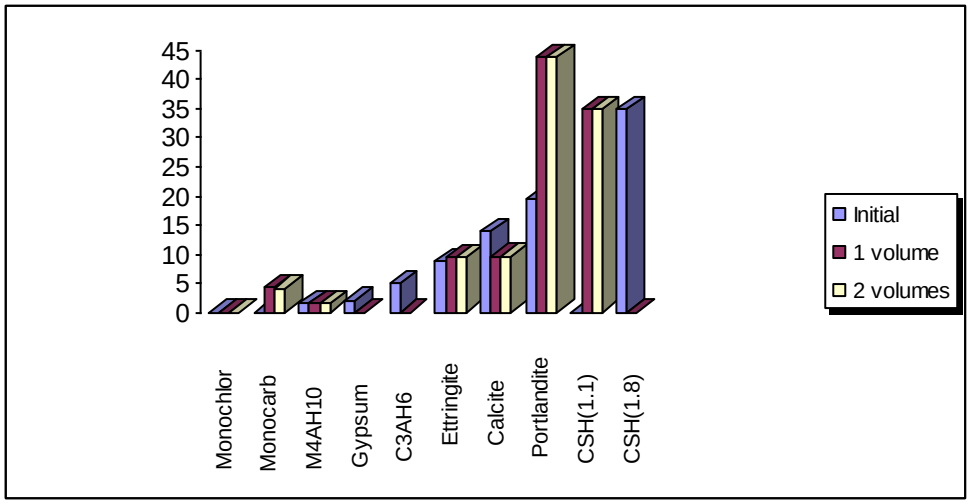

Figure 3.1 *Molar quantities of hydrates following reaction with acetogenic leachate. Binder type is CKD-PFA as used in cells 2 & 3 and proposed for Poplars site*

Applying the same approach to the binder material used in the bottom layer of cell 2, a similar prediction of longevity is made:

	Moles of solid	
	1 volume	**2 volumes**
Ca-Monocarboaluminate	3.55E+00	3.52E+00
Ca-Monochloroaluminate	5.46E-02	8.12E-02
Ettringite	8.01E-01	8.08E-01
Portlandite	1.74E+00	1.70E+00
M4AH10	7.54E+00	7.54E+00
Calcite	1.47E+01	1.47E+01
CSH(1.1)	6.74E+01	6.74E+01

Table 3.8 *Molar quantities of hydrates following reaction with acetogenic leachate. Binder type is CKD-PFA as used the bottom layer of cell 2*

The binder shown above contains much less portlandite than the previous mix, yet it will still take over 100 exchanges of pore solution to exhaust this phase.

3.3.3 Reactive Transport

PhreeqC simulates both advective and diffusive flow by using a compartmental model in which the solutions contained in each are sequentially moved along the column, after reaction with the solid phases they contain. Certain assumptions are made in the implementation of this model, for example, ions must diffuse at a common rate, boundary conditions are fixed (in type and flux) for the duration of the simulation and high ionic strengths (> 0.5M) may result in misleading results as the theoretical basis of the activity correction model are exceeded. Nonetheless, the code offers a route by which acid-base, redox, ion exchange, surface complexation and solid solution models may be simulated in the same system. The transport algorithm allow simulation of diffusive, and / or advective flow, effectively coupling the chemistry model to one of saturated flow.

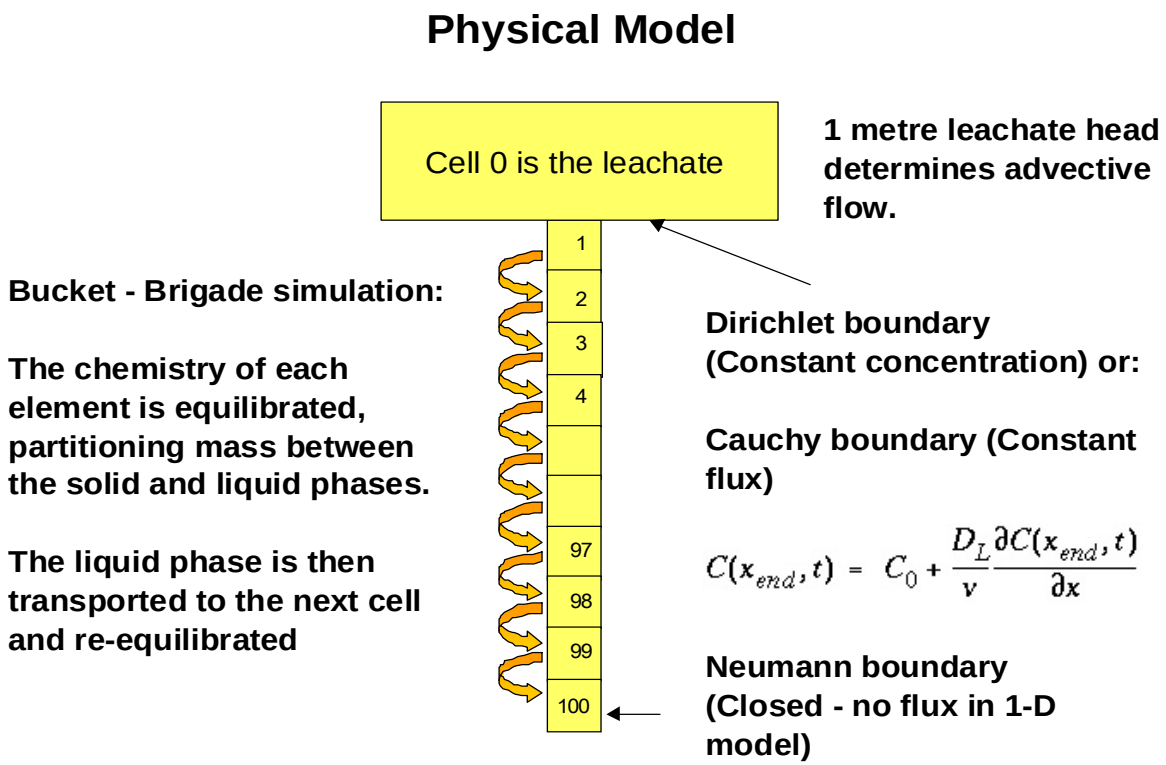

Figure 3.2 *Schematic diagram of the "bucket brigade" compartmental model invoked in PHREEQC in which looose coupling between chemistry and transport allows reactive transport calculations to be undertaken.*

As a comparison with the calculations presented using the conservative transport model developed at Coventry, the mass transfer through the top layer concretes at the site trials have been simulated. In these calculations, the mineral hydrates and pore solutions shown in table 3.5 occupy each cell and leachate is eluted through the column under a head of one metre. Diffusion is allowed to operate in addition to advection and selected heavy metals were considered in the simulations.

The comparison involves eluting the leachate measured for Cell 2 of the site trial through the upper layer concrete and into the clay layer. As transport is very slow and there are no useful data with which to make a comparison, the lower concrete was disregarded for this simulation. The average concentration measured on site over two years show that for the major elements, temporal changes in concentration are slight, being within the analytical variations of the measurements. Similarly, the measured solution concentrations in the liquid collected from the base of this layer (on top of the clay) are reported in table 3.9.

All quantities are molal	Leachate (Analytical)	Interface pore solution (Analytical)	Model predictions of interface pore solution	
			After equilibration with cements	After equilibration with heavy metal salts
pH	7.7	13.24	12.464	12.464
K	1.36E-01	3.49E-01	3.49E-01	3.49E-01
Na	1.02E-01	6.59E-02	6.59E-02	6.59E-02
Cl	Assumed 0.1M		1.45E-02	1.45E-02
Ca	1.05E-02	3.57E-04	1.44E-02	1.44E-02
S	1.39E-02	Assumed 1 mM	2.68E-05	2.68E-05
Mg	6.41E-03	1.67E-05	4.44E-09	4.44E-09
Ni	3.19E-05	2.22E-05	3.19E-05	6.27E-08
Sr	2.00E-05	4.06E-06	1.96E-05	1.96E-05
As	1.96E-05	2.48E-05	1.92E-05	1.92E-05
Si	Not determined	Not determined	1.64E-05	1.64E-05
Al	Not determined	Not determined	1.24E-05	1.24E-05
Zn	1.91E-05	2.46E-05	1.87E-05	1.21E-05
Pb	1.20E-05	5.59E-04	1.18E-05	1.18E-05
C	Not determined	Not determined	9.45E-06	9.45E-06
Cr	1.56E-06	2.28E-07	1.53E-06	1.53E-06
Cu	3.15E-06	2.75E-06	3.09E-06	4.60E-07

Table 3.9 *Starting solution compositions used in coupled chemical transport simulation of Risley cell2*

The leachate and pore solutions from the site were routinely analysed by ICP spectroscopy for their metal content, but this does not determine the major anions (carbonate, chloride, ammonium or sulphate) nor does it account for organic species. To restore electrical charge balance in the solution, it was re-equilibrated with the cement hydrate assemblage from table 3.5, as shown in the third column. The metals determined in the cement pore solutions were

included in the calculations but where the solution was over saturated with a solubility limiting phase (Ni, Zn, Cu) these were allowed to control the quantities present in solution.

Allowing reactive transport to move leachate through the top layer concrete both by diffusion and advection, we see that the major aqueous species behave largely conservatively, albeit with minor reaction between the solid phases with calcium and sulphate ions. The heavy metals under the control of a solubility limiting phase precipitate in the upper region of the concrete and remain strongly bound there, whilst the others behave conservatively.

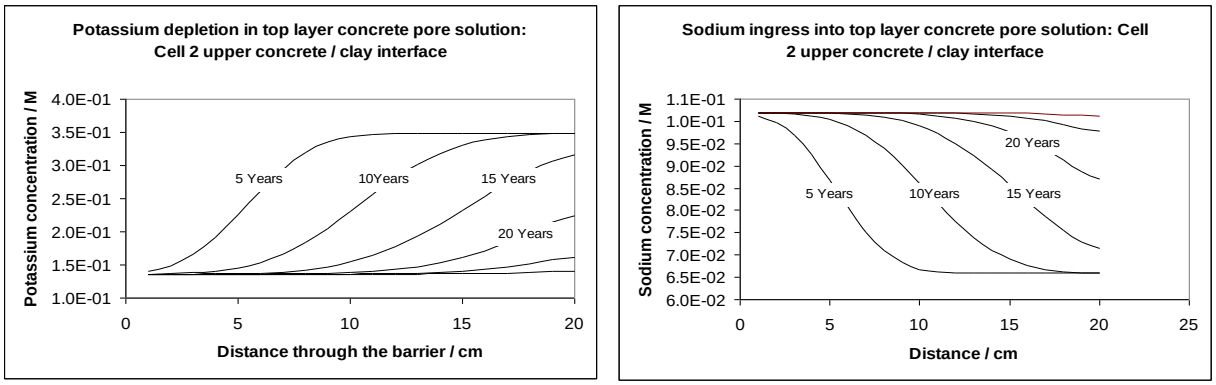

Figure 3.3 *Predicted elution of major ions through the top layer concrete as a function of distance*

Calcium concentrations are predicted to be constant for at least 200 years, as the alkaline reserve (portlandite, CSH and to a lesser extent calcite) remain in excess. No significant change in mineral assemblage is predicted over this time scale.

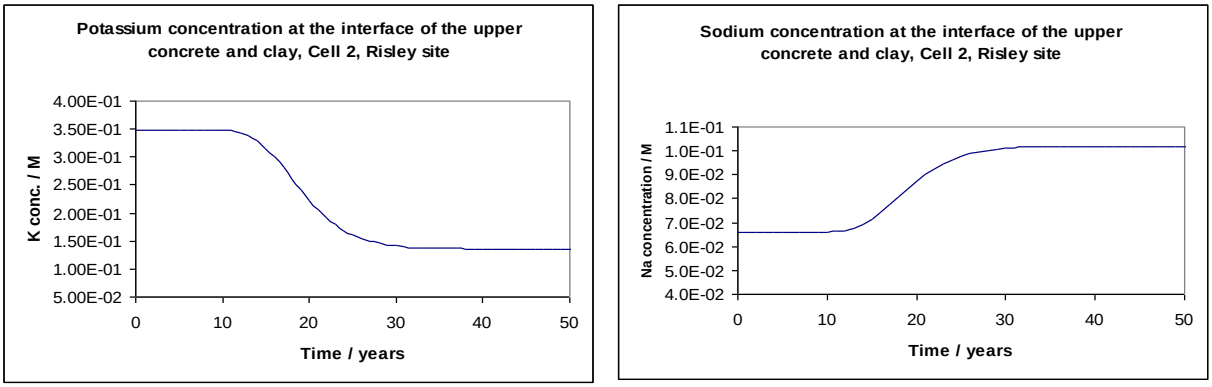

Figure 3.4 *Predicted elution of major ions through the top layer concrete as a function of time*

Comparing the figures above with figures 5.15 and 5.16, there is obvious agreement between both approaches and the experimental data. The leachate is somewhat higher in sodium than the binder pore solution, whilst for potassium, the reverse is true.

Considering next, the precipitation of metal ions by the binder, it is predicted that there will be solubility limiting phases for some elements as shown:

Nickel	Nickel Hydroxide	$Ni(OH)_2$
Copper	Tenorite	CuO
Zinc	Zincite	ZnO

Note that both nickel and zinc have less soluble silicates than the phases shown above, which are predicted to be massively oversaturated in the solution. However, owing to the slow kinetics of their formation at low temperatures, these have discounted. The solubility limiting phases give rise to very low concentrations of the metals (see table 3.9) in solution and it is predicted that they will precipitate in the surface layers of the upper concrete:

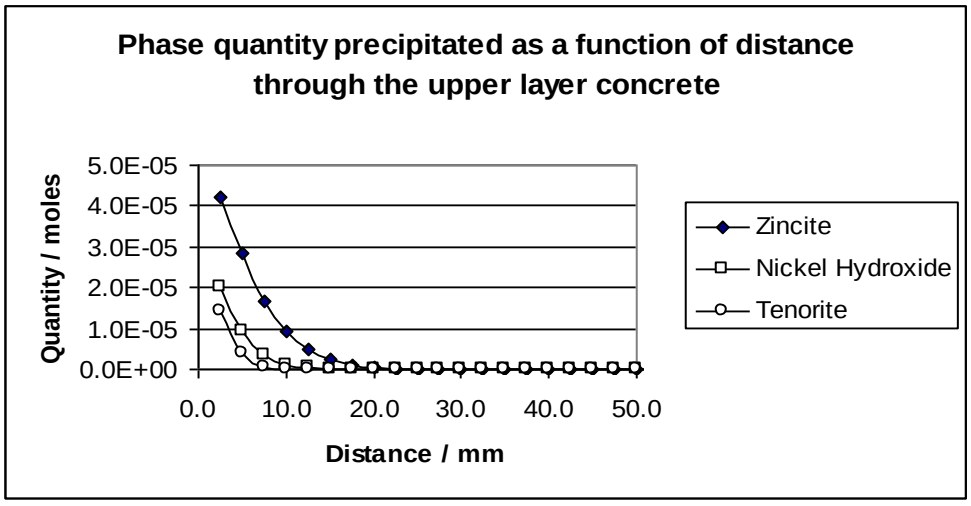

Figure 3.5 *Predicted elution of major ions through the top layer concrete as a function of time*

In conclusion, the experimental results of the site trials can be simulated using both conservative and reactive chemical transport modelling.

3.3 Landsim II

The concepts and use of probabilistic risk assessment models is addressed extensively elsewhere and discussed in some detail in the Landsim-2 manual (EA, R&D Publication 120, 2001). This modelling tool has become the *de facto* standard for landfill performance assessment in this country and its recent revision, commissioned from its authors, Golder Associates Ltd, has increased both its capabilities and user base.

The code contains a description of the source term, which can be made to evolve with time (according to a half-life) and modules of the simulator are available to describe infiltration, cell geometry and local or regional groundwater flow. In operation, simple chemistry is described in terms of sorption and dilution, which are coupled to a three-dimensional transport code. Practically, many calculations are performed in a run (typically over 1000) during which input parameters are sampled using a Monte Carlo method. Such parameters, for example concentrations in the source term inventory or barrier thickness, are assigned a range of likely values which are sampled stochastically. On completion, a risk assessment module combines these results and estimates the probability of an event (such as a concentration / distance combination) occurring and presents the results as shown below:

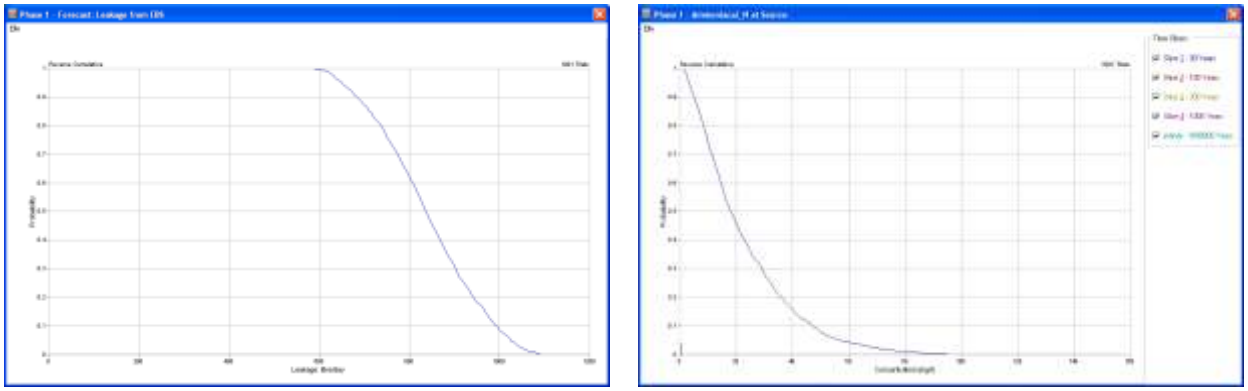

Figure 3.6 *Typical probability predictions of (left) leakage through the barrier and (right) ammoniacal nitrogen concentrations generated for the Poplars site using Landsim.*

One of the most sophisticated modules available is that describing the engineered barrier system. The user is required to select one of several pre-defined geometries which, by and large, describe most of the landfill cell constructions in the UK. At the time that the code was commissioned by the Environment Agency, there was no anticipation of novel sacrificial

barriers being adopted. Consequently, use of Landsim to model the barrier types described here presents considerable problems.

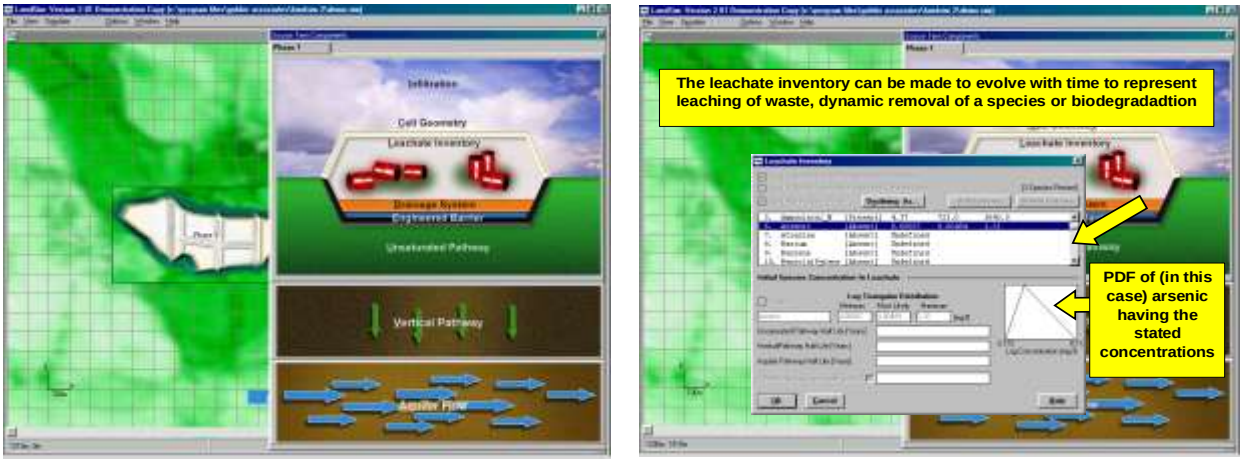

Figure 3.7 *Typical probability predictions of (left) leakage through the barrier and (right) ammoniacal nitrogen concentrations generated for the Poplars site using Landsim.*

As no formal clay chemistry is simulated by Landsim, use of the simple, single clay liner would seem a pragmatic choice as its physical properties (strictly the hydraulic conductivity) can be adapted to represent those of the cementitious barrier. At this point, a conceptual model with which to describe our system remains elusive. If default concentrations are chosen in the inventory module, mass is distributed around the site as in a conventional calculation. If however, the inventory is set with the extremely low concentrations of transition metals which are known to prevail in the cement environment, no release of these elements are simulated at all.

It remains unclear how an assessment of such technology could be made numerically. Uncertainties in material properties, consistencies and availability preclude the detailed deterministic modelling described here, at least as a routine assessment. As conceptual models become more sophisticated, the uncertainties associated with the interrelationships between their component parts becomes great. Moreover, sophisticated calculations often lead to impracticably long run times, numerical instability or more predicted information, than is desirable. In conclusion, Landsim-2 offers a reasonable compromise between flexibility and complexity, but its limitations to conventional liner designs preclude its use in this case.

4 LABORATORY TESTS

4.1 High pressure tests

4.1.1 Experimental Programme

This test is a major component of the laboratory programme for evaluation of the cementitious liners. The broad objectives of these experiments are to investigate the evolution of bulk permeability, the chemical evolution of the eluting leachate and the micro structural evolution of the materials.

The specific objectives are to measure the following:

1. The permeability of the samples to water.
2. The change in permeability in the presence of leachate.
3. The adsorption of ions from the leachate by measuring eluent chemistry.
4. The relationship between numbers of sample volumes passing and changes in permeability.
5. The effect of different residence times in the sample by running the test at different pressures and/or sample thicknesses. This determines whether the leachate achieves chemical equilibrium with the barrier. It also checks the sensitivity of the observed permeability to changes in pressure.
6. The effect of cracking by casting some samples with glass fibre in them which can be pre-cracked on the compression machine before testing
7. The performance of multi-layer systems by testing them in the cells
8. The ability of the clay to seal cracks by testing multi-layer samples with cracked concrete.
9. The effect of sample size and boundary effects by testing samples in the 100mm cell.

The principal experimental technique employs a confined leach cell (1) a modification of the Hoek cell, in which a solution is eluted through a column of barrier material under a pressure gradient. To maintain the structural integrity of the sample, and prevent flow past its sides, a confining pressure is applied (as in a triaxial cell) around an impermeable sleeve surrounding the sample. By maintaining the pore solution pressure below that of the confining pressure, the internal structure of the barrier material is maintained. In addition to providing a reaction

vessel, the cell is used as a constant head permeameter, allowing dynamic measurement of permeability changes over the duration of each experiment.

Both deionised water and a synthetic (acetogenic) leachate have been eluted through the materials to examine their effects on permeability evolution and buffering capacity of the mixes.

The composition of the synthetic leachate used in this work was obtained by comparing the composition of various natural and synthetic leachates and is given in table 4.1. This solution was chosen as it represents a leachate from the early (acetogenic) phase of a landfill and is therefore the most aggressive solution to which a cementitious barrier would be likely to be exposed. The evolution of leachate chemistry during the service life of a landfill, normally shows a decrease both in acidity and ionic strength as the landfill matures, so experiments using this solution are thought to be conservative.

2.043g	Concentrated Sulphuric acid
4.48g	Acetic acid
1.897g	Potassium chloride
7.755g	Calcium acetate
1.186g	Ammonium chloride
0.91g	Sodium chloride
2.588g	Sodium hydroxide

Table 4.1 *Composition of synthetic leachate, per litre of solution(pH=5.1)*

The permeability testes for the specific objectives listed previous page were carried out on duplicated samples of candidate trial site mixes given in table 2.4 and / or the purposed designed mixes given in table 2.6. In addition to these tests all the initial mixes considered in the study were tested in duplicate. These mixes were designed with consideration for requirements for strength, permeability, through pH and cost benefit analysis. The result shows the wide variation in strength, through pH and permeability and it can be seen that there are a large number of mixes that satisfy the strength, permeability, through pH and cost criteria.

Two samples from each mix design were tested with leachate and two more were tested with water to give a programme of over 200 permeability tests.

4.1.2 Description of apparatus

The permeabilities of the specimens were determined using a continuous high-pressure flow experiment in which solution is eluted through the materials at pressures up to 10 MPa depending on the compressive strength of the particular specimen. See figures 4.1 and 4.2. The apparatus is adapted to measure both the flow and pressure drop across the sample. Measurements were made after one sample volume of liquid had passed through the concrete or mortar specimens. Assuming an average permeability of 10^{-9} and a maximum leachate head of 1m above the liner, this corresponds to 16 years of exposure in service. Tests were carried out with deionised water and a synthetic (acetogenic) leachate to examine their effects on permeability evolution and buffering capacity of the concrete.

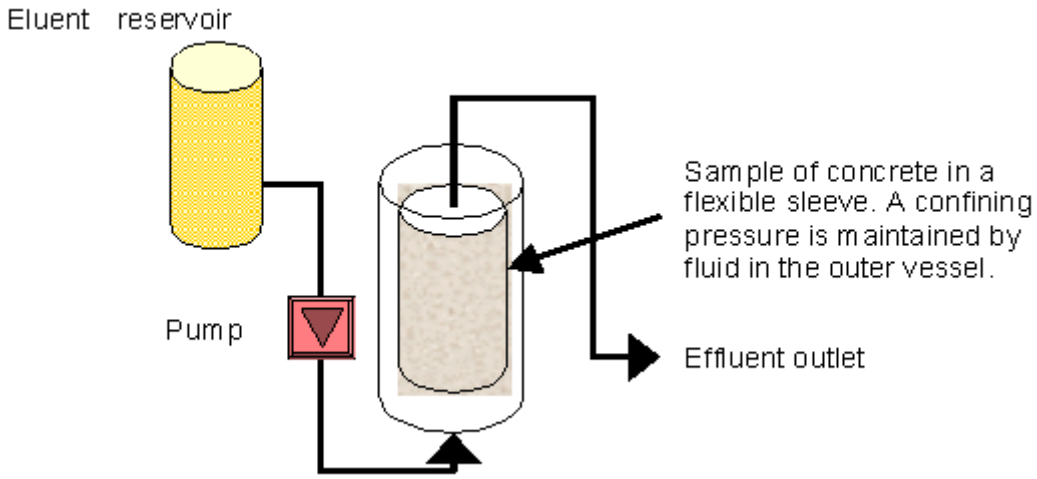

Figure 4.1: *Schematic view of high-pressure permeability apparatus.*

Figure 4.2: *High-pressure apparatus at Coventry, showing two small cells (for 54 mm diameter samples) and one big cell (for 100 mm diameter samples) together with liquid pump and pressure gauge.*

4.1.3. Sensitivity to sample size and pressure

Three different mortar mixes were tested as a validation check of the High pressure tests by eluting synthetic leachate and deionised water. The designs of these mortar mixes are given in Table 2.6. Two of these mixes were cement mortar mixes with different strength and permeability coefficients and one other mix was one of the several trial cell mixes used for site trials (i.e. top layer mix of the trial cell 2 at Risley). A low strength of about 5 MPa was deliberately engineered to find the effect of applied pore pressure and number of sample volumes eluted on the coefficient of permeability.

The effect of eluted volume on the coefficient of permeability at different pore solution pressures is shown in figures 4.3 to 4.5. For low strength materials such as materials being used in the novel liner mixes, increased eluted sample volumes slightly decrease the coefficient of permeability but this is contrary to higher strength materials in which the permeability increases. This could be because high strength materials are rigid whereas low strength materials are compliant and weak bonding fine particles cause blockage of the pore routes in these types of materials.

The effect of specimen size on the coefficient of permeability at different pore solution pressures is shown in figures 4.6 to 4.8. Increasing the specimen size slightly increases the coefficient of permeability in lower strength mixes and decreases the coefficient in higher strength mixes. From the figures it can also be seen that the permeability coefficient does not change significantly with pressure.

Fig. 4.3: Permeability Vs. eluted sample volume for 5 MPa. Top layer cell2 (i.e. CKD, LA, ferrosilicate) mix.

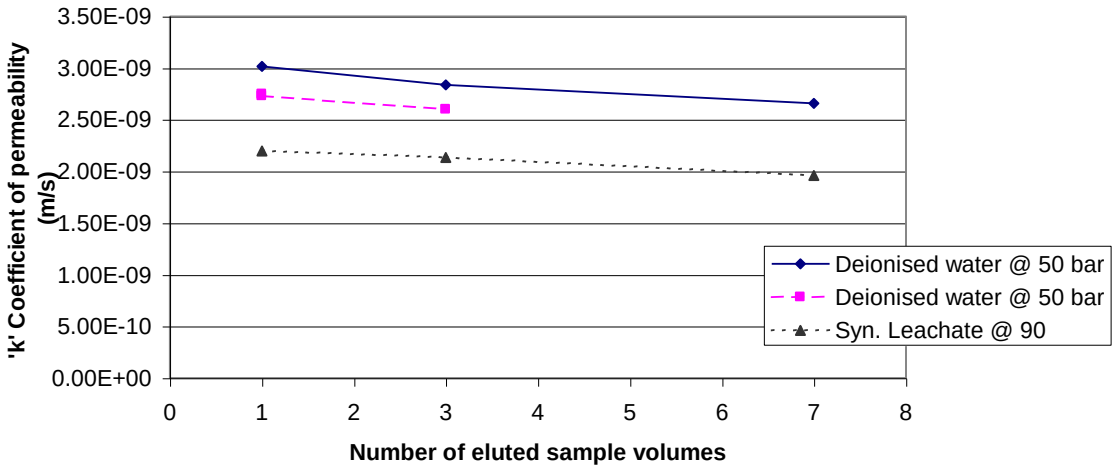

Fig. 4.4: Permeability Vs. eluted sample volume for 15 MPa. cement mortar mix.

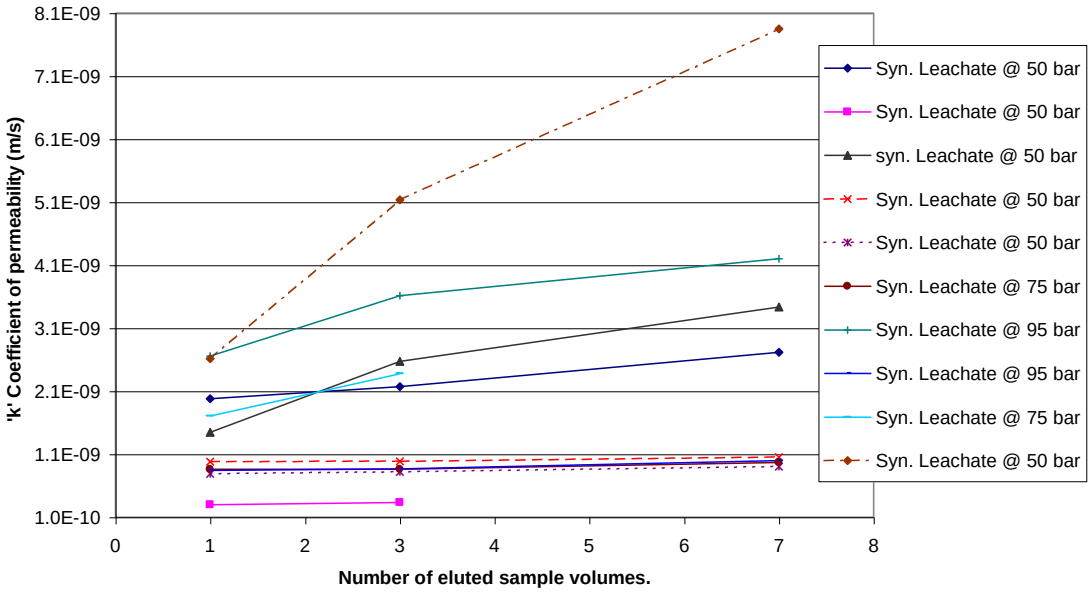

Fig. 4.5: Permeability Vs. eluted sample volume for 20 MPa. Cement mortar mix.

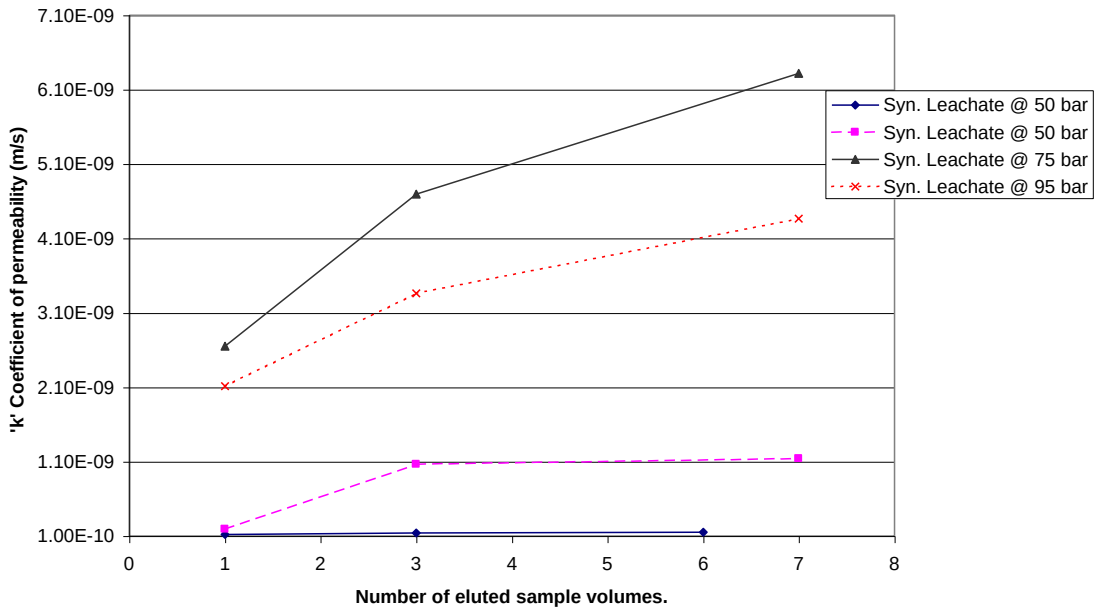

Fig. 4.6: Coefficient of permeability Vs. Sample size for 5 MPa. top layer cell 2 (i.e. CKD, LA, FerroSilicate) mix.

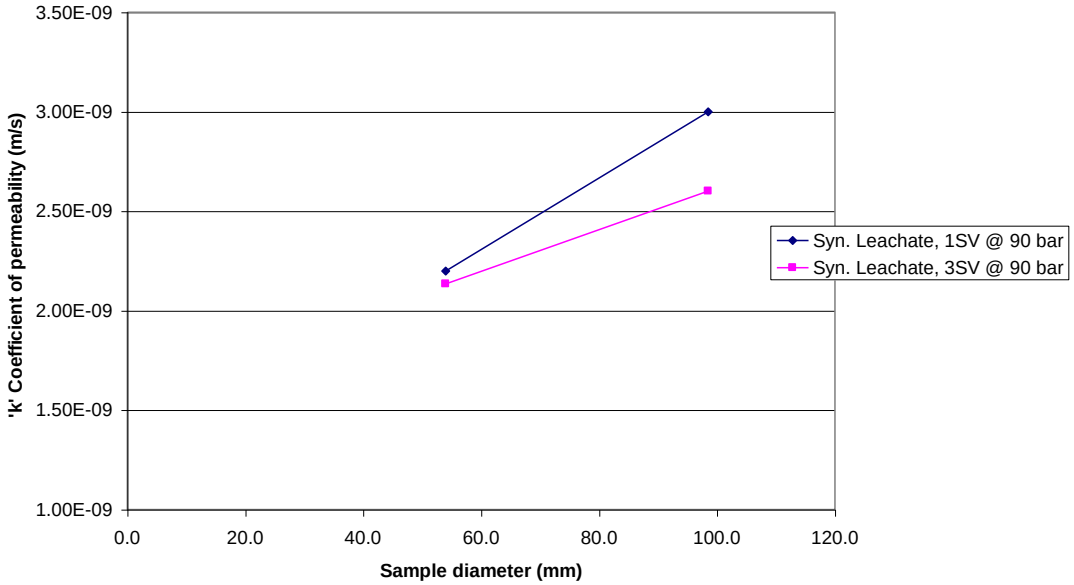

Fig. 4.7: Coefficient of permeability Vs. Sample size for 15 MPa cement mortar mix

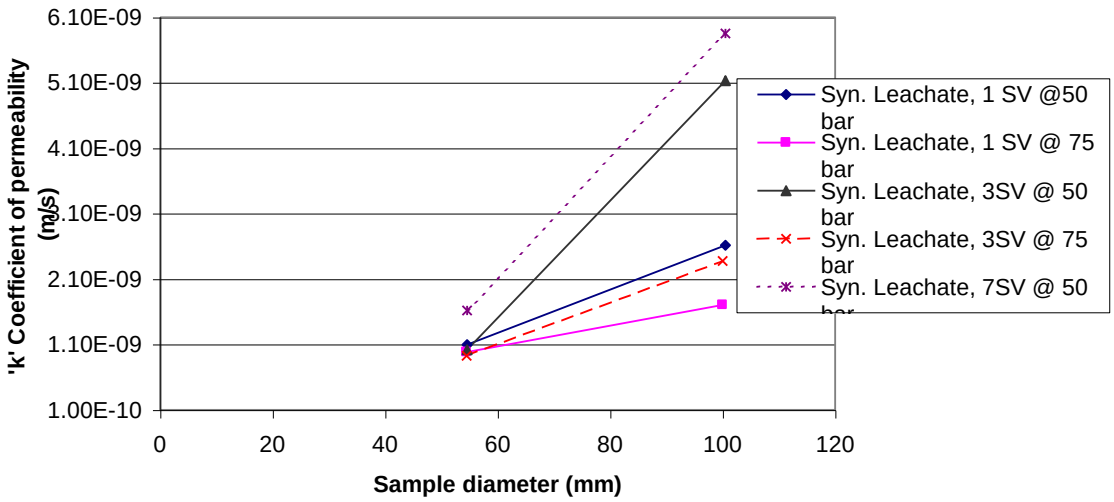

Fig. 4.8: Coefficient of permeability Vs. sample size for 20 MPa cement mortar mix.

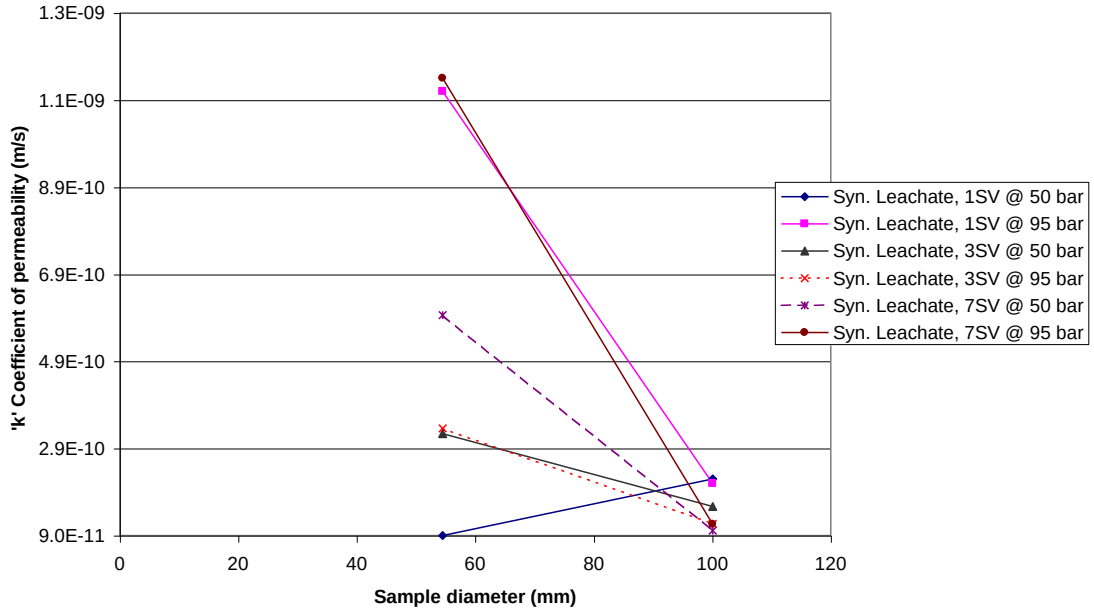

4.1.4 Cracked samples

Two sets of different tests were carried out to check the self-sealing property of the multi layer barriers. In the first set of test a 100 mm diameter Fibre Reinforced OPC mortar disc of 33.4 mm thick was cracked by applying small loads using a compression test machine. The cracks induced in the disc were clearly visible by naked eye and were measured between 0.5 mm and 1.2mm wide (see figure 4.9). By placing a 55 mm thick metal spacer ring packed with the Risley site clay on the top of the cracked disc, a two-layer test was next carried out on the high pressure cell apparatus using the synthetic leachate with Fluorescein dye. After running the high pressure cell for about an hour at 95 bar pressure liquid stated to leached out showing the fluorescein colour. When left for another 5 hours at 95 bar the leaching stopped and about 0.8 sample volumes of liquid were collected during this period. No more leaching was observed when the cell was continuously run at the same pressure for another 24 hours (see figure 4.10).

In the second set of test hair line cracks (about 0.2 mm wide) were induced in the mortar sample (similar to cell number 2 bottom layer mix) and the clay material (passing 5 mm sieve mesh) was packed inside the sample (see figure 4.11). A mortar disc (similar to the cell

number 2 top layer mix) was placed on top of clay and cracked sample (Fig. 4.12). The thicknesses of the three layers were proportional to the site trial cells. Running this multi layered sample at 100 bars for 3 days showed no leaching from it at all. After dismantling the multi-layered sample it was noticed that the top mortar was disintegrated under high-pressure leachate jet but no trace of leachate could be found in the bottom cracked mortar (see figures 4.13 and 4.14).

Fig. 4.9: Narrow cracks induced in the F.R. mortar disc.

Fig. 4.10: Cracked sample after clay has sealed the cracks.

Fig. 4.11: The set up of bottom layer mix and compacted clay with silicone rubber round the rim and inside wall to prevent ingress of leachate from rim and interfaces.

Fig. 4.12: Multi layer sample with partially compacted clay inside it.

Fig. 4.13: Multi layer sample after taken out of the test rig.

Fig. 4.14: Cut through the dismantled multi layer sample.

4.2. Diffusion tests

4.2.1 Experimental Programme

Initial scoping trials were carried out to indicate the diffusion coefficients for a range of materials. Subsequent to this a wide range of different mix designs were tested with synthetic pore solutions and leachates for up to six months. In the main programme one sample from each mix design from the top and bottom mixes used in Risley trial cells number 2 and 3 was tested. (Table 2.4).

4.2.2 Scoping trials.

Two sets of diffusion cell experiments have been conducted to examine the transport properties of these barrier materials. In one group, a synthetic cement pore solution was used, containing group I and group VII elements with ammonium as a counter ion to maintain constant ionic strength. It is assumed that as the electrolyte is chemically, closely matched to the solid phases in the matrix, dissolution is negligible.

Schematically, the diffusion cell is shown below:

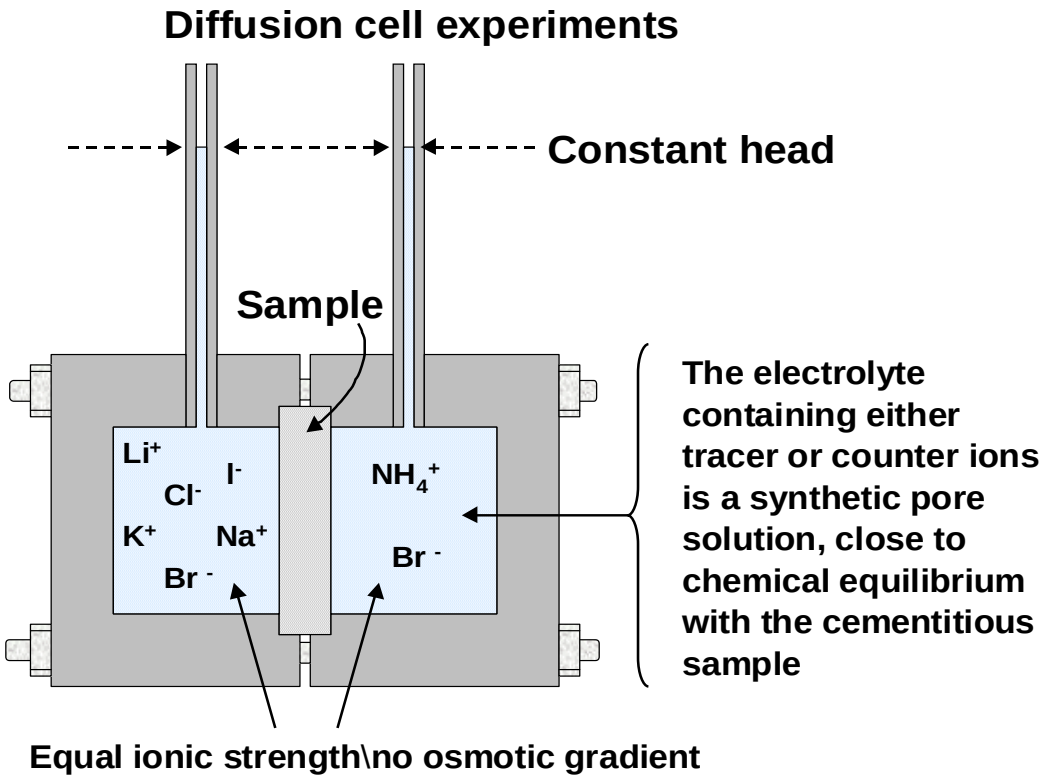

Figure 4.15 *Schematic section through diffusion cell*

By maintaining a constant average ionic strength on either side of the sample, osmotic transport of water is minimised, ensuring that diffusion is the dominant transport mechanism. For pseudo-steady state diffusion:

$$J = (V/A)*(dC_2/Dt) = (D/x)*(C_1-C_2)$$

Where:
- J = Flux
- V = Volume of low concentration side
- A = Cross sectional area
- C_1 = Concentration on high concentration side of sample
- C_2 = Concentration on low side

t = time

x = specimen thickness

D = Diffusion coefficient

To calculate the diffusion coefficient, a rectilinear plot of concentration versus time is drawn, the gradient of which yield the diffusion coefficient, such that:

$D = \text{gradient} * M_w * (1/A) * (V/1000) * (1/(C_1-C_2))$

Where: M_w is the molecular weight of the ion

and: The diffusion coefficient has units of $cm^2.s^{-1}$

For example, compare the "upstream" and "downstream" concentrations of chloride and bromide ions diffusing through a mortar similar to that used in the site trials described in chapter 4. The mix contains a ferrosilicate slag sand aggregate (65.9% by mass) and a binder comprising both cement kiln dust (20.5%) and lagoon ash (13.6%) at a water, binder ratio of 0.37. The diffusion experiment began on mortar cured at 25°C for 28 days at 100% relative humidity.

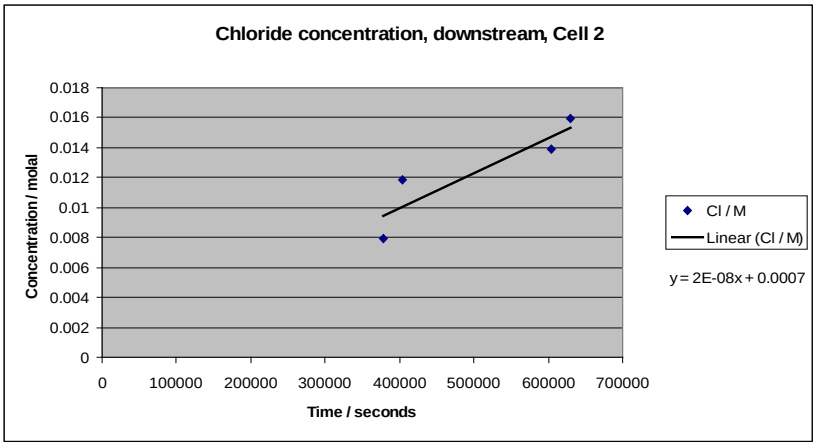

Figure 4.16 *Chloride ion concentration increase on "downstream" side of diffusion cell*

Similarly, for bromide ions:

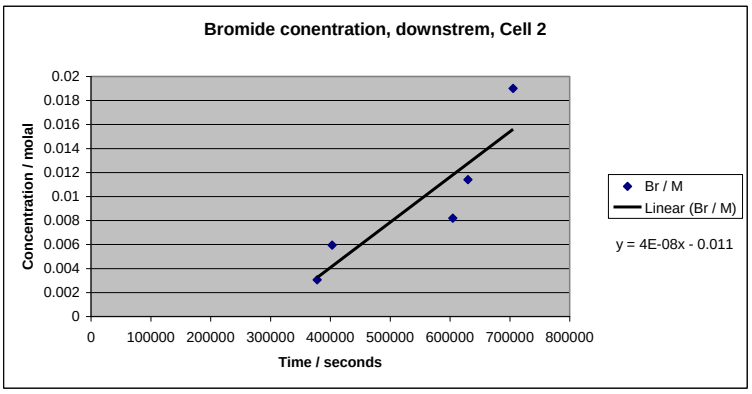

Figure 4.17 *Bromide concentration increase on "downstream" side of diffusion cell*

As ions diffuse across the sample, their concentration decreases on the "upstream" side of the cell:

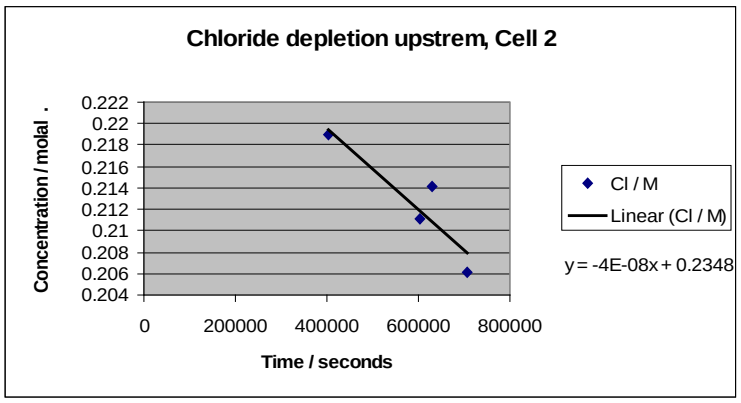

Figure 4.18 *Chloride concentration decrease on "upstream" side of diffusion cell*

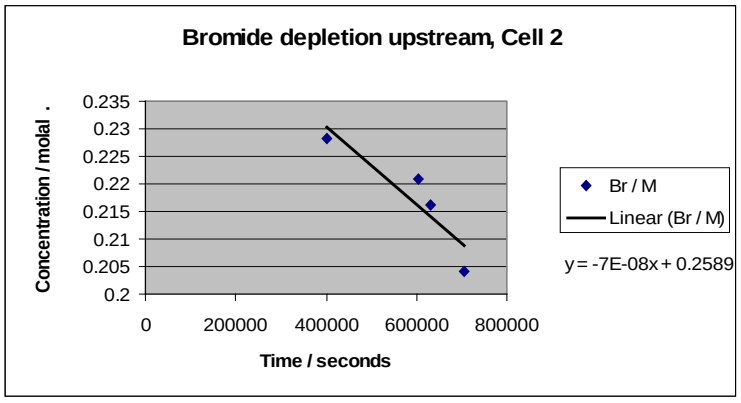

Figure 4.19 *Bromide ion concentration decrease on "upstream" side of diffusion cell*

It important to realise that this approach is only valid for the central, linear portion of the plot, as the initial break-through concentration is non-linear.

Using this method, estimates have been made for the diffusion coefficients of Li, Na, K, and Cl, Br, I ions along with arsenic as As(V), through a range of cementitious materials. The latter (arsenic) species is important, as it is not readily fixed by either cements or clays, owing to the relative stability of its uncharged arsenate complexes with potassium or (especially) sodium as shown in figure 2.9.

	Li	Na	K	Cl	Br	I	As	**Mean**
1	2.8E-10	1.3E-11	1.9E-11	2.1E-11	1.8E-11	7.2 e-11	6.6 e-11	**5.0E-11**
2	2.8E-10	1.1E-13	2.9E-13	6.6E-13	9.9E-14	4.5E-13	6.2E-14	**4.0E-11**
3	1.1E-12	4.3E-12	6.0E-13	6.7E-12	2.1 e-13	3.2 e-12	3.3E-13	**1.9E-12**
4	9.6E-13	1.2E-14	3.2E-13	4.3E-13	1.5E-14	2.3 e-12	1.0E-14	**2.5E-13**
Mean	**1.4E-10**	**4.4E-12**	**5.1E-12**	**7.2E-12**	**4.5E-12**	**1.1E-13**	**1.0E-13**	**3.2E-11**

Mix number	1	2	3	4
OPC (control)	100 %			5.2 %
CKD		60 %	60 %	69.8 %
PFA		40 %	40 %	25 %
Mix solution	Water	Water	Na_2SO_4 (aq) 11%	Water
Aggregate	Ferrosilicate slag sand	Ferrosilicate slag sand	Greensand & Cr-Alumina slag	Greensand & Cr-Alumina slag

Table 4.2 *Experimental determination of diffusion coefficients for mortars used in thin-disk diffusion experiments (above) and key to binder compositions and aggregate type (below)*

Although there is considerable scatter in these data, to a first approximation they are a useful guide to the likely contribution made by diffusion in the transport process. Considering the relative sizes of the ions, it is not a simple matter to relate hydrated ionic radius to the diffusion coefficient. As the ionic radius decreases, so to its charge density increases, such

that it attracts more water molecules in its hydration sheath. Estimation of the size of a hydrated ion is a function of ionic strength and in general, cat ions attract more water molecules than anions.

Taking the hydration numbers of the alkali and halide ions as follows $Li^+ = 4$, $Na^+ = 3$, $K^+ = Cl^- = 2$, $Br^- = 1$, $I^- = 0.7$, allows a plot of the relative scatter of the experimentally derived diffusion coefficients to be made with respect to hydrated ionic radius. Figure 4.21 illustrates the effect schematically.

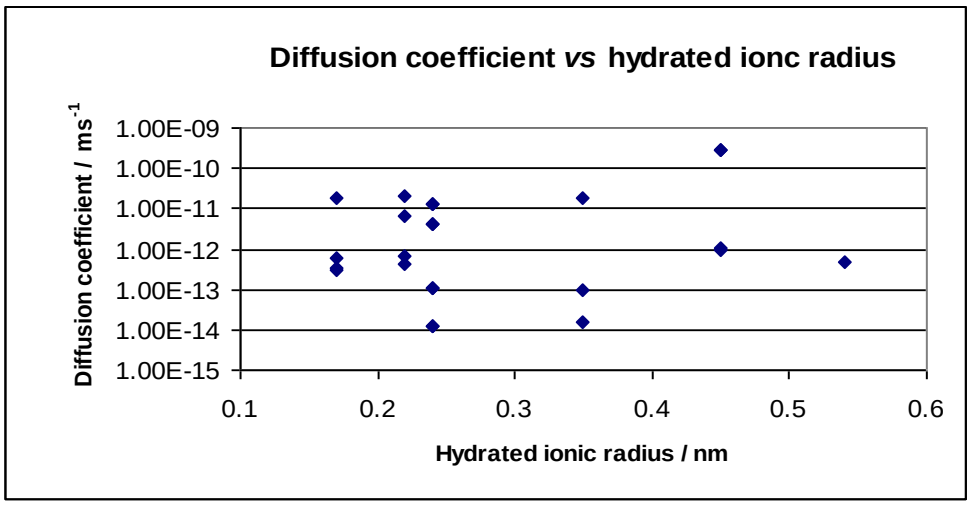

Figure 4.20 *Variation in diffusion coefficient as a function of hydrated ionic radius*

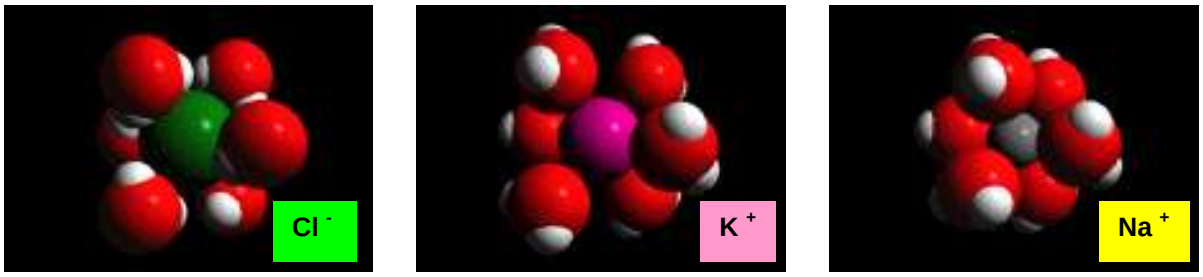

Figure 4.21 *Hydration sheath around ions used as conservative tracer elements in diffusion experiments*

4.2.3 Diffusion tests using simulated leachate.

Subsequent to these initial experiments, the diffusion cells were used to examine mass transport in reactive systems. An aggressive solution, simulating an acetogenic leachate typical of the early stages of landfill evolution (Table 4.1) was allowed to react with the sample, whilst concentration changes due both to diffusion and reactive transport were monitored in the cells.

This application of the diffusion test is intended to measure both the diffusion coefficient and capacity factor of those species partitioned between the solution and porous sample. The basis of the test is a divided cell with the sample in the centre. Artificial leachate is placed on one side and deionised water on the other; chemical analysis is used to track changes with time on each side.

The apparatus is a modified ASTM (C1202) test. The C1202 test has an applied electric field and in this work the same cells were used without the field but with extra reservoirs on the top. Using an electric field would have accelerated the tests but made interpretation very uncertain.

Two symmetric poly methyl methacrylate ('Perspex') chambers with fluid reservoirs of 85 mm diameter and about 47 mm depth are made with extra liquid storage reservoirs of 50 ml on top of the chambers. Figure 4.22 shows the arrangement of cells and the specimen between them. The specimens are a 100 mm diameter disc with about 10 mm thickness.

Fig.4.22 *Diffusion cells used in this investigation.*

The specimen-cell is sealed by using rubber gaskets on each side of the specimen, tightening the bolts, and applying silicone rubber round the specimen and inner face of cells. The apparatus was kept in a temperature controlled room at 20°C. Periodically, 10 ml of liquid was taken out from the reservoirs and the chemical composition was analysed.

Synthetic leachate was used on one side of the sample and de-ionised water on the other.

Extensive modelling of Na, K, Ca and S (concentration versus time in the top layer of Cell 2 and 3) has been carried out

From the diffusion tests on the mixes used for the site cell capacity factor (α**)** and D (diffusion coefficient) values were calculated using the optimisation routine in the CU model for the four major elements in the mixes with synthetic leachate on one side and deionised water on the other.

Table 4.3: Capacity factor (**α)** and D (diffusion coefficient) values for the four major elements in the trial cells 2 and 3.

Chemical Element	**Top layer mix Cell 2 & 3 (Porosity = 12%)**		**Bottom layer mix Cell 2 (Porosity = 9%)**		**Bottom layer mix Cell 3 (Porosity = 9%)**	
	α	**D**	**α**	**D**	**α**	**D**
Ca	7.74	3.7E-10	0.67	$5E^{-10}$	0.09	1.35E-10
Na	0.43	1.19E-10	0.09	$1E^{-14}$	1	4.58E-13
K	0.86	1.07E-10	0.67	$9.33E^{-12}$	1	6.73E-12
S	1	2.07E-12	1.37	$1E^{-14}$	27.67	2.93E-14

The modelled input – output and experimentally measured (real) input- output concentrations of the diffusion cell are plotted for the major elements of Na, K, Ca, and S in figures 4.23 to 4.26 for top layer mix of cells 2 and 3 and in figures 4.27 to 4.30 for bottom layer mix of cell 3. The results show that the model optimisation gave a very good agreement between the modelled values and the experimental values. (Note that more toxic elements i.e. As, Mg, Zn, Pb, Cr, Al, Sr, Cu, Ba, Hg, were studied in the diffusion cells and the results are presented in the last part of this section).

Fig. 4.23: Modelled 'Ca' Concentration Vs time in Diffusion cell for top layer mix of site cell 2 & 3.

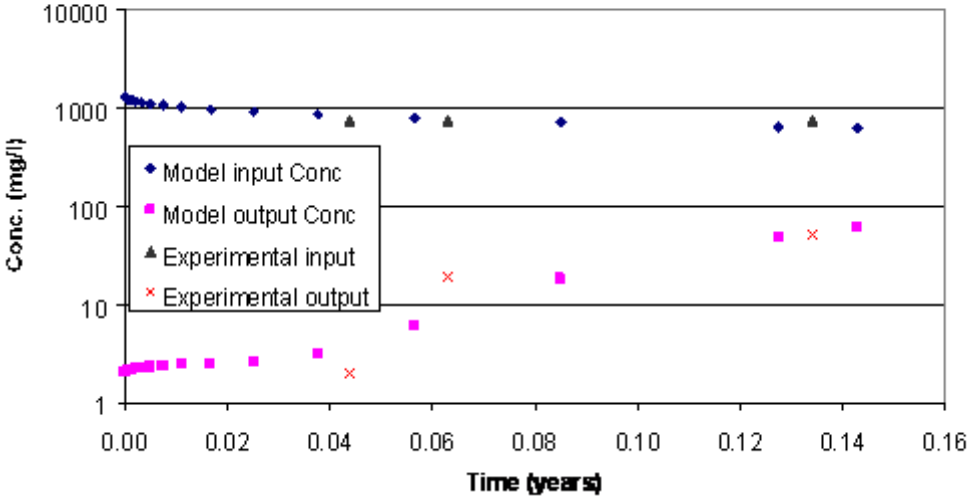

Fig. 4.24: Modelled 'S' concentration Vs. time in Diffusion cell for top layer mix of site cell 2 & 3.

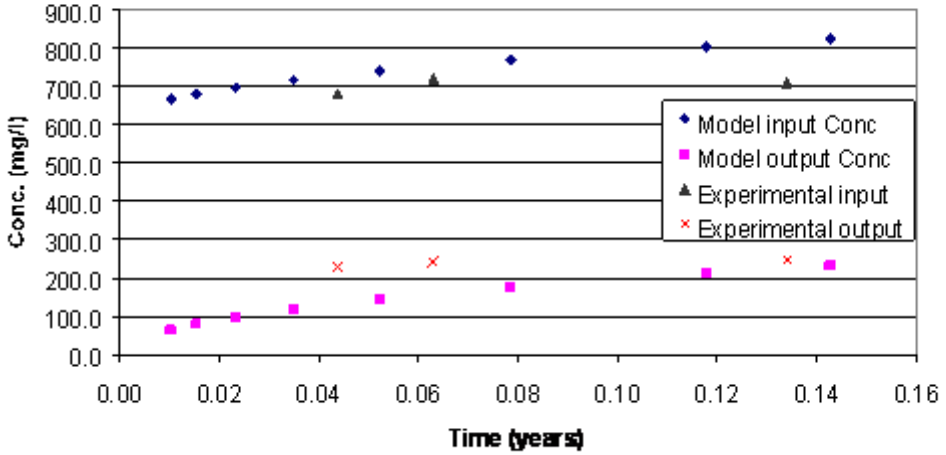

Fig. 4.25 : Modelled 'Na' concentration Vs. time in Diffusion cell for top layer mix of site cell 2 &3.

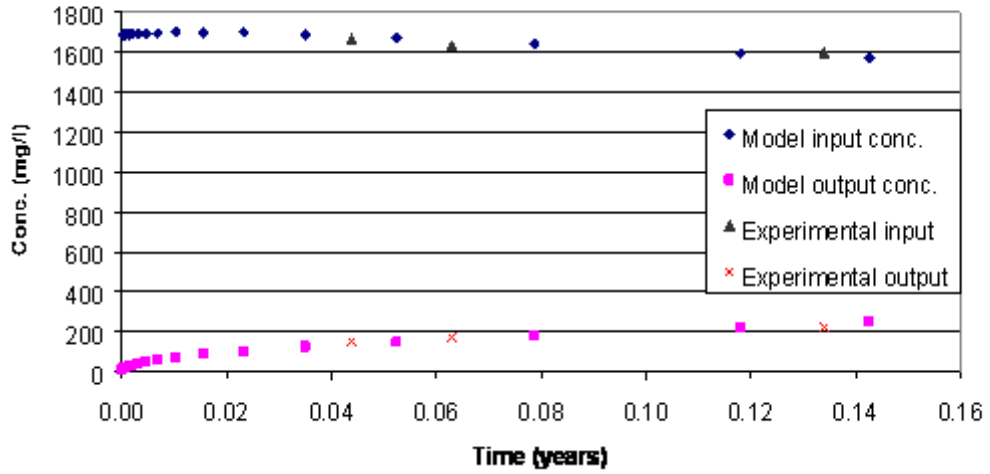

Fig. 4.26: Modelled 'K' concentration Vs. time in Diffusion cell for top layer mix of site cell 2 &3.

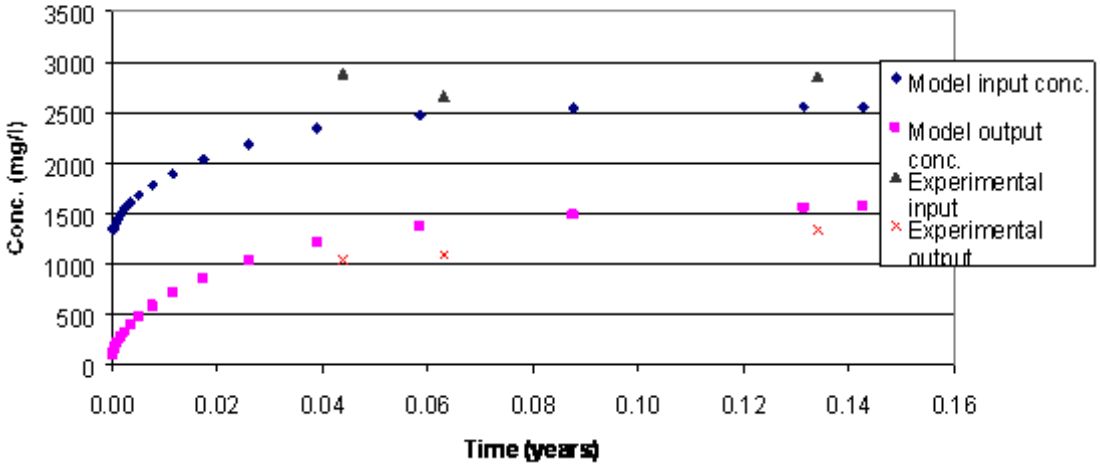

Fig. 4.27 : Modelled 'Ca' concentration Vs. time in Diffusion cell for bottom layer mix of site cell 3.

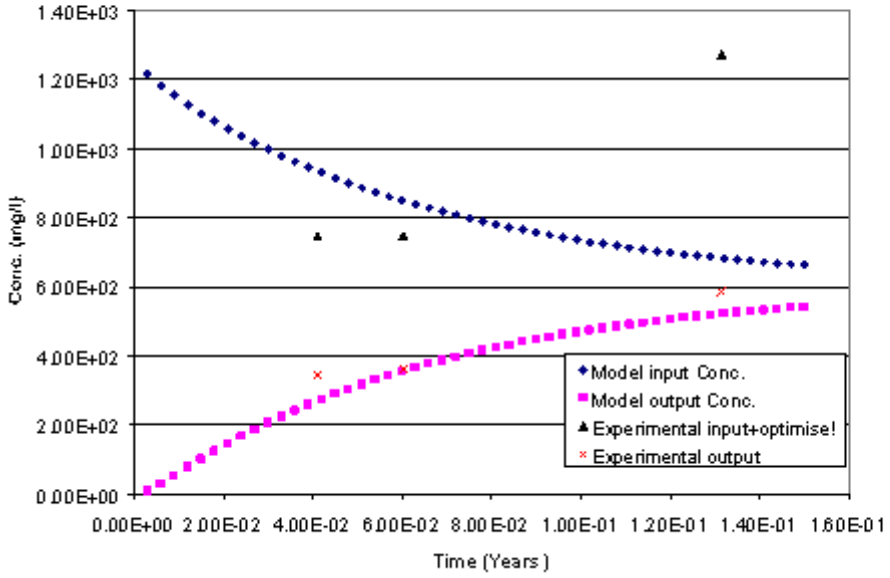

Fig. 4.28 : Modelled 'Na' concentration Vs. time in Diffusion cell for bottom layer mix of site cell 3.

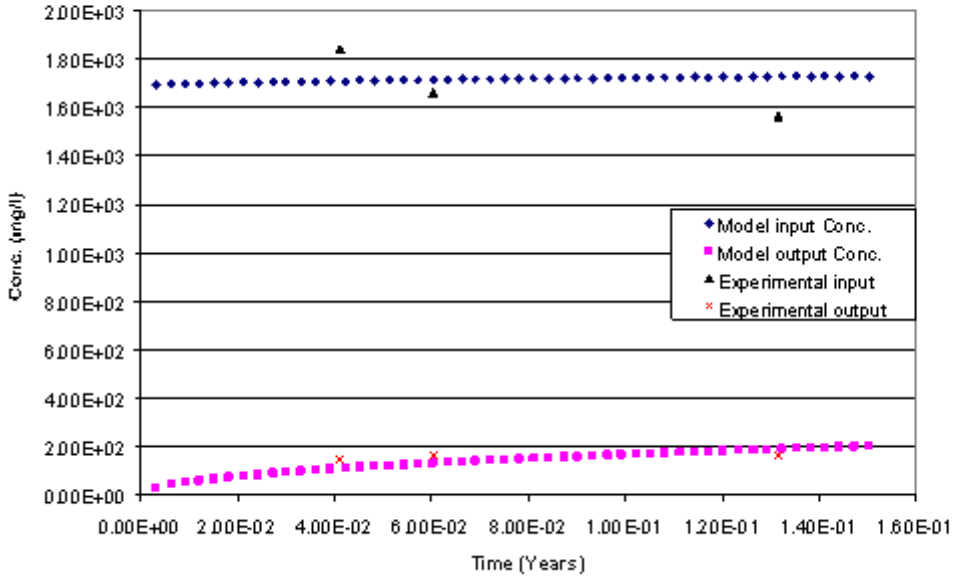

Fig.4.29 : Modelled 'K' concentration Vs. time in Diffusion cell for bottom layer mix of site cell 3.

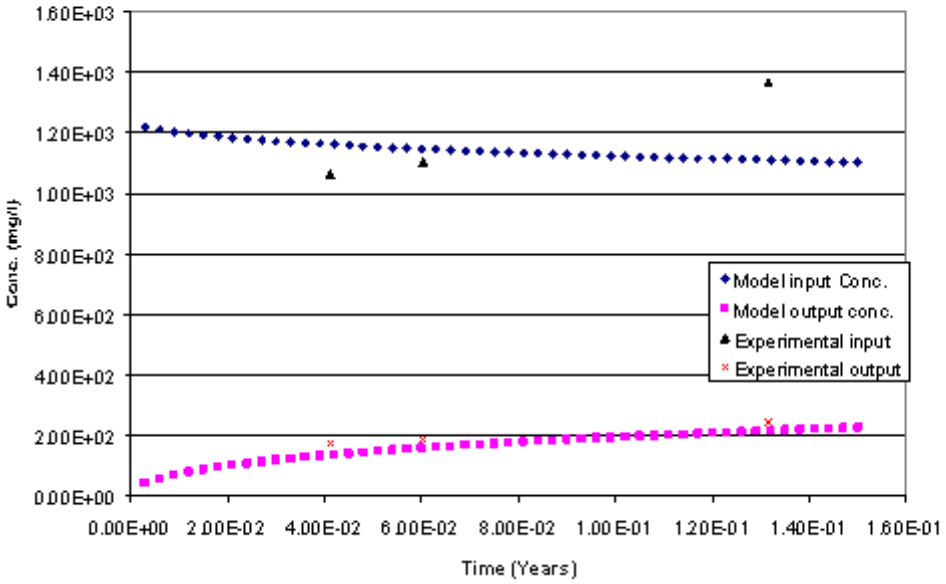

Fig. 4.30 : Modelled 'S' concentration Vs. time in Diffusion cell for bottom layer mix of site cell 3.

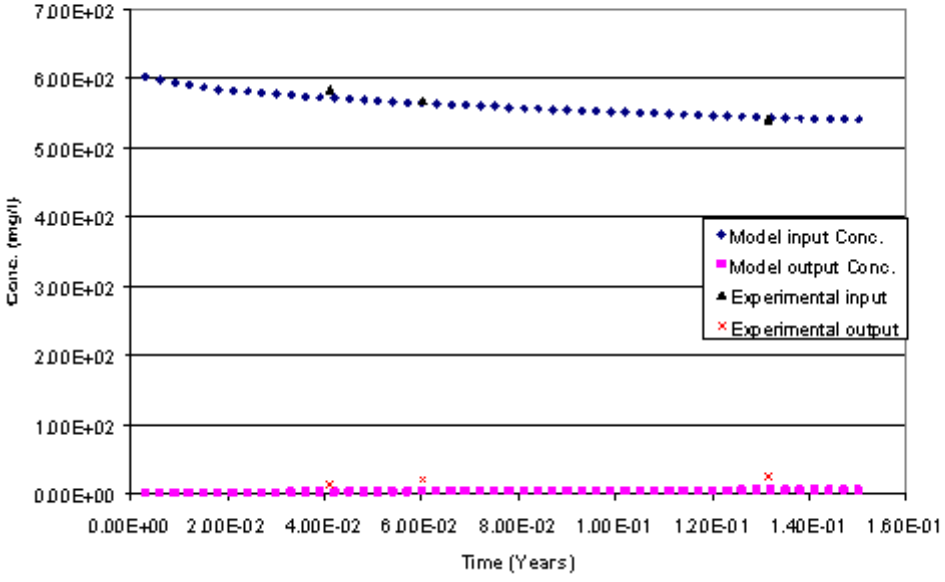

4.2.4 Diffusion tests using “hit list” solution

A synthetic leachate containing significant quantities of heavy and more toxic elements i.e. As, Mg, Zn, Pb, Cr, Al, Sr, Cu, Ba, Cd and Hg, was introduced into the diffusion cells containing the trial cells 2 and 3 mixes.
The composition of the ‘hit list’ solution is given in the second column of the table 4.4.
From the diffusion tests on the mixes used for the site cells, the capacity factor (**α)** and D (diffusion coefficient) values (shown in table 4.4) were calculated using the CU model for the toxic elements with synthetic toxic leachate on one side and deionised water on the other.

The composition of the toxic leachate, the capacity factor (**α)** and D (diffusion coefficient) values are given in table 4.4. The results show initially a substantial amount of heavy metals were contained in the mixes. After a period of two months nothing appreciable has been found at the outlet (see figures 4.31). The modelled input – output and experimentally measured (real) input- output concentrations of the diffusion cell are plotted for some typical elements of the toxic leachate in figures 4.32 to 4.35. As before the results show that the optimisation gave a very good agreement between the modelled values and the diffusion tests experimental values.

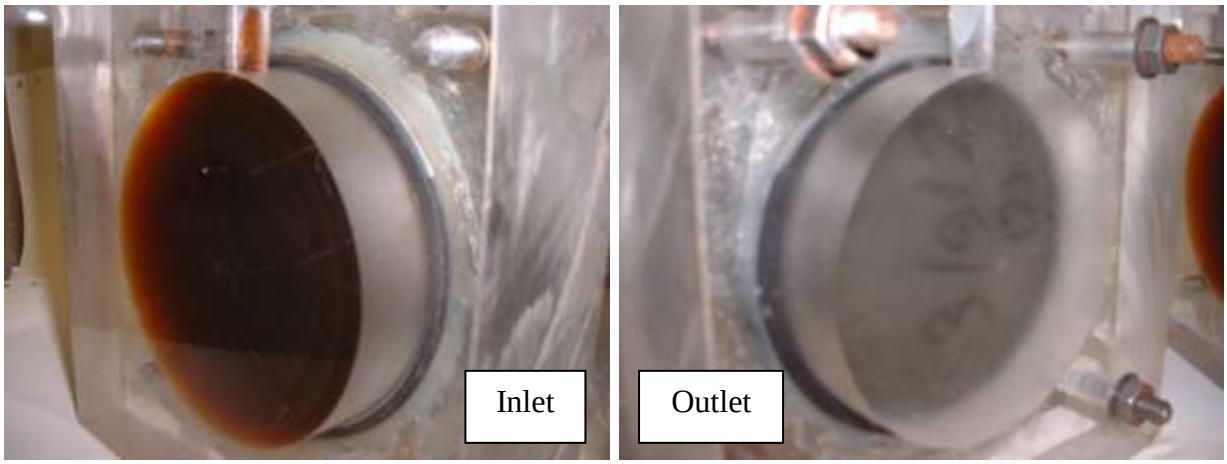

Fig. 4.31: Upstream (Inlet) and downstream (Outlet) of toxic leachate diffusion cell.

Table 4.4: The composition of the toxic leachate and the calculated capacity factor (**α)** and D (diffusion coefficient) values for the mixes used for trial cells 2 and 3.

Elements	**Start of upstream (Toxic leachate) (ppm)**	**Final upstream (ppm)**	**Final downstream (Deionised water) (ppm)**	**Bottom layer mix Cell 2**		**Bottom layer mix Cell 3**	
				α	**D**	**α**	**D**
As	454	158	0.1	4.43	5.69E-12	11	6.01E-12
Mg	194	143	0.7	1	1E-17	1.04	7.7E-12
Zn	400	241	0.1	16.9	1.55E-12	1.12	9.24E-12
Pb	395	87	0.2	10.8	1.7E-10	2.94	2.23E-11
Cr	392	234	0	1	1.68E-11	2.36	1.68E-11
Al	400	214	1.8	4.64	6.98E-12	3.58	1.5E-11
Cu	415	204	0.4	26.7	2.31E-12	2.1	1.07E-11
Sr	427	310	6	0.76	1.39E-11	2.36	1.4E-11
Ba	385	310	0.1	1	5.69E-9	1.26	3.37E-13
Cd	450	250	0	3.09	8.42E-12	2.1	5.94E-12
Hg	600	75	6	10.8	2.08E-11	11.3	3.57E-11

Fig.4.32 : Modelled 'Zn' concentration Vs. time in Diffusion cell for bottom layer mix of site cell 2.

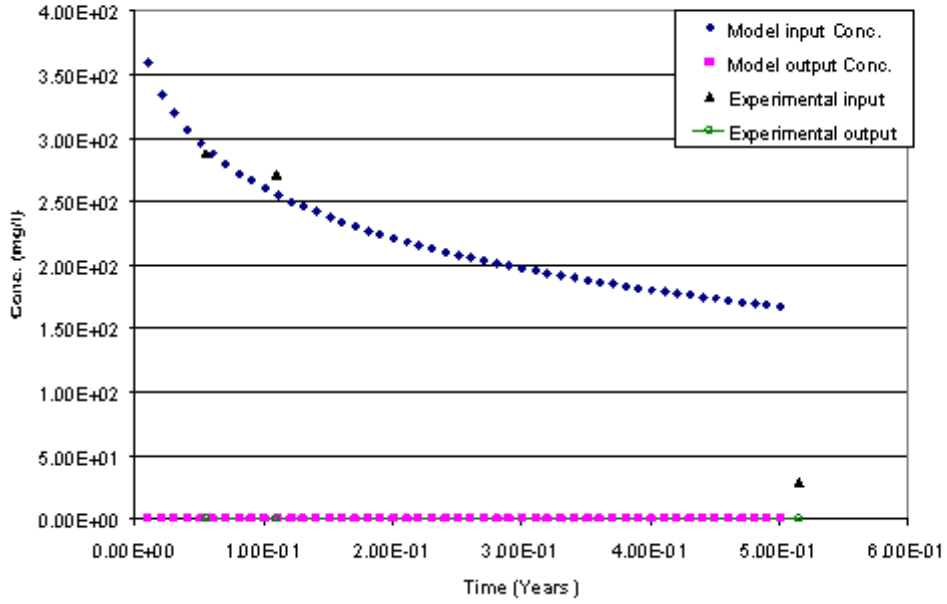

Fig.4.33: Modelled 'Pb' concentration Vs. time in Diffusion cell for bottom layer mix of site cell 2.

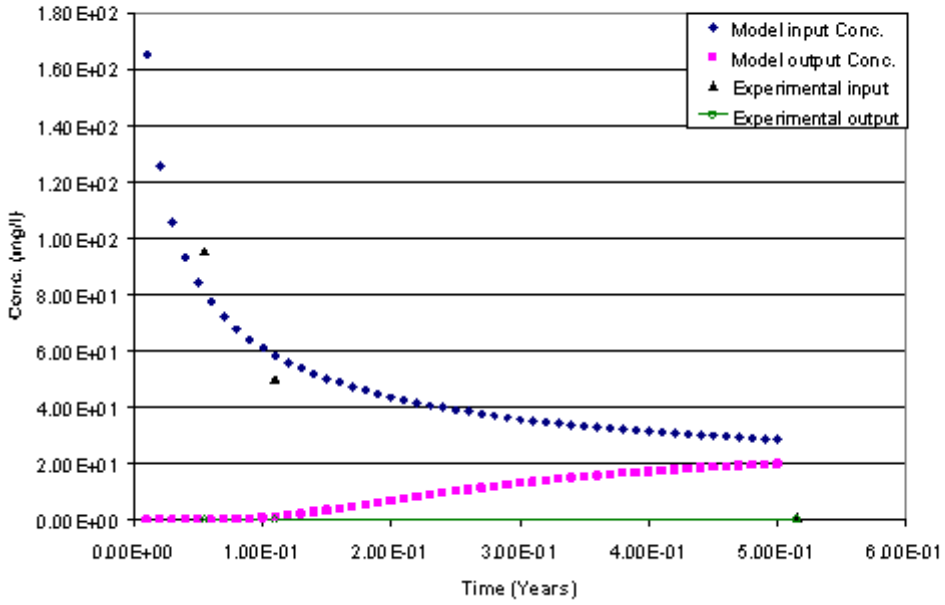

Fig. 4.34 : Modelled 'As' concentration Vs. time in Diffusion cell for bottom layer mix of site cell 2.

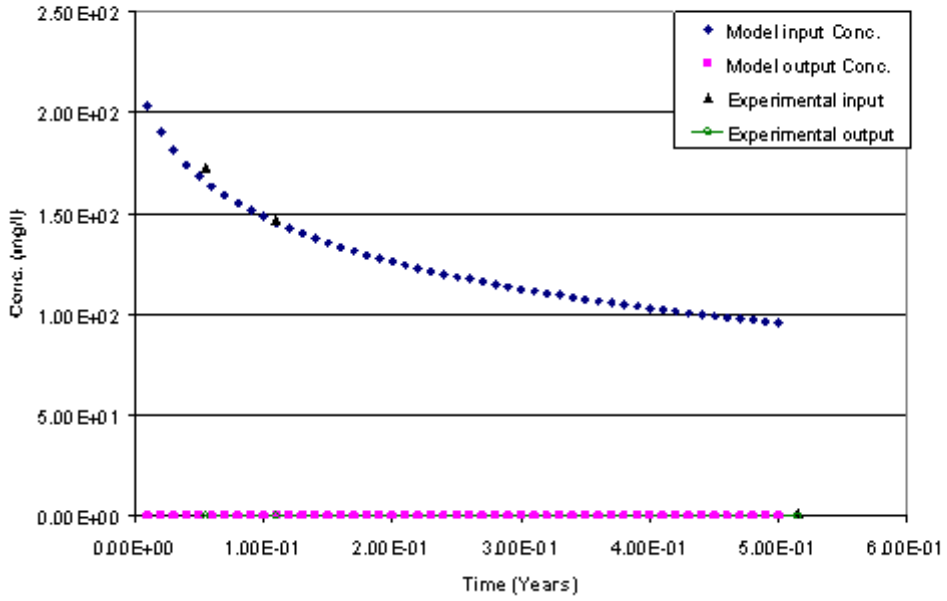

Fig. 4.35 : Modelled 'Hg' concentration Vs. time in Diffusion cell for bottom layer mix of site cell 2.

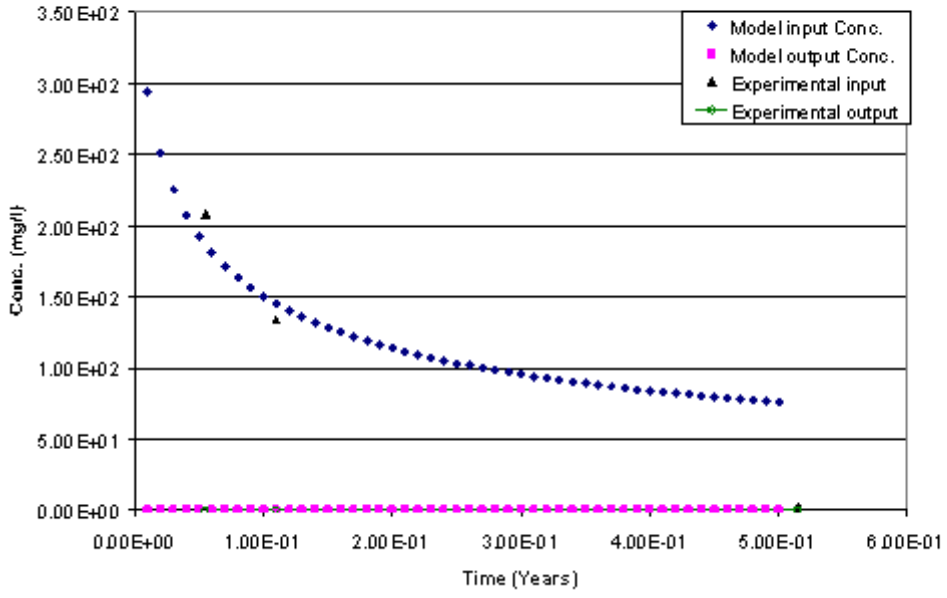

4.3 Physical tests

The compressive strength of pastes and mortars were determined by casting 50 mm cubes and the compressive strength of concrete by 100 mm cubes. All the specimens were cured at 95 per cent relative humidity at 20± 2°C and tested according to B.S. 1881,part 116. The results of the compressive strength of the mixes used for site trials are given in table 2.5 and the results of the compressive strength of the mixes intended for use in Poplars site are shown in table 2.7.

4.4 Leaching tests

The basis of the test is to expose a known mass of barrier material to a known volume of leachate and bring them to equilibrium. Since the present model assumes that the materials in the barrier do not move this does not provide data for it.

The new EC standard leach tests have recently been published. These are BS EN 12457-4:2002 Characterisation of waste- Leaching- Compliance test for leaching of granular waste materials and sludges. (Part 4: One stage batch test at a liquid to solid ratio of 10 l/kg for materials with particle size below 10 mm (without or with size reduction). As these tests do not apply for hydraulically bound mixtures a batch-leaching test was carried out using barrier mixtures and synthetic leachate as explained in this section.

Blocks of cementitious mortars were immersed in the synthetic leachate (10 volumes liquid: 1 volume solid) and allowed to react with it. Periodically (typically 1,2 4, 7 days and weekly, reducing to monthly thereafter) the leachate was replaced, such that fresh solution was continuously supplied to the samples. Analysis of the leachate at each change allows an estimate of the rate of dissolution to be made as a function of sample surface area. Each sample cube had an edge dimension of 50mm, giving a surface area at the start of 1.5 e-2 m^2. At certain intervals, a sample was removed and cut parallel to a face, allowing a determination of reaction depth to be made.

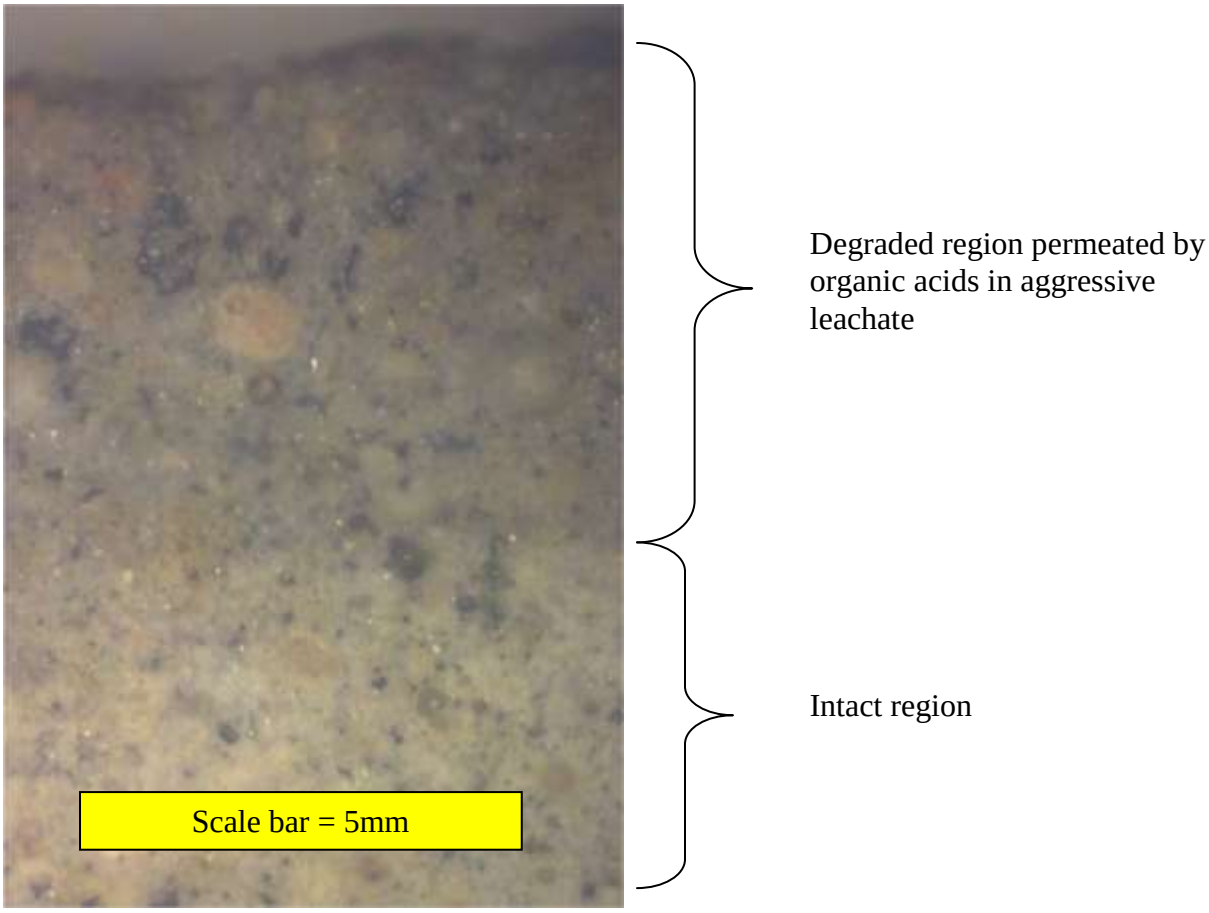

Fig. 4.36 *Reflected light micrograph showing interface between the region degraded during ingress of the acidic leachate and material underlying it, which remains unchanged.*

The composition of the leach solution remained fairy constant over the duration of the experiment, suggesting that once the initial reaction between the solid and liquid had occurred, the rate of mass transfer was slow, even after replacement of the leach solution. The pH after two days, became stable at pH 12.3□0.1 and the major species in solution were sodium, potassium and calcium. Acetate was obviously persistent throughout (noticeable by it's smell) although not measured directly. The alkali metals present in the solid quickly leach out and the concentration of these ions is subsequently buffered by their concentration in the leach solution. Calcium is continuously (though slowly) leached from the solid and sulphate is continuously partitioned into the solid phase. Dissolution of calcite from the CKD presumably maintains the carbonate concentration in solution.

	Leachate	**4 days**	**7days**	**28 days**	**289 days**
CO3		6.9 E-03	4.2E-03	N.D.	5.0E-03
SO4	2.0E-02	8.2 E-04	2.1E-03	3.3E-03	1.8E-02
NH4	2.2E-02	Ammonium not determined			
K	2.5E-02	4.5 E-02	6.1E-02	3.5E-02	3.2E-02
Ca	6.0E-02	6.9 E-02	6.5E-02	6.0E-02	6.2E-02
Cl	6.3E-02	5.5 E-03	3.3E-03	1.5E-03	5.6E-03
Na	8.0E-02	9.9 E-02	1.1E-01	9.1E-01	8.6E-02
COOH	1.9E-01	Acetate not determined			
pH	5.1	12.3	12.2	12.4	12.3

Table 4.5 *Leachate composition during batch leaching experiments. The sample binder is CKD and conditioned ash, hydrated with water. This binder type was used on cells 2 (upper layer concrete) cell 3 (both layers and is proposed for use at the Poplars site.*

A similar experiment was undertaken in which a small quantity of transition metal nitrates were included in the leachate. The object of this experiment is to examine the uptake of these metals into the solid phase. It is well established that most transition metal elements exhibit low solubility as hydroxides and one of the principal mechanisms by which the barrier system is intended to work, is by providing an alkaline buffer, promoting precipitation of transition metal salts. Milli molar additions of zinc, lead, mercury and cadmium were made to one batch of leachate and these metals were analysed for by ICP spectroscopy. The solid phases were mortars, one a Portland cement reference mortar and the other, similar to that shown above (CKD – Lagoon ash blend) and proposed for use at the Poplars site. The results show a steady concentration for each analyte, suggesting that the availability of these elements is under the control of a solubility limiting phase.

	7days		28 days		180 days		289 days	
	OPC	**CKD-PFA**	**OPC**	**CKD-PFA**	**OPC**	**CKD-PFA**	**OPC**	**CKD-PFA**
Cd	2.1 E-7	3.2 E-7	2.0 E-7	4.5 E-7	7.2E-7	6.2 E-7	4.5 E-7	1.1 E-6
Hg	All mercury determinations were below detection (<0.01 ppm = 5 E-8M)							
Ni	1.1 E-6	1.6 E-6	4.3 E-6	9.1 E-7	1.1 E-6	5.5 E-7	3.5 E-7	4.5 E-6
Pb	4.1 E-4	3.3 E-4	2.9 E-4	4.8 E-4	2.1 E-4	1.0 E-4	9.0 E-5	8.8 E-5
Zn	1.6 E-5	1.2 E-5	1.3 E-5	4.2 E-5	3.2 E-5	5.4 E-5	8.2 E-6	4.1 E-5

Table 4.6 *Uptake of heavy metals by cementitious binders from acetogenic leachate. Concentration is molal units*

Periodic sectioning of the samples allowed an estimation of the rate of movement of the reaction front through the materials. This approach can only by an approximate method, yet it is a useful guide to the rate of degradation in this relatively aggressive environment.

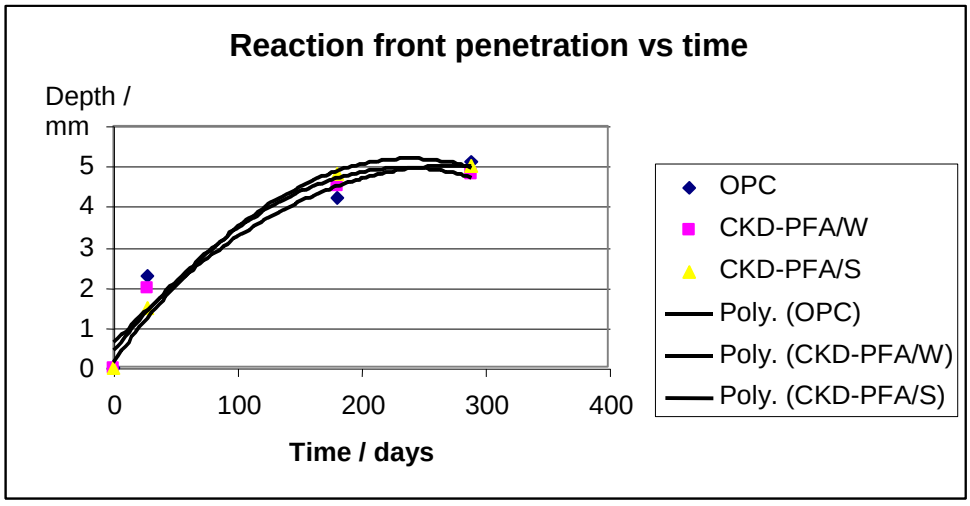

Fig. 4.37 *Depth of penetration of the reaction front developed within the cementitious barrier materials when immersed in acetogenic leachate. Note CKD-PFA/W is water hydrated binder (as proposed for Poplars site) and CKD-PFA/S is sulphate activated, using n 11% w/w sodium sulphate solution*

As with the solution analyses, the rate of change diminishes with time, suggesting that the process is under diffusion control, which is confirmed in the plot below

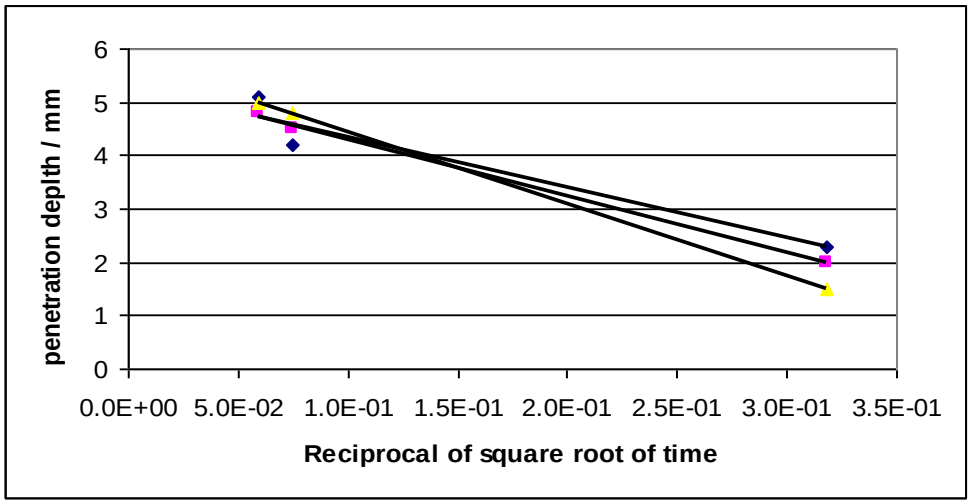

Fig. 4.38 *Depth of penetration results of leaching tests, plotted as 1/√*time, showing the process to be limited dominantly by diffusion

4.5 Pore expression (squeezing)

The pore solutions of the mixes used in the Risley site trials 2 and 3 were extracted by applying high pressure to a purpose built cell in compression machine. The concentrations of some elements for these mixes are given in table 5.5 of the chapter 5 in this document.

5 SITE TRIALS

5.1 Introduction:

The first three-layer experimental barrier test cell was successfully constructed in autumn 1999 on a licensed landfill operation site at Risley, Cheshire operated by Biffa Waste Services Ltd. Two more cells were constructed adjacent to this cell in winter 2000 with different cementitious composite mineral waste materials. This landfill site receives both domestic and industrial waste. The first cell was dismantled in March 2001. Cells number 2 and 3 are still being monitored.

The purpose of the cells is as follows.

- To provide validation data for the modelling of the performance of the barriers in service.
- To demonstrate a construction method.
- To demonstrate that the novel mixes can be made in industrial quantities (150t of concrete were used in the three test cells).
- To provided samples for on-site workability testing and long-term physical testing in the lab.
- To provide samples for mineralogical analysis when the cells are dismantled.

5.2 Layout and construction methods of the cells:

A typical test cell is shown schematically in Figure 5.1. These inverted pyramid shape cells measure 8 metres wide and contain waste to a maximum depth of 1.1 metre. The slopes of the cells are 30°and the cells contain 5.4m^3 of waste. Table 5.1 gives the dimensions and volume of each layer in the test cells. The excavation was carried out with an excavator which was also used to place the concrete and mortar mixes designed for the different cells. The concrete layers were placed and levelled by the excavator. The compaction of concrete layers was carried out by two poker vibrators and the compaction of clay layer was carried out using the outside surface of the excavator's bucket.

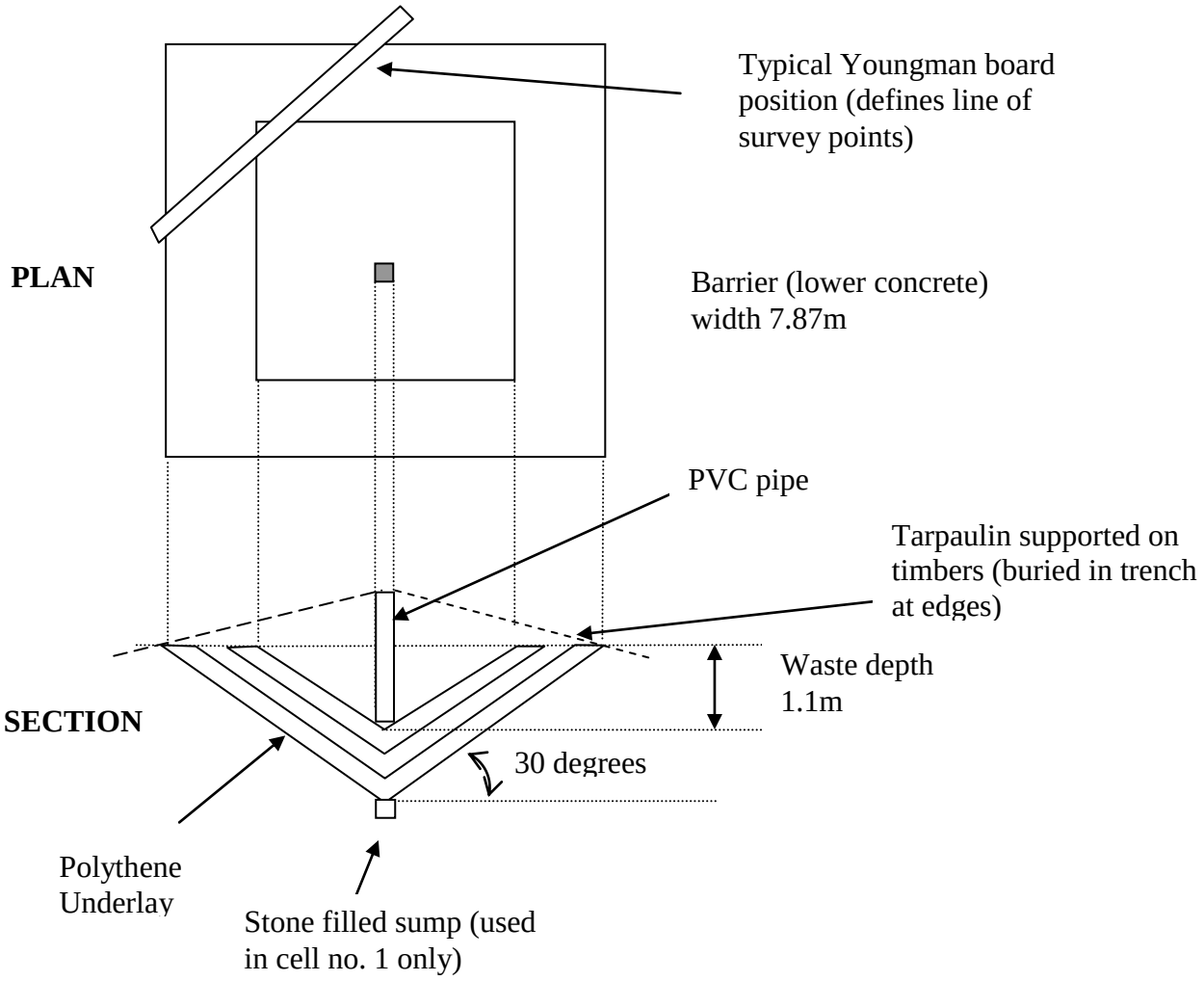

Figure5.1: *Typical trail test cell layout.*

	Thickness (m)	Depth to lowest point (m)	Width (m)	Volume (m^3)
Waste	-	1.1	3.84	5.4
Upper Concrete	0.2	1.33	4.65	4.16
Clay	0.5	1.9	6.66	18.61
Lower Concrete	0.3	2.25	7.87	18.28

Table 5.1: *Dimensions and volume of each layer of test cells.*

Observations from the construction

Limestone aggregate used in the top layer of the first cell caused an adverse chemical reaction with the spent borax cementitious material. The limestone was used due to difficulties with the intended aggregate (a slag from BRM) at the concrete batching plant when the mixing was taking place. The strength of the concrete was reduced by time and micro-cracks were observed in the lab specimens but no cracks or traces of leaking leachate could be observed in the top layer when dismantling the first cell. In this cell even higher permeability coefficients of about $1.5 – 4 \times 10^{-8}$ m/s was found to be acceptable and no leachate was detected on top of the clay layer. Although suitable for the purpose intended the borax did not bind well with the limestone; it would be best used on its own or with siliceous aggregate but shows great potential owing to its resistance to organic acids.

During the construction of cell numbers 2 and 3 the mix proportions actually used were different to what was designed in Laboratory due to some practical problems encountered in the batching plant and placement of some of materials (in correct weightings of different materials and partial hydration of CKD in the plant).

The mixes actually made showed higher permeabilities than the mixes designed initially in the laboratory (see table 2.5).

5.3 Emplacement of waste and leachate:

Due to size and shape constraints of the cells shredded waste was used. It was placed and compacted up to the top level of the test cells. A leachate which provided the most aggressive solution representing the leachates found in the landfill was obtained from the leachate treatment plant for the site and it was pumped to 100 mm below the top level. This level was checked during operation and just before the dismantling process. The cells were covered with a tarpaulin rain cover to prevent rainwater ingress and contain odour.

5.4 Instrumentation and sampling:

Two types of sampling lines were used between the layers of the cell liners using 3 mm plastic tubes in both. In one type the end of the 3 mm plastic tubes were glued inside porous stone discs of 60 mm diameter. In the other type the layer was drilled and the 3 mm plastic tubes ends were sealed in place in the set concrete with sponge around the end of the line. The sampling lines were placed as an array in the various liner materials and levels. Liquid samples were obtained by applying a vacuum to the lines.

A 10mm sampling line was also placed in the sump below the barrier to monitor the water table or any liquid, which accumulated below the bottom concrete layer in the first cell. Cells 2 and 3 are placed on top of an existing operational landfill cell.

A thermocouple was placed in bottom layer concrete of each cell to monitor the temperature variation with time. Cores were cut through the liners in the first cell when it was dismantled after about fifteen months of exposure. Cores will be cut through the liners in cell numbers two and three when they are dismantled.

Operation of Vacuum Lines

On the end of the extract lines there is a sponge or a stone to form a void. If there is gas in adjacent pores or cracks etc. samples may be extracted easily with a vacuum. If there is no gas or other pathway the flow up the line must be from advection from a spherical region around the void. The velocity of flow up the pipe is given by:

$$V = \frac{4khr_1}{r_0^2} \qquad \ldots[5.1]$$

where:

k is the permeability (10^{-9} m/s)

h is the head of water corresponding to the atmospheric pressure (m)

r_1 is the radius of the void (10mm)

r_0 is the bore radius of the pipe (1.5mm)

The outer radius of the integral is insignificant provided it is much greater than r_1. Using the values in brackets gives a calculated flow of 640mm per hour. Flow rates of approximately this value were observed.

5.5 Dismantling

Dismantling objectives:

1. Determine the extent of leachate penetration through the barriers.
2. Investigate the effect of leachate exposure on the materials in the different layers.
3. Investigate interactions between the layers in the presence of leachate.

Principles of dismantling method used on cell 1.

The most interesting samples come from near the centre of the cell. The cell were completely emptied and all leachate removed before dismantling. If this is not done the leachate will spill down onto all recovered samples. Concrete core cutting on site is difficult and the cutting water would also wash out leachate from samples. Concrete samples were therefore recovered by breaking. Clay cores were taken as well as the concrete samples.

5.6 Modelling transport in the tests cells

5.6.1 Observations from leachate sampling

Table 5.2 gives the results of monitoring leachate level and liquid between the layers and the temperature at the top of the lower layer concrete in the first cell. Tables 5.3 and 5.4 give the corresponding results for cells 2 and 3 up to date.

Table 5.2: *Monitoring of the leachate level and liquid between the layers of cell No:1. filled on 17/12/99:*

Date	2000						2001	
	11/1	**13/3**	**20/4**	**19/7**	**11/9**	**28/11**	**29/1**	**6/3**
	PH level							
Below lower layer	**9**	**9**	**10**	**10**	**9.7**	**8.4**	**7.8**	**8.2**
Inside lower Layer	**-**	**-**	**-**	**-**	**-**	**-**	**-**	**-**
Top of clay layer	**13**	**13**	**13**	**13**	**-**	**-**	**-**	**-**
Inside top layer	**12**	**-**	**-**	**-**	**-**	**-**	**-**	**-**
Leachate at 163 mm below ground level	**6**	**6**	**6**	**6**	**6.5**	**6.5**	**6.6**	**6.7**
Temp. at top of lower concrete layer (°C)	**10**	**10**	**11**	**17.5**	**18.8**	**13.6**	**8.9**	**8.9**

Table 5.3 *Monitoring of the leachate level and liquid between the layers of cells No:2. filled on 29/01/01*

Year	**2001**					**2002**					**2003**			
Date	**06/ 03**	**06/ 06**	**17/ 07**	**27/ 09**	**27/ 11**	**29/ 01**	**12/ 03**	**14/ 05**	**16/ 07**	**01/ 10**	**15/ 01**	**01/ 04**	**03/ 07**	**26/ 11**
Leachate at:	**pH level**													
163 mm	7.5	7.5	7.8	7.8	7.5	-	-	-	-	-	-	-	-	-
272 mm						8	7.6	7.9	8.2	8.5	8.5	8.5	8.3	8.1
378 mm														
below GL														
Top of clay layer	13.2	13.3	13.2	13.0	13.0	13.3	13.2	13.1	13.0	12.9	12.9	12.9	13.0	12.1
Top of base layer	-	-	-	8.2	8.2	8.5	8.5	8.4	8.3	8.4	8.4	8.4	8.3	8.3
Below base layer	-	12.7	12.9	12.2	12.2	12.9	12.4	12.4	12.2	12.2	12.2	12.2	12.3	11.6
Temp. at top of base layer (°C)	6.6	14.7	17.5	16.5	11.5	7.2	7.7	12.1	17	17.3	7.1	9.5	18	10.7

Table 5.4 *Monitoring of the leachate level and liquid between the layers of cells No:3. filled on 29/01/01*

Year	**2001**					**2002**					**2003**			
Date	**06/ 03**	**06/ 06**	**17/ 07**	**27/ 09**	**27/ 11**	**29/ 01**	**12/ 03**	**14/ 05**	**16/ 07**	**01/ 10**	**15/ 01**	**01/ 04**	**03/ 07**	**26/ 11**
Leachate at:	**pH level**													
163 mm	8.8	-	-	-	-	-	**Refill**	-	-	-	-	-	-	-
272 mm		7.9	7.9	7.9	-	-	(7.9)	8.4	8	8.3	8.4	8.2	8.4	-
378 mm					8.5	-								-
below GL														
Top of clay layer	-	12.9	13.1	-	12.3	12.9	12.4	12.2	12.2	12	-	12	11.8	10.7
Top of base layer	-	-	-	-	8.7	8.2	8.5	8.1	8.1	8.1	7.8	7.8	7.5	7.1
Below base layer	-	-	-	-	-	-	-	-	-	-	-	-	-	-
Temp. at top of base layer (°C)	8.9	16.2	19	18	13.2	8.3	8.2	13.4	19.5	17.9	7.9	10.3	18.6	11.3

The chemical analysis and changes of site leachate in cell 1 are shown in figure 5.2, these results indicate that no liquid had leached through any layers in this cell and the major element concentrations had not changed during the 15 months of monitoring this cell. Furthermore, the underground water chemical changes in cell 1 indicate that these changes had occurred independently of the leachate variation in a particular element (See figure 5.3). For example Na and K reduced in concentration in the underground water but they were constant in the leachate. The concentrations of elements in the leachate are also different to the ones monitored from the liquid extracted from bottom of the lower layer (See figures 5.2 and 5.3). Concentration of Na in the leachate was about 10000 mg/l but it is about 1000 mg/l in the underground liquid. Ca concentration in the leachate was about 5000 mg/l but in

underground water was about 50 mg/l. Monitoring cell number one in service showed that the leachate had not penetrated the liner and that no liquid was collected from the sampling lines at the interface between clay and either concrete. This indicates that the integrity of the liner has been maintained over the duration of this study.

Monitoring of Cells 2 and 3 has continued for 36 months.

The concentration changes in each of the cells number 2 and 3 are shown for Na, K, Mg and Ca. in figures 5.4 to 5.11.The results of the these two cells are similar to those from Cell 1, showing nearly constant concentration of elements in the leachate contained in Cell no. 2 and 3.

For the reasons given in the last paragraph of this section, it was expected that the leachate would leach through the layers in cells 2 and 3, since the top layer concretes were not prepared and mixed as designed to specification and also the clay was not properly compacted during construction of the cells.

In Cell No. 2 some liquid was collected from below the top of bottom concrete layer, but since a higher vacuum pressure was used for collecting samples in cells Nos. 2 and 3, the pore solution is believed to have been extracted from clay layers in these cells.

It is suggested that a reduction in the K concentration in the bottom of the top layer concrete to be due to the sorption of K in the top concrete layers (Figs 5.5 and 5.9). It was noted that the increase of Na was due to the high solubility of Na in the top concrete layers (Figs 5.4 and 5.8).

The reduction in the Ca concentration in the bottom of top layer concrete was due to precipitation of Ca in the concrete layers (Figs 5.6 and 5.10).

The reduction in the Mg concentration in the bottom of top layer concrete was due to precipitation of Mg by concrete layers governed by high pH (Figs 5.7 and 5.11).

It was noted that the concentration reduction or increase in each case generally follows the same pattern in these cells. This is because chemically similar types of materials used in Cell 2 and 3.

All of the factors described above are well explained by the linear isotherm ‘Coventry’ model. See section 5.6.2.

Figure 5.2: Leachate's chemical changes in Cell 1

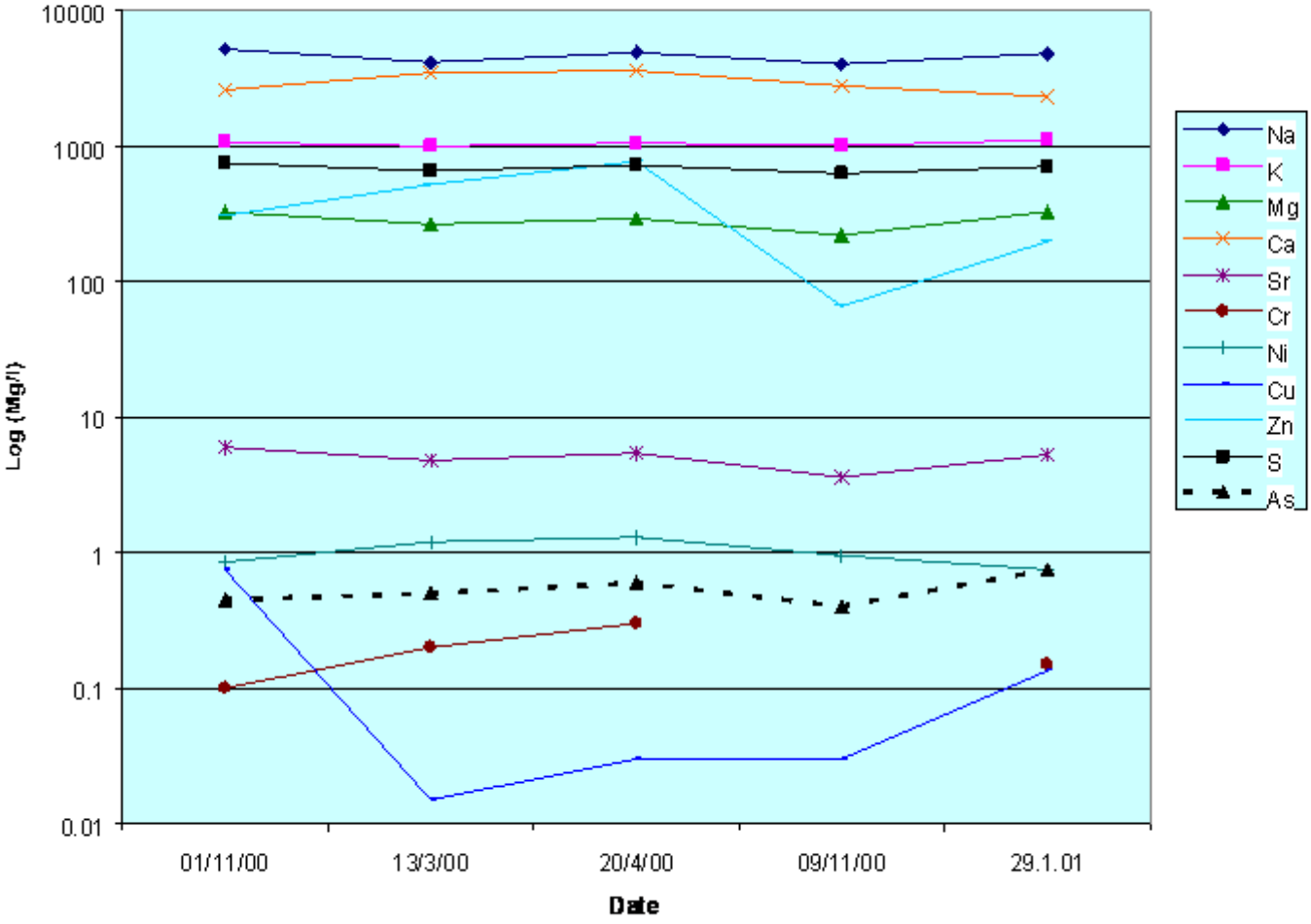

Figure 5.3: Underground water chemical changes in cell 1

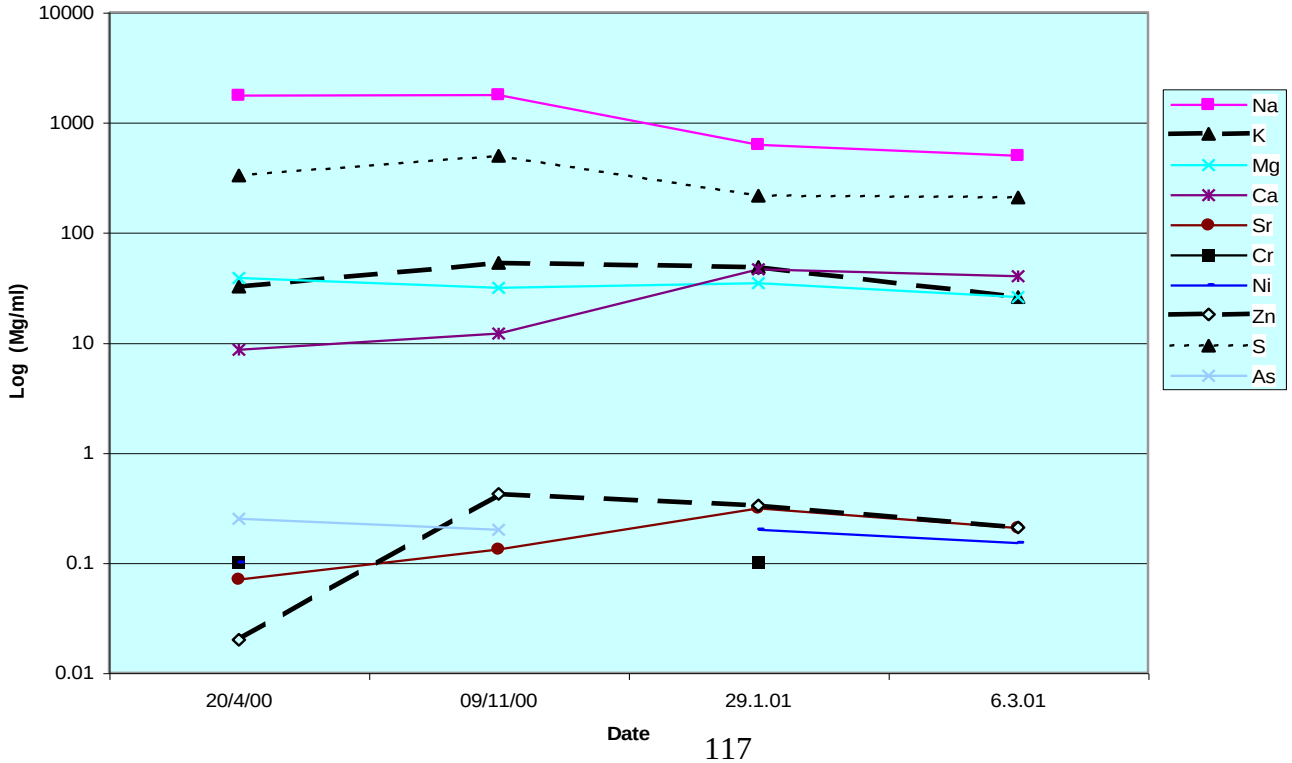

Fig. 5.4: 'Na' concentration changes in cell 2.

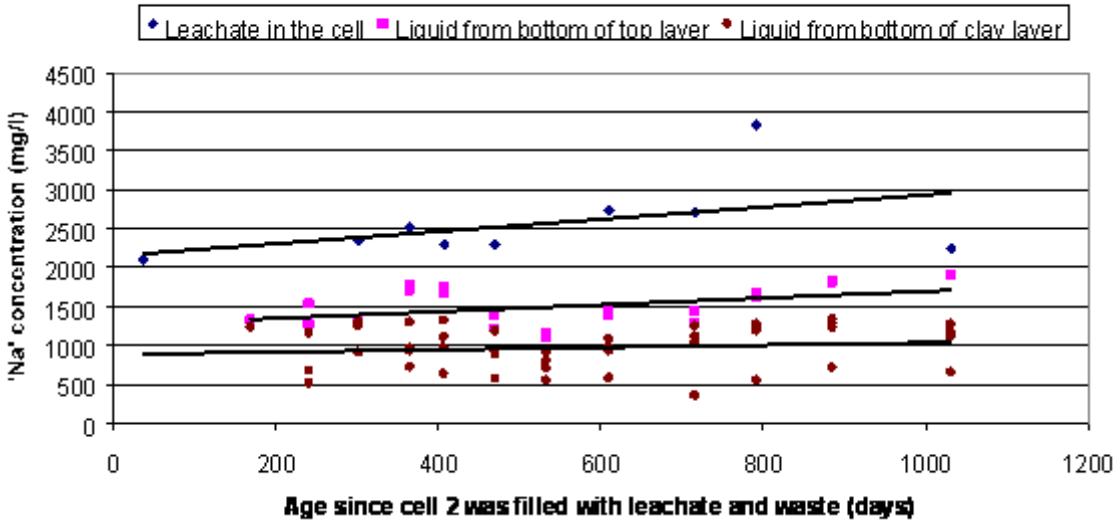

Fig. 5.5: ' K' concentration changes in cell 2.

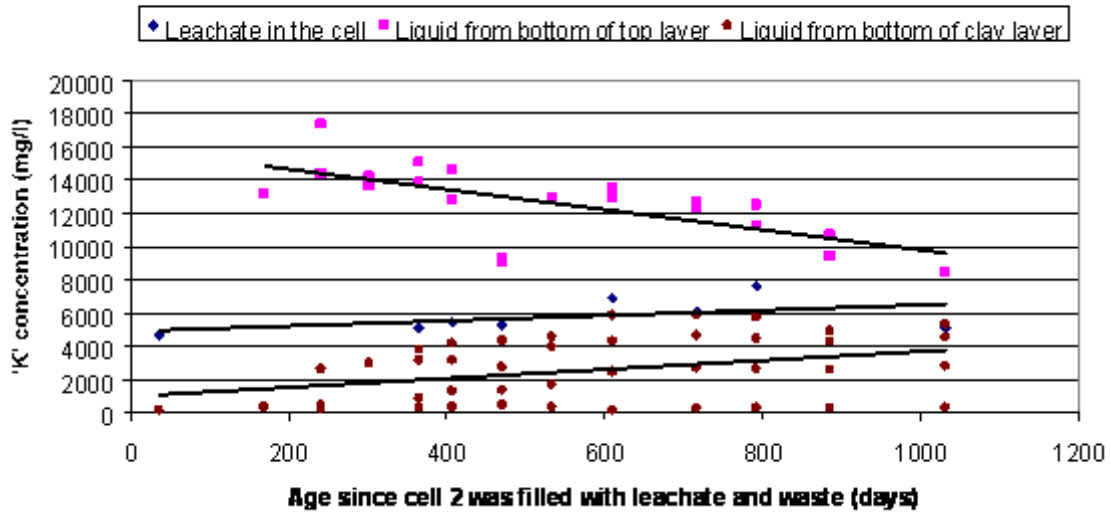

Fig. 5.6: ' Ca' concentration changes in cell 2.

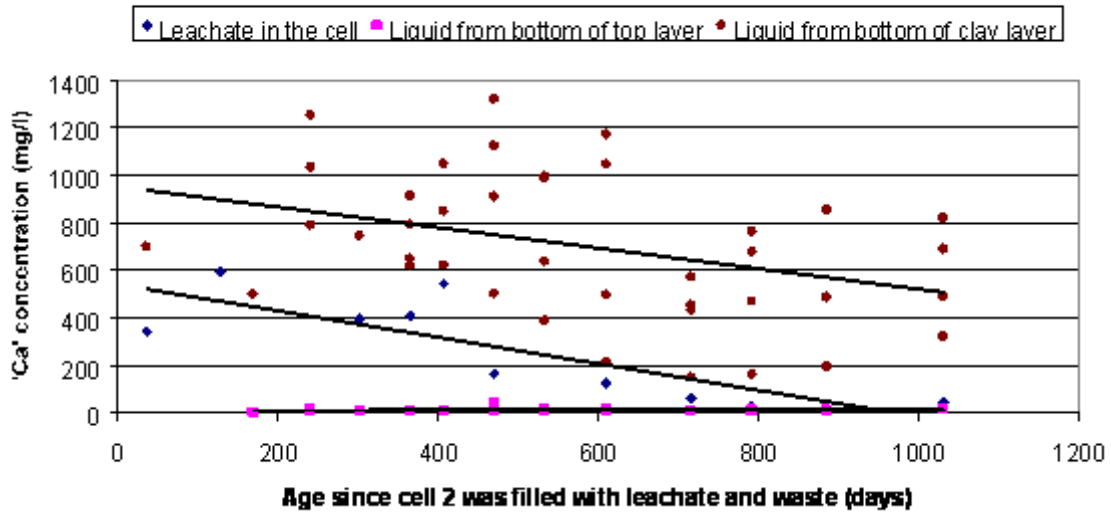

Fig. 5.7: ' Mg ' concentration changes in cell 2.

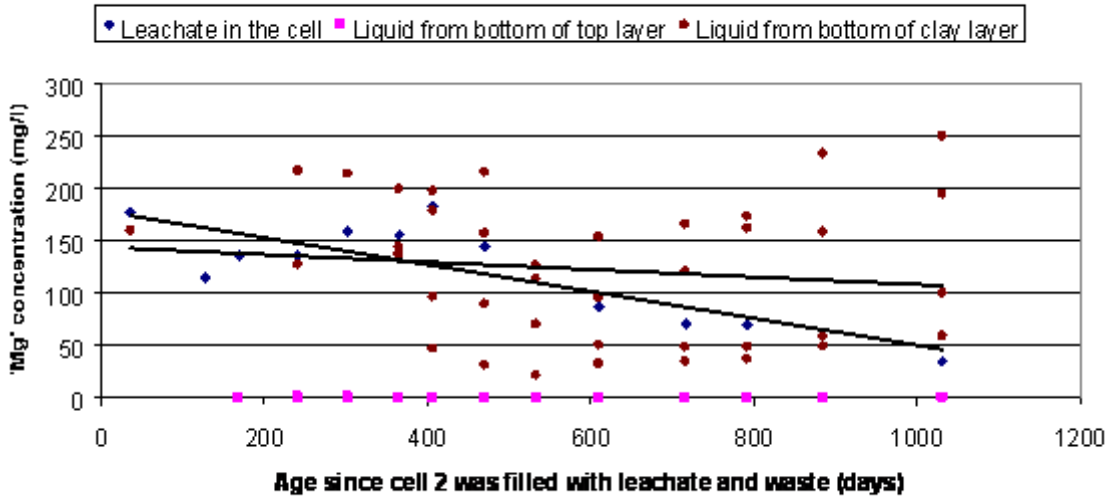

Fig. 5.8: 'Na' Concentration changes in cell 3

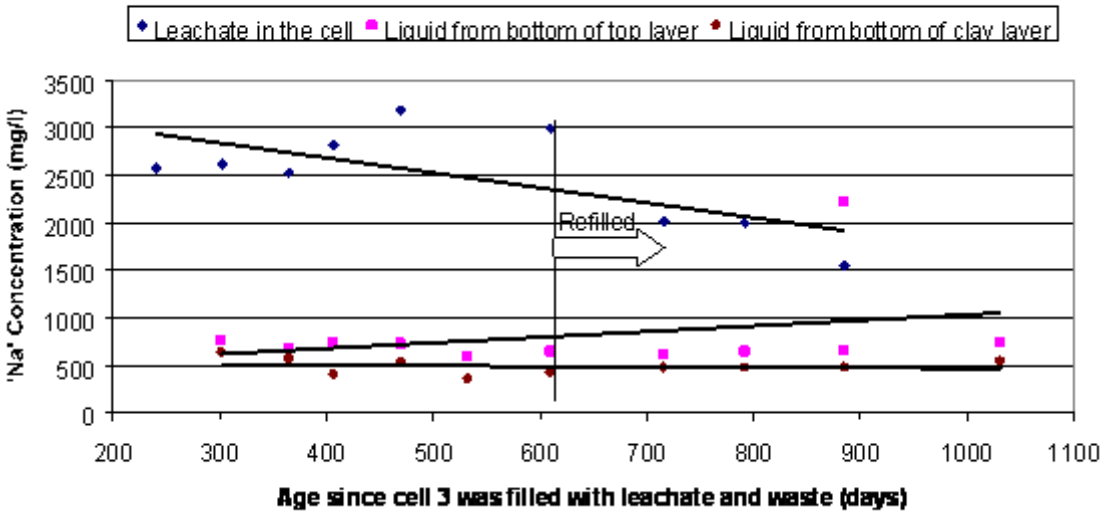

Fig. 5.9: 'K' Concentration changes in cell 3

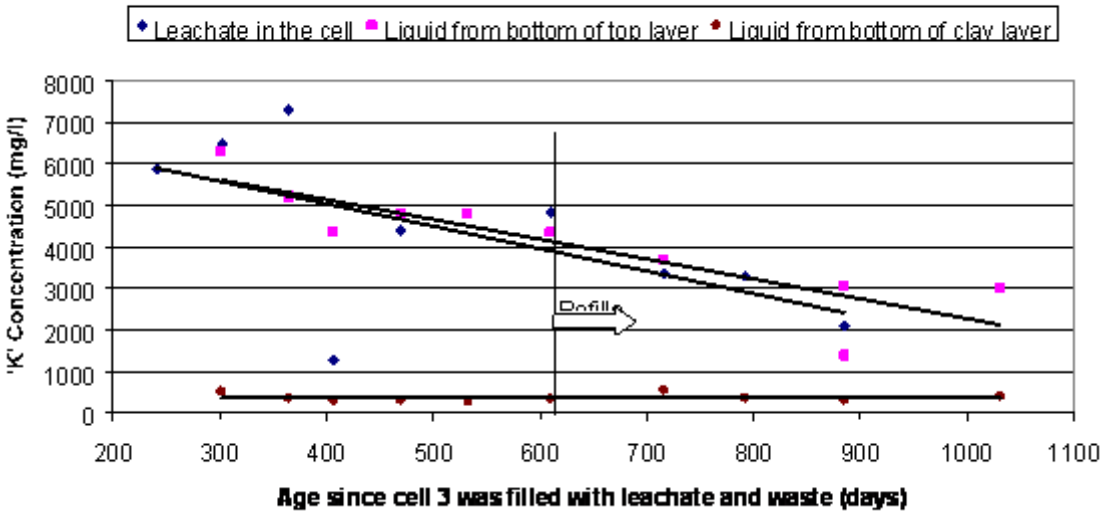

Fig. 5.10: 'Ca' Concentration changes in cell 3

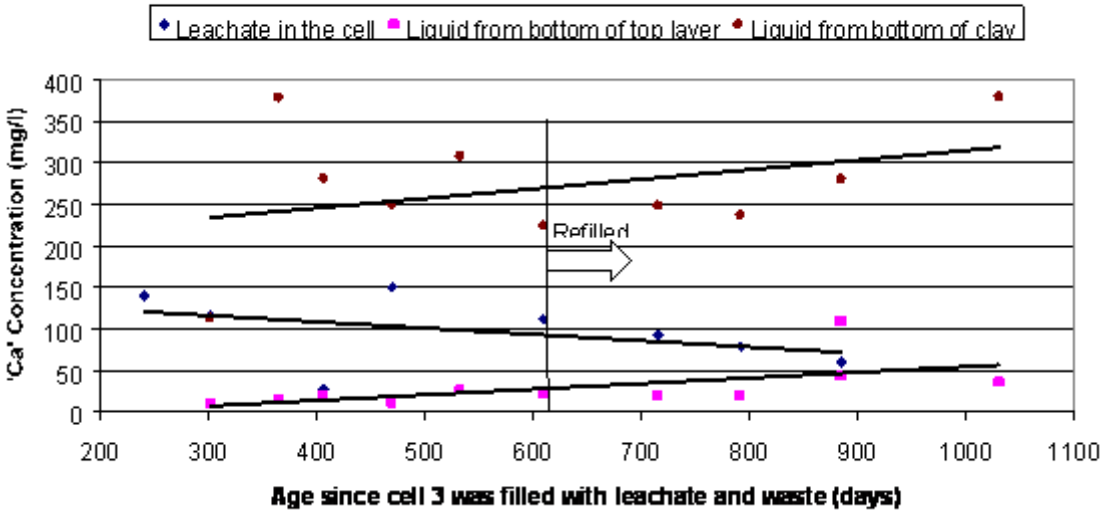

Fig. 5.11: 'Mg' Concentration changes in cell 3

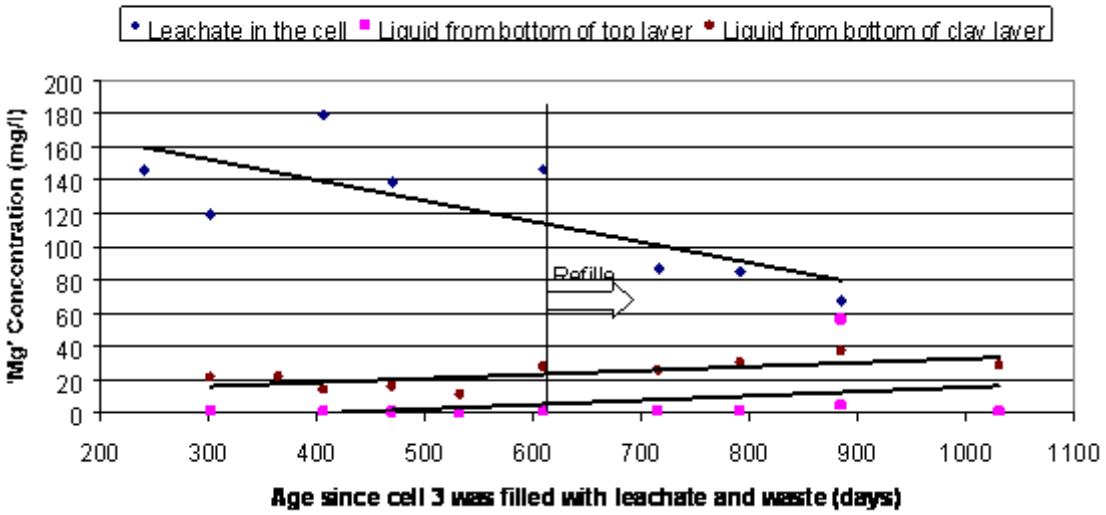

During the monitoring of Cell 3 a leak was identified, caused by:

- Inadequate compaction of the clay during construction of Cell 2 and 3 as reported previously.
- Partial hydration of the CKD in the top concrete layer due to the storage of uncovered CKD bags in the batching plant.
- The poorer quality of the top layer mixes than designed, due to a driver adding water to mixes on the road to produce more flowable mixes to facilitate discharge.

Cell 3 needed to be refilled after 12 months. The effective indicated premeability was calculated as follows:

Total Volume of the leachate leaked $\cong 4.54\ m^3$

Surface area of pyramid in bottom of clay layer $=25.3\ m^2$ (See Fig. 4.12)

Thus indicated permeability $k = 5.2 \times 10^{-9}$ m/s

This corresponds to nearly the same permeability as a Bentonite Enhanced Sand liner and indicates satisfactory performance even when very poor construction practice was evident.

5.6.2 Comparison between model and observations

The capacity factor, alpha (α) and diffusion coefficient (D) values obtained from the diffusion tests on the top and bottom mixes used in the site trial cell number 2 and 3 together with the initial concentrations of different elements in site leachate and the mixes used in the cell (from the pore pressed solutions) were used (see table 5.5) to verify the modelled concentration against measured collected samples concentration values. These are shown in figures 5.12 to 5.19 for Ca, Na, K, and S for cell 2 and 3 respectively.

Table 5.5 *Initial liquid concentrations used to simulate models for site trials at Risley (mg/l).*

		Cell 2			Cell3		
Elements	Site leachate	Top layer	Clay layer	Bottom layer	Top layer	Clay layer	Bottom layer
Ca	344	4	350	1214	4	350	14
Na	2300	450	450	10802	450	450	2157
K	4730	15193	300	1761	15193	300	761
S	770	2000	500	549	9294	500	50

It had been observed that the compaction of the clay using the excavator bucket was not as good as it would have been using a roller in a full size cell. The permeability of the clay layer was therefore unknown and was estimated from the observed loss of volume of leachate. All the material data (e.g. concrete permeability, diffusion and adsorption) was obtained from laboratory observations. It may be seen that the observations generally lie within the standard error bars for the computer model. In the case of Sulphur more experimental results are being processed in due course.

Fig. 5.12: Modelled and experimental 'Ca' concentration Vs. time at different levels in site trial cell no. 2.

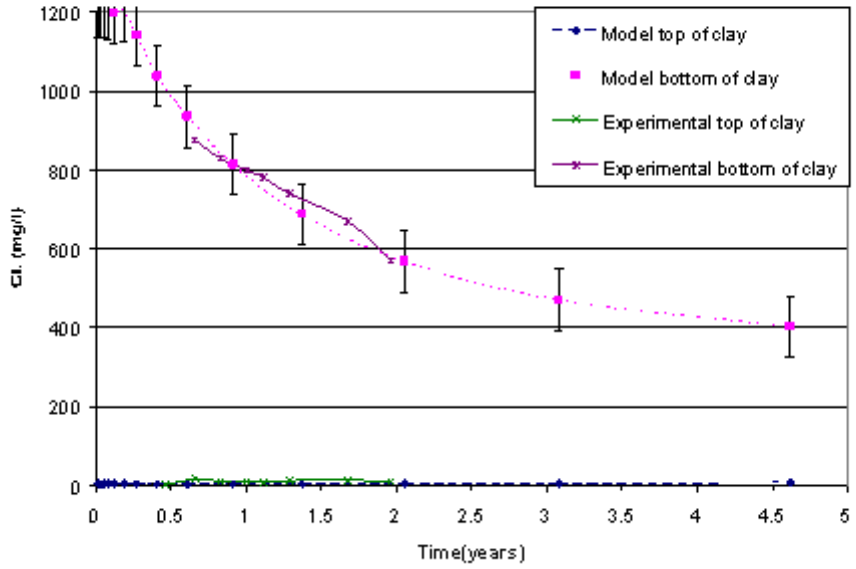

Fig. 5.13 : Modelled and experimental 'Na' concentration Vs. time at different levels in site trial cell no. 2.

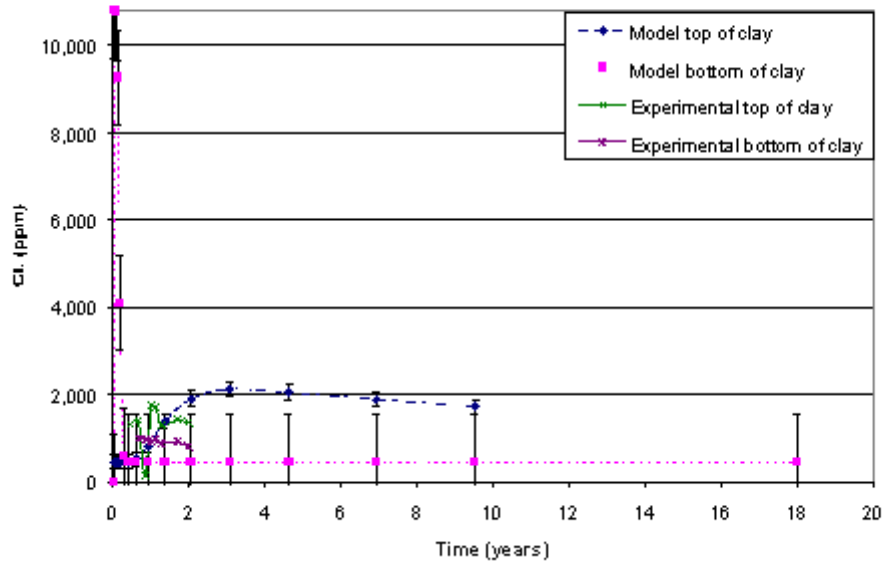

Fig. 5.14 : Modelled and experimental 'K' concentration Vs. time at different levels in site trial cell no. 2.

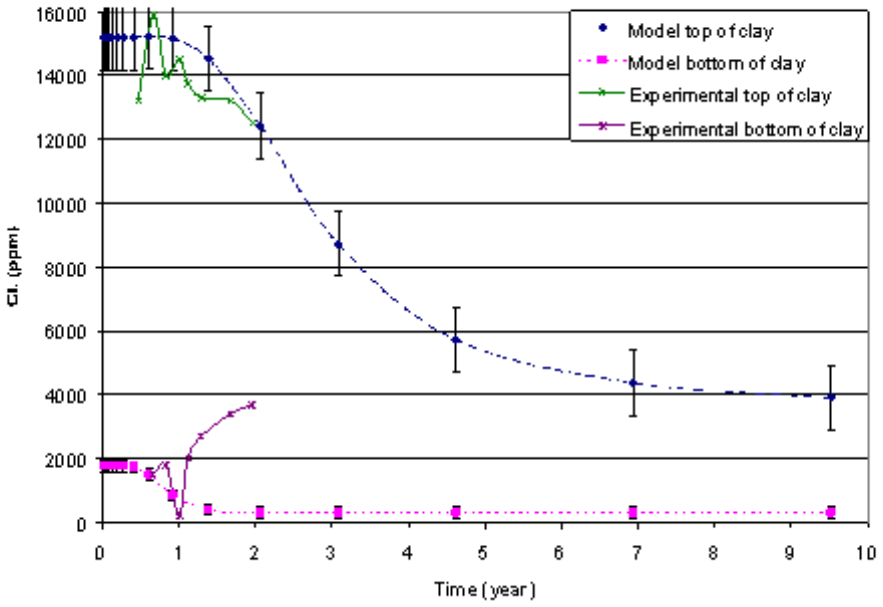

Fig. 5.15: Modelled experimental 'S' concentration Vs. time at different levels in site trial cell no. 2

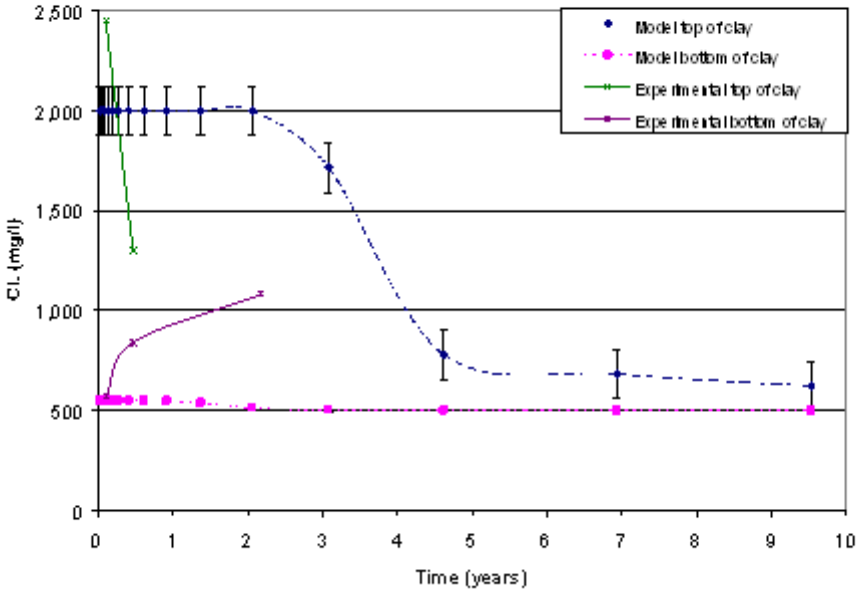

Fig. 5.16 : Modelled and experimental 'Ca' concentration Vs. time at different levels in site trial cell No. 3.

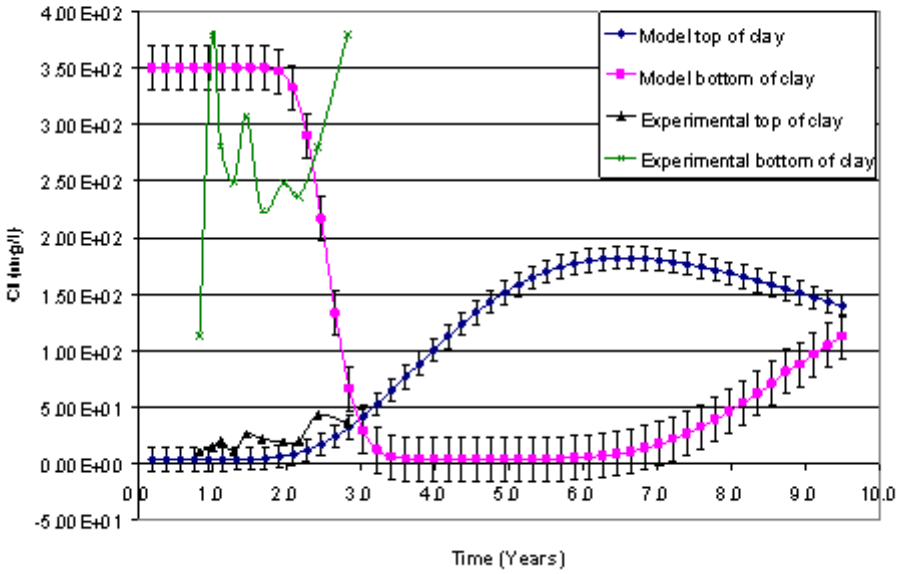

Fig. 5.17: Modelled and experimental 'Na' concentration Vs. time at different levels in site trial cell No. 3.

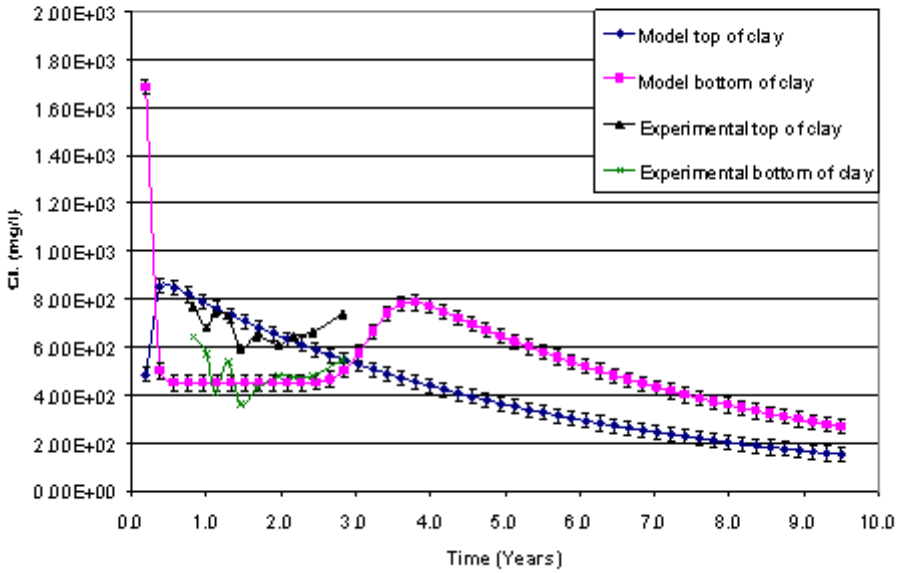

Fig. 5.18 : Modelled and experimental 'K' concentration Vs. time at different levels in site trial cell No. 3.

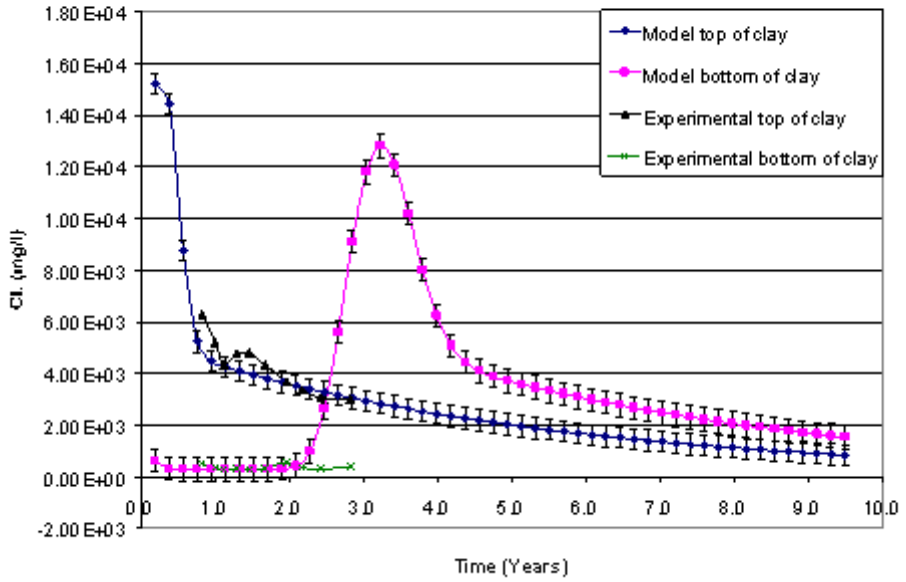

Fig. 5.19: Modelled and experimental 'S' concentration Vs. time at different levels in site trial cell No. 3

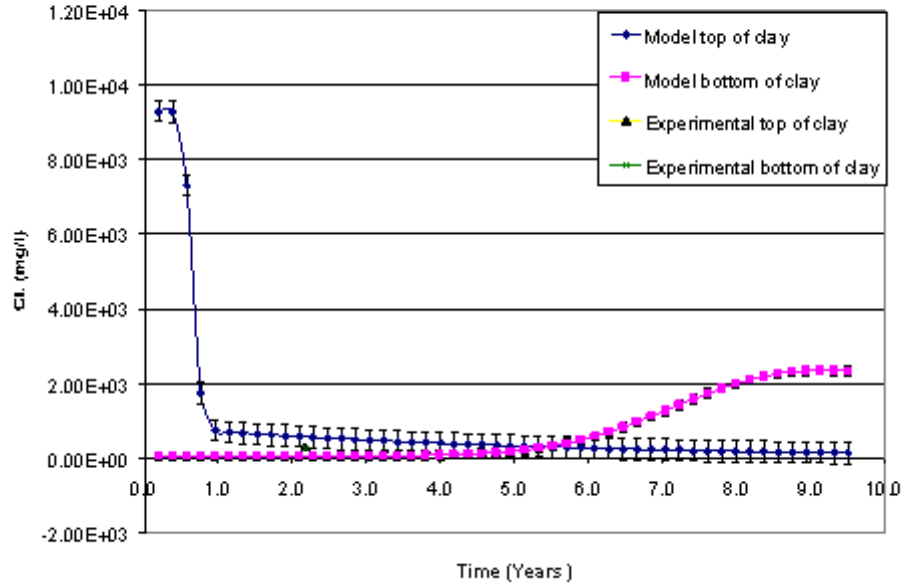

6 PHYSICAL STABILITY OF THE BARRIER

The barrier is a 300mm thick layer of concrete with a characteristic strength of 3 MPa (target mean of 5 MPa) in unconfined compression and a density of 2300 kg/m^3. A density of 1500 kg/m^3 for the waste has been assumed.

Three different locations for the barrier are considered:

Horizontal
30 degree slope
Vertical

Horizontal Barrier

In a horizontal barrier the mode of failure would be shear due to local compression of the substrate. The possibility of cracking caused by general compression of the substrate resulting in progressive bending and slight tensile strain in the barrier is not considered to be a failure and has been considered elsewhere in this report. The direct compression of the barrier due to the waste load will be just 0.75 MPa at 50 m depth.

Severe local failure shall be prevented by following the procedures in the construction quality assurance plan which is given in chapter 7.

30 degree slope

For the purposes of this design a slope length of 50m is considered giving a depth of 25m.

On a slope the mode of failure would be slippage in which the barrier slides down and causes buckling or compressive failure near the bottom.

Buckling will only be possible during the waste emplacement phase because there will be lateral restraint once the waste is consolidated into place.

The mass of the barrier per m of width will be 34,500 kg. Assuming no friction with the substrate this will give a load of 172 kN at the base resulting in a stress of 0.57 MPa. For 3 MPa concrete this will be well below the threshold for buckling.

When the waste is emplaced there will be a mass of 811,000 kg of waste above the barrier slope. If the very conservative assumption is made that there is no slippage of the waste above the liner (very high friction) and the shear strength of the clay under the liner is 50 kPa this will give a stress of 5MPa in the concrete.

Vertical Barrier.

This barrier would not actually be absolutely vertical. An inclination of, possibly, 3 degrees towards an existing slope would be used to give stability during the emplacement phase. The mode of failure would be by compression at the base. A 25m high barrier would have a mass of 11,250 kg per m width giving a stress 0.37 MPa which is insufficient to cause compression or buckling failure.

CONSTRUCTION QUALITY ASSURANCE PLAN FOR POPLARS LANDFILL SITE

The construction quality assurance plan prepared by Biffa waste services Limited are given in the following pages.

8 QUALITY ASSURANCE

This section describes the proposed quality assurance procedures for the concrete barrier. All other aspects of the works shall follow the quality procedure for a geosynthetic barrier system which is included in chapter 7.

1. The concrete shall be mixed and placed by contractors who have previous experience with large volume concrete construction.

2. Materials for the barrier shall be supplied from organisations with QA procedures and shall be supplied with QA documentation recording their production history. Water will be from main supply.

3. Materials shall be tested for consistency by recording strengths of trial concrete cubes (or other approved method) at a rate of one set of 3 cubes from every 300 Tones of material.

4. The materials for the concrete production will be stored on a clear level surface. All hydraulic materials (e.g. Cement Kiln Dust) shall be kept dry and used in rotation.

5. The contractor shall demonstrate the accuracy to which the materials will be proportioned in the mix. Trial mixes shall be made at the extremes of these ranges and tested for strength and permeability.

6. Prior to placing any barrier a 500 m^2 trial pour will be carried out on a roadway and also on a 30 degree slope.

7. The concrete may be placed directly onto the substrate.

8. The contractor shall use an approve method of placing the concrete to achieve an average thickness of 300mm and a minimum of 230mm. The thickness shall be determined by survey before and after placing at a rate of one set of levels every 50 m^2. The modelling

has been based on a coefficient of variation of 15% indicating that for a 300mm layer only 95% of the observations should show a thickness within 72mm of the mean.

9. The concrete shall be compacted with a vibrating screed. No special precautions shall be required for day-joints. Stop-ends shall not be required and the concrete shall be permitted to rest at its angle of repose.

10. A set of 3 concrete cubes shall be made to EN12390 part 1 from each 100 m^3 of concrete and tested for strength to EN 12390 part 3. The minimum mean unconfined compressive strength will be 5 MPa and the maximum standard deviation shall be 1.2 MPa.

11. One sample shall be tested for permeability from each 300 m^3 of concrete. Permeability may be measured to EN12390 part 8 if accompanied by an approved method of calculation to yield results in m/s or another test (such as the high pressure test used by Coventry University) may be used to give the results directly. The maximum mean permeability shall be 5×10^{-9} m/s and the maximum standard deviation shall be 2×10^{-9} m/s.

12. One sample shall be tested for diffusion/adsorption every 1000 m^3. The maximum permitted values for each element shall be determined from the transport model.

13. In hot conditions with direct sunlight or strong wind curing by water spray shall be applied for the first 24 hours.

14. The contractor shall determine when the concrete has sufficient strength for waste emplacement. Any concrete that is damaged by waste emplacement shall be replaced or overlaid.

9 WORK IN PROGRESS

This programme is funded until Autumn 2004 and we aim to provide all of the necessary technical input for regulatory approval by then.

Our initial work plan is:

- Respond to input from the EA
- Refine the input data to the Coventry model to provide a better explanation of the 8m trial cells and use this data to improve the modelling of the 100m cell.

Extend the application of PHREEQE to provide increased experimental validation.

PART 2 THE 300mm BARRIER FOR THE POPLARS SITE

10 INTRODUCTION

10.1 General Description

Location of proposed barrier

Poplars landfill site at Cannock (a Biffa site).

Current Barrier System in use at the site

This is a clay site where the owners currently only use "Bentomat" (this consists of layers of fabric with bentonite powder between them and is about 20mm thick) on top of milled and compacted layers of existing clay. Geotextiles are then used to protect the Bentomat. The novel barrier is proposed as an alternative.

Basic Design

A 300mm layer of concrete on the clay. Note that this simple design has been chosen for this particular site but much of our research relates to multi-layer systems intended for less secure sites.

Construction Method

One hectare (10,000 m2) of barrier this will need 3000 m3 of concrete. A pump will be used and target placing rates should be at least 200m3 per day.

There is plenty of space to stockpile material before starting mixing.

10.2 Mix design

A candidate mix design for the proposed barrier is made up of the materials given in table 10.1.

Material	Kg/m3	Total quantity Tonnes
Cement Kiln Dust	150	450
Steel slag Dust (0-5mm)	700	2100
Conditioned ash	150	450
Shell sand	700	2100

Table 10.1: *Candidate materials proposed for use in Poplars site.*

11 TRANSPORT MODELLING

11.1 Results from the CU model

Mix number two (i.e. CKD and ROSA) of the candidate mixes given in section 2.2.4 (table 2.7) is selected for modelling transport in the new barrier in the Poplars site. For this site a 300 mm thick mortar mix with 500 mm thick clay layer is proposed. However an 800 mm thick clay only and 300 mm mortar only barrier was also analysed.

Figures 11.1 to 11.4 shows the cumulative concentration of different elements by time. As it can be seen 300 mm mortar layer performs same or better than mortar plus clay barrier (this is due to the extra head being generated by clay layer and as this is advection driven transport it gives higher concentrations) and without an exception clay layer only barrier performs worst for the elements considered.

By keeping the head constant for all different types of barriers in the CU model, the cumulative concentration of different toxic elements (i.e. As, Pb, Zn and Hg) by time is shown in figures 11.5 to 11.7 respectively. The geosynthetic clay barrier is also included in these analyses. As theses figures show the mortar or mortar clay barriers perform better than GCB as its thickness is much less and in the advection driven transport that would have immense effect on rate of transport. The break through time and steady state rate of these toxic elements together with some of their 10^{th} and 90^{th} percentiles for these layers are given in table 11.1 A 300 mm DBM asphalt layer is also included in table 11.1.

The concentrations assumed above the liner are those in the ‘hit list’ solution used in our laboratory work and well above any found in a normal landfill.

The statistical terms shown in table 11.1 are worked on the following Standard Deviations values: Alpha (α) for mortar 50, diffusion coefficient (D) 4, coefficient of permeability (k) 3.165 and thickness 15. These SD values were derived from experimental values obtained from laboratory experiments. For the coefficient of permeability 26 twin samples of similar strength were tested at same pressure and sizes to determine the SD for coefficient of permeability.

Table 11.1: Break through time and Steady state rate of some toxic elements for 2 layer barrier using mixes 2 and 3 in table 2.7.

Type of layers	Elem-ents	Assumed concentration above the barrier (mg/l)	Break through time (Years)	Break through time percentiles		Rate at 160 years (mg/m^2/year)	Rate percentiles	
				10th	90th		10th	90th
300 mm mortar and 500 mm clay	As	454	92.2	30	151	6.6	0.13	13.6
	Zn	395	120.7	64	156	2.3	0.0	10.5
	Pb	400	155.6	63	142	4.4	0.1	10.5
	Hg	600	147.2	71	154	0.4	0	15.9
800 mm clay only	As	454	0.5	0.17	1.57	32.2	13.5	79.4
	Zn	395	0.5	0.17	1.57	28.0	12.1	66.6
	Pb	400	0.6	0.17	1.57	28.4	12.1	67.0
	Hg	600	0.6	0.17	1.57	42.6	18.6	99.1
300 mm mortar	As	454	74.2	21	150	8.1	0.32	21.3
	Zn	395	112.2	0.0	157	4.6	0.0	18.3
	Pb	400	283.6	39	140	7.1	0.27	18.3
	Hg	600	144.4	50	155	3.0	0.0	28.1
30 mm GCB and 500 mm clay	As	454	12.7	3.3	20.7	5.3	2.6	13.6
	Zn	395	9.9	13	104	4.6	1.6	10.7
	Pb	400	44.2	4.1	21.5	4.7	1.8	10.5
	Hg	600	24.3	8.1	53	7.0	2.8	16.0
300 mm DBM asphalt	As	454	64.0			0.081		
	Zn	395	98.8			0.064		
	Pb	400	101.2			0.067		
	Hg	600	94.4			0.093		

Fig. 11.1 : Modelled 'Ca' concentrations for multi layer and clay only barriers using site leachate.

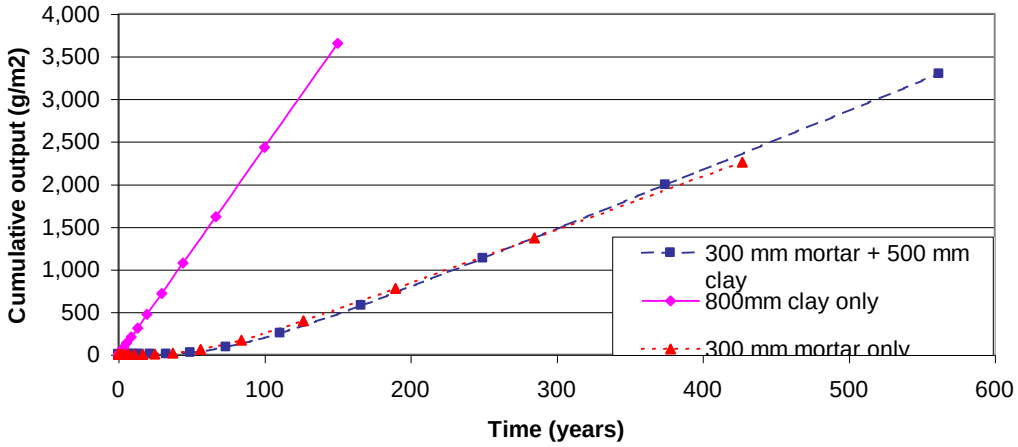

Fig. 11.2: Modelled 'Na' concentrations for multi layer and clay only barriers using site leachate.

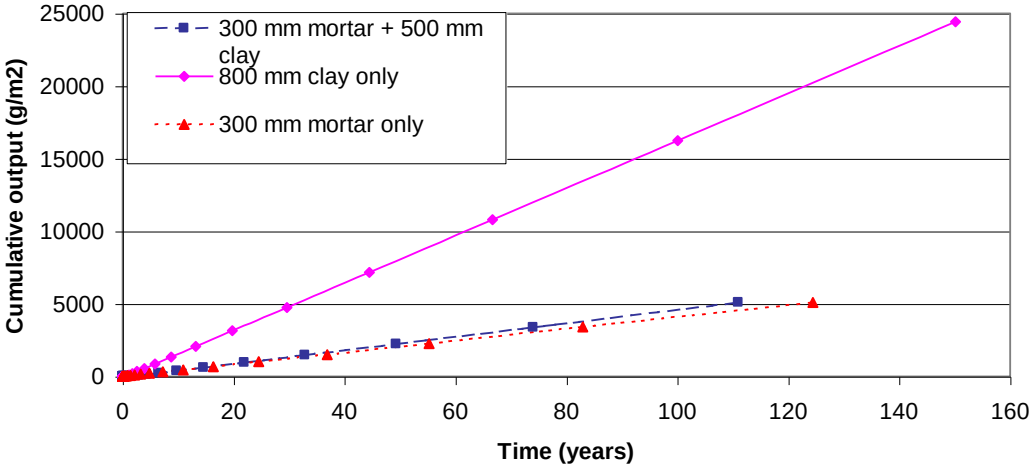

Fig. 11.3: Modelled 'K' concentrations for multi layer and clay only barriers using site leachate.

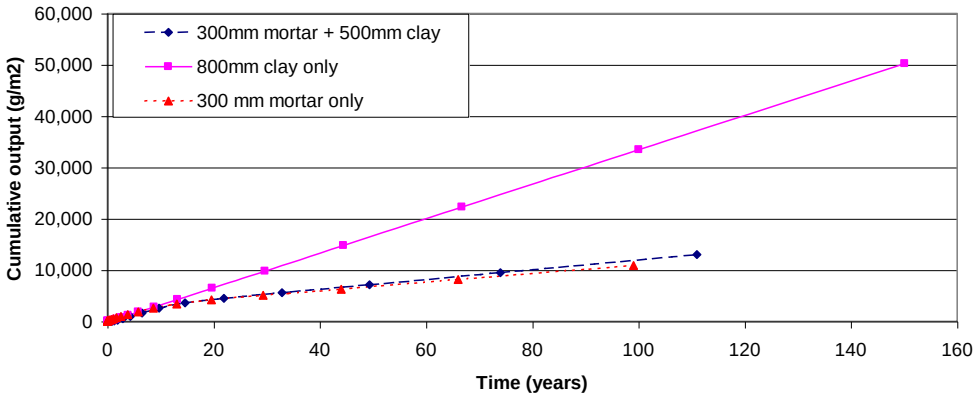

Fig. 11.4: Modelled 'S' concentrations for multi layer and clay only barriers using site leachate.

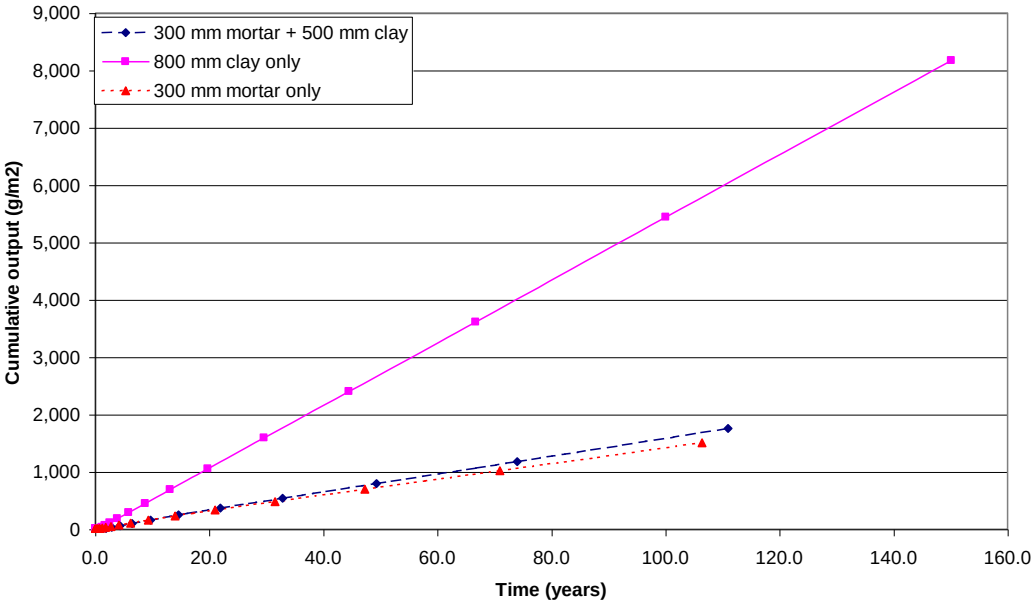

Fig. 11.5: Modelled 'As' concentrations for multi-layer and clay only barriers using toxic leachate.

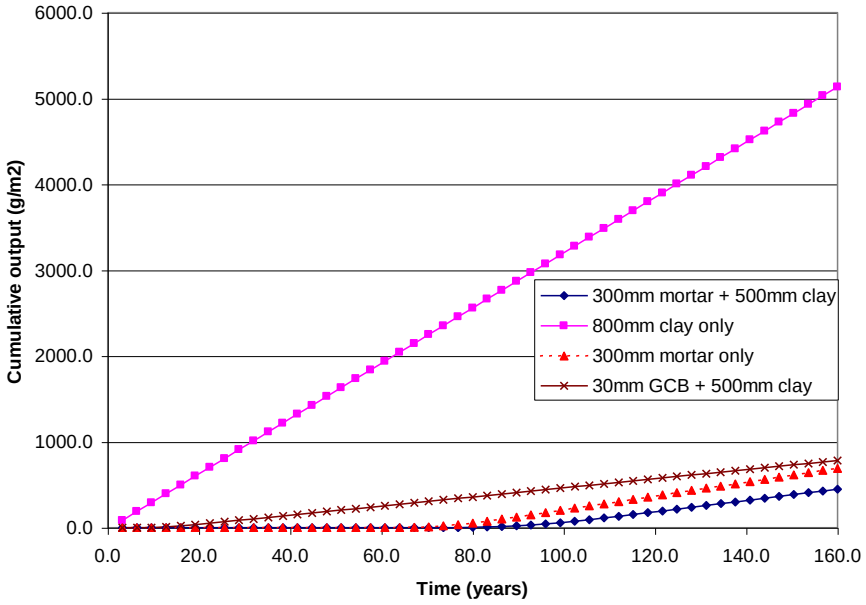

Fig. 11.6: Modelled 'Pb' concentrations for multi-layer and clay only barriers using toxic leachate.

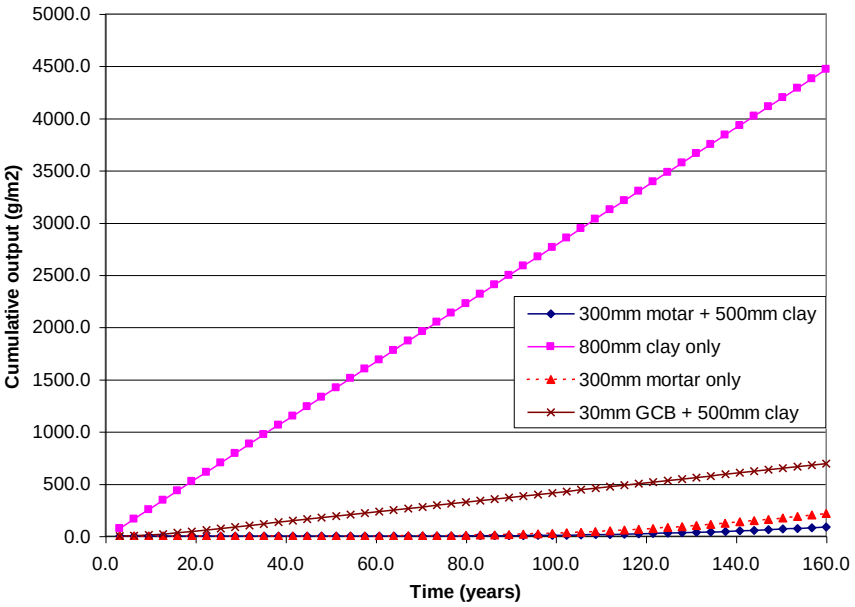

Fig. 11.7: Modelled 'Hg' concentrations for multi-layer and clay only barriers using toxic leachate.

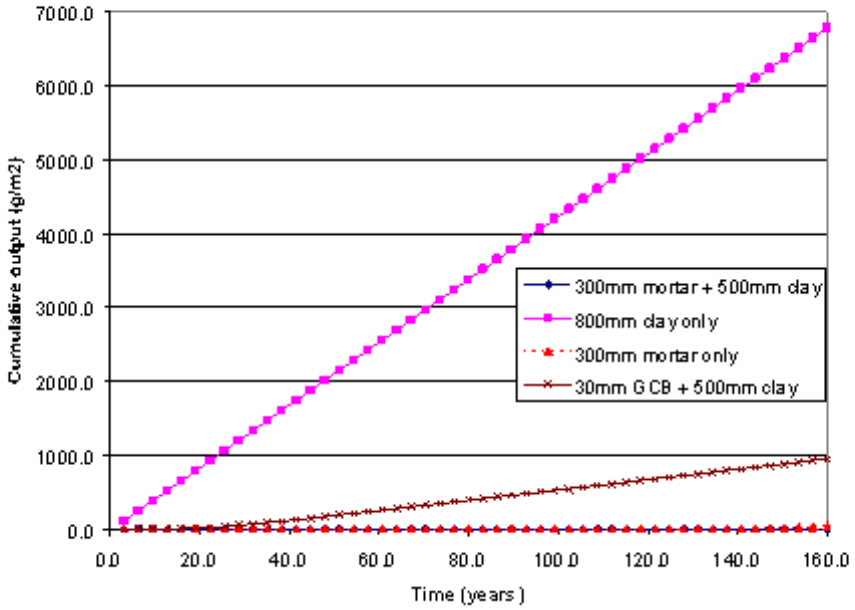

11.2 Results from PHREEQE

The initial calculations concerning modelling the binder at the Poplars site considered the action of a slightly oxidised, acetogenic leachate typical of the early stage of landfill evolution. Whist this has moderate impact on the binder materials, its high redox potential has a major impact on the speciation of the transition metals in solution. Many are both amphoteric and redox sensitive and their concentration in solution will very much be dependent on their chemical environment. This effect has been seen in the experimental site trials at Risley, where after approximately one year, the concentration of lead falls by a factor of four:

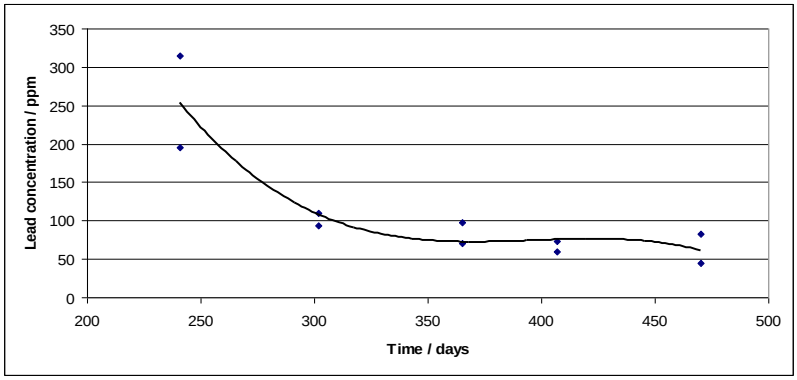

Figure 11.8 *Evolution of lead concentration in upper layer concrete pore solution as a function of time. Risley experimental site, Cell 2*

For this reason, the leachate composition at the Poplars site will be considered as exclusively anoxic, with an pe of –8 (equivalent to an E_H of –473 mV). Considering the leachate composition at Poplars, relatively few toxic metal species are reported present in the leachate; indeed, previous modelling has used the UK default inventory and concentration, supplied with the risk assessment code "Landsim". For the purposes of modelling the likely performance of the proposed barrier, the following composition is used (Table 11.2). This is based on the Poplars leachate composition (where available) and other elements have been added in order to examine their likely transport through the barrier. It must be stated however that such a leachate would not be expected to exist under any circumstances; it simply serves to illustrate the effect of chemical environment on the speciation of these elements. The major ions however are realistic, but at the upper levels of concentration which might be expected to prevail in a landfill leachate.

	Concentration		Present at Poplars?	Notes
	ppm	Molal		
As	1.310	1.78E-05		Maximum estimate in UK 'default' leachate *
Ca	420	1.048e-002		No concentration reported at Poplars. Estimate
Cl	7760.000	2.22E-01	Yes	Maximum estimate in UK 'default' leachate *
Cr	1.750	1.53E-05		Maximum estimate in UK 'default' leachate *
K	3120.000	8.11E-02		Maximum estimate in UK 'default' leachate *
NH4	3640.000	2.64E-01	Yes	Maximum estimate in UK 'default' leachate *
Na	1000.000	4.42E-02		No concentration reported at Poplars
P	22.600	7.41E-04		Maximum estimate in UK 'default' leachate *
Pb	1.020	5.00E-06		Maximum estimate in UK 'default' leachate *
S	100.000	1.06E-03		No concentration reported at Poplars. Estimate
Zn	208.000	3.23E-03	Yes	Only 0.433 ppm reported at Poplars

Table 11.2 *Leachate composition used in Poplars simulation*

** The "UK Default Leachate Inventory and Concentration" is taken from the software package'Landsim' and represents a reasonable estimate of leachate chemistries based on UK experience. The values reported here are maxima and represent an extreme case; it is most unlikely that all these elements would be present in any single leachate*

The Poplars leachate also contains mercury, cadmium, nickel and copper ions all of which are highly toxic. It was not practical to simulate coupled chemical transport of all elements in the same solution, owing to the complexity of their interactions. In order to scope their likely behaviour in the cementitious barrier, batch calculations were performed, in which the leachate (above) additionally containing these four metals, was equilibrated with the cement hydrates. The concentrations of Hg, Cd, Ni and Cu was in excess of 1E-5 molal at which concentration, each is under the control of a solubility limiting phase.

Table 11.3 illustrates the predicted chemistry of the surface layer of the upper concrete proposed for the Poplars site, in contact with such a leachate. Each of the transition metals is under the control of a sparingly soluble salt, such that whilst the alkaline and reducing environment persists, its concentration will be governed by that compound. In the event of conditions changing, such as a reduction in pH, the speciation and solubility of the elements will also change. It is for this reason that a large alkaline reserve in a low permeability barrier is important in ensuring maximum retention of metals in a mineral barrier such as this.

	Solid phase chemistry				Pore solution	
*	**Phase**	**Quantity**	**Description**		**Element**	**Concentration**
	C3AH6	1.22E+00	Ca3Al2(OH)12		NH3	2.64E-01
	Calcite	4.60E+00	CaCO3		Acetate	2.00E-01
Cd	CdS	9.50E-07			CO3	9.09E-02
Cu	Chalcocite	9.04E-06	Cu2S		K	8.11E-02
Hg	Cinnabar	9.88E-09	HgS		Na	4.42E-02
	CSH(1.1)	3.48E+01	Ca1.1SiO7H7.8		Ca	4.32E-02
	Ettringite	9.51E+00	Ca6Al2(SO4)3(OH)12:20H2O		S	5.85E-03
P	Hydroxylapatite	2.47E-04	Ca5(OH)(PO4)3		Cl	5.01E-04
Mg	M4AH10	1.67E+00	Mg4Al2O7:10H2O		As	1.78E-05
Pb	Pb	5.00E-06	Colloidal lead		Si	3.32E-06
	Portlandite	4.37E+01	Ca(OH)2		Al	1.15E-06
	Tricarbo	3.05E+00	Ca6Al2(CO3)3(OH)12:24H2O		Mg	1.63E-08
	Trichloro	4.62E-02	Ca6Al2Cl6(OH)12:24H2O		Pb	5.48E-09
Ni	Vaesite	3.83E-05	NiS2		P	2.15E-11
Zn	Wurtzite	3.23E-03	ZnS		Zn	5.19E-13
Cr	ZnCr2O4	7.67E-06	Zinc Chromate		Ni	1.05E-13
*	Solubility limiting phase for specific element				Cr	2.51E-15
					Cd	1.07E-21
	Notes on cement hydrate nomenclature:				Cu	7.36E-24
	M4AH10 is hydrotalcite-like phase = Magnesium sink in cements				Hg	6.33E-42
	C3AH6 is hydrogrossular				pH	12.43

Table 11.3 *Predicted leachate composition after conditioning by cement hydrates in the Poplars barrier*

Considering next, the persistence of alkaline conditions in the barrier, coupled chemical transport modelling is used to simulate reactions of the cement hydrates as leachate permeates the barrier:

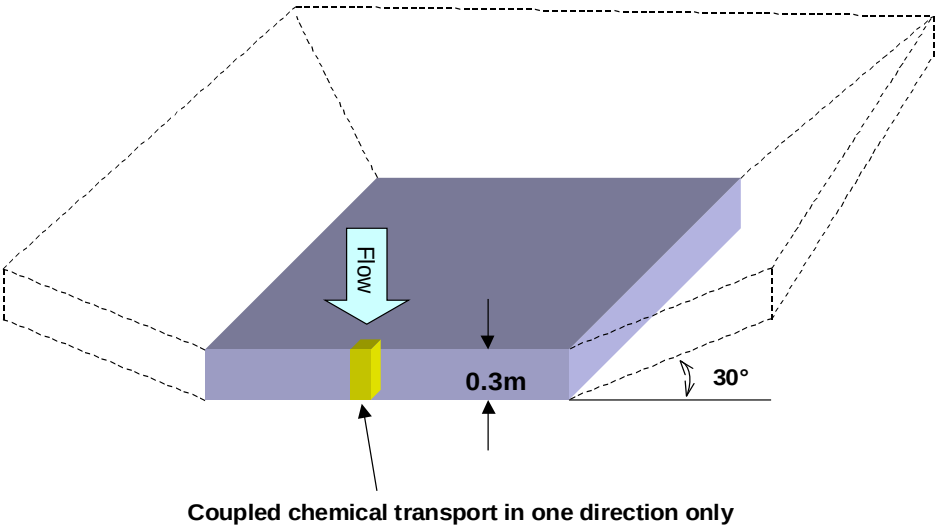

Figure 11.9 *Flow path through the barrier simulated by coupled chemical-transport modelling. At 0.3m thick, the surface are occupied by* $1m^3$ *of liner is* $3.3m^2$*. At a permeability of* $1e^{-9}$ ms^{-2}*, this suggests a solution transfer rate of 0.3 litres per square meter per year*

Two geometries have been simulated, the 300mm concrete barrier in isolation and the barrier underlain by 800mm of compacted local clay. This latter reflects that much of the Poplars site is covered by made ground, as the area has had a number of industrial uses extending back into the nineteenth century. Much of the surface contains demolition waste from previous uses of the land, so a compacted clay layer underlying any liner system emplaced on this site is considered essential.

Considering first, the single cementitious barrier with no underlying clay. The hydrate assemblage is as shown below along with its pore solution composition.

Solid phase assemblage			Pore solution chemistry	
Phase	**Moles / dm^-3**		**Element**	**Concentration / molal**
Calcite	9.55E+00		Al	9.97E-06
CSH(1.1)	3.48E+01		As	3.30E-10
Cu	3.59E-11		C	8.14E-06
Ettringite	9.51E+00		Ca	1.19E-02
M4AH10	1.67E+00		Cl	1.17E-02
Monocarb	5.20E-02		Cr	5.74E-15
Monochlor	3.04E+00		Cu	7.38E-12
Portlandite	4.37E+01		K	8.93E-06
ZnCr2O4	9.78E-13		Mg	3.87E-09
			Na	2.87E-06
			Ni	3.78E-10
			Pb	2.70E-09
			S	1.11E-05
			Si	4.48E-06
			Sr	4.63E-11
			Zn	3.75E-10
			pH	12.429

Table 11.4 *Solid and liquid phase chemistry of the Poplars concrete barrier before reaction with leachate. Note that the transition metal content reflects analytical values determined at the Risley site trial*

The leachate described in table 11.2 was allowed to elute through the mortar, maintaining equilibrium with those phases above and with new substances, where appropriate. A total path length of 0.3m was simulated as thirty cells and run times simulating 200 years were around three hours (P4, 2.33GHz PC). This allowed both the spatial distributions of transition metals within the barrier and the evolving phase and pore solution chemistry to be simulated.

The graphs shown in figures 11.10 and 11.11 show the predicted spatial distributions of dissolved species moving through the porous barrier.

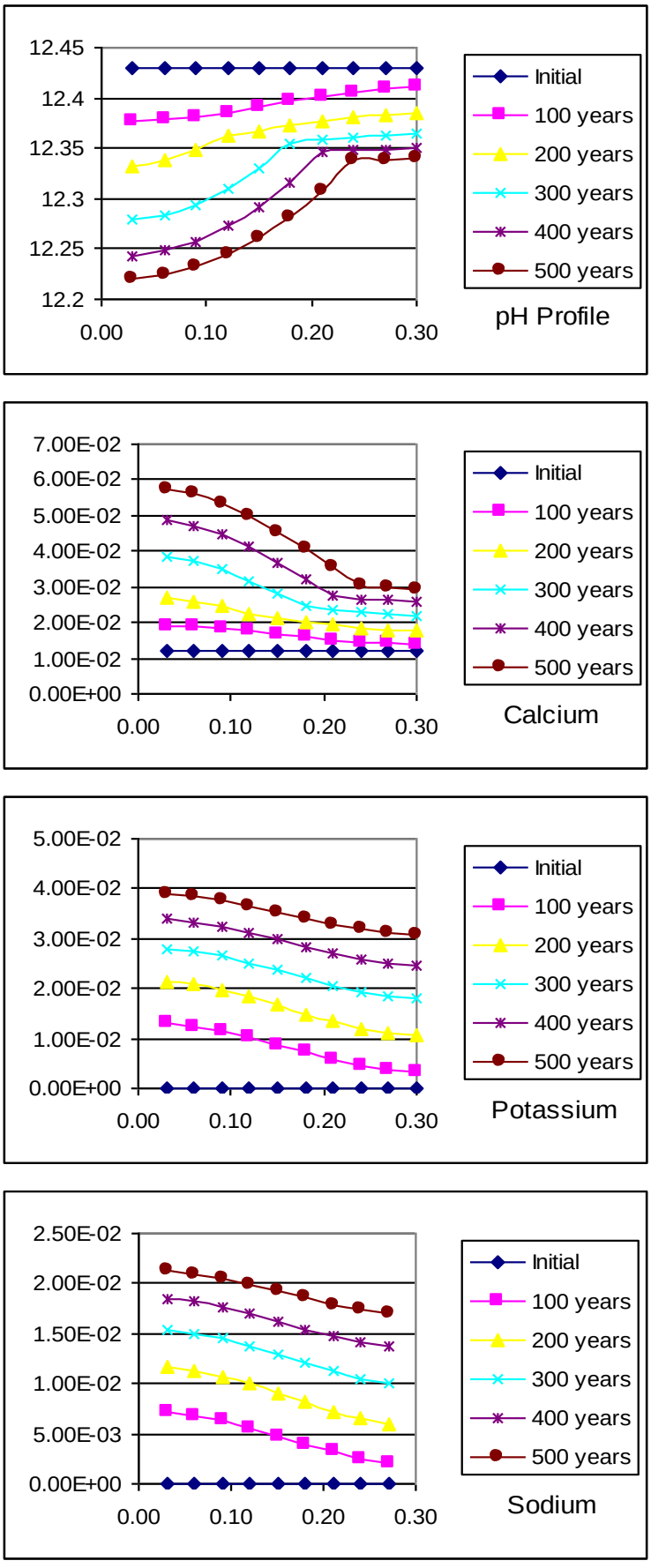

Figure 11.10 *Ingress of sodium, potassium and calcium ions into the Poplars liner. These graphs show molal concentrations (vertical axes) against distance through the barrier in metres, where the left of each graph is the top of the liner*

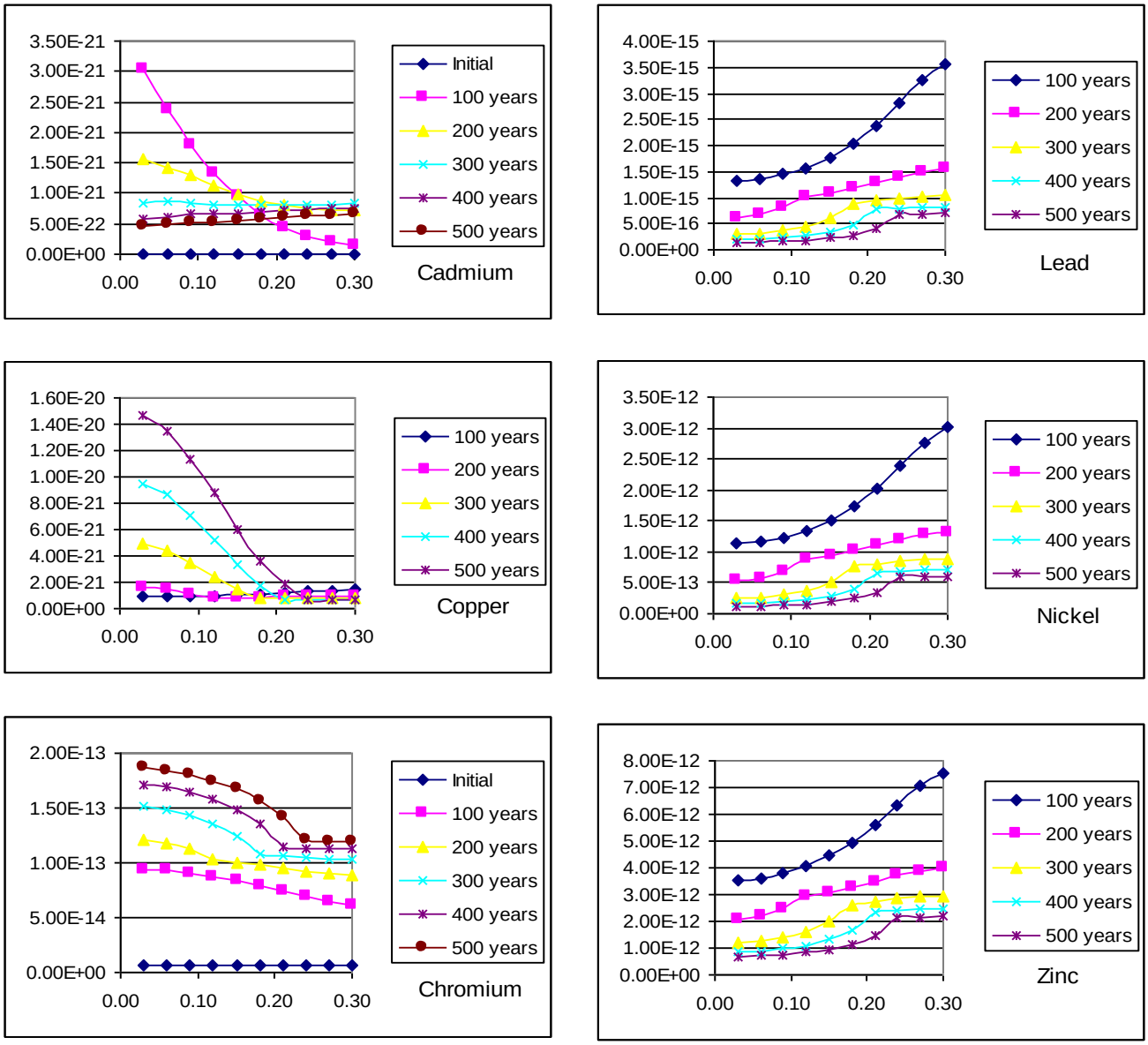

Figure 11.11 *Ingress and retention of transition metal species in the Poplars liner. These graphs show molal concentrations (vertical axes) against distance through the barrier in metres, where the left of each graph is the top of the liner*

Sodium and potassium move conservatively through the liner, where as the transition metal distributions are governed by solubility limiting phases, as shown in table 11.3. Continued simulation of these systems, excluding the many possible transition metal compounds which may influence their distributions, allows a prediction to be made about the integrity of the

liner. Of paramount importance, is the ability of the system to precipitate metals from solution. As leachate continues to elute through the binder system, it sequentially dissolves solid phases from the mineral hydrate assemblage. Table 11.5 and figure 11.12 show the order in which the alkaline reserve will be exhausted. Whilst these simulations attempt a rudimentary transport calculation, they are intended to as the understanding of multiphase chemistry, rather than problems in hydraulics. The simplifications of the transport algorithms require the user to use a single diffusion coefficient for all species, but more importantly, define a transport rate, rather than permeability. As a result, changes in permeability must be modelled by scoping the transport parameters appropriately. It is important to realise therefore that temporal predictions about the later changes in system chemistry must be treated with some caution, as dissolution of, for example portlandite, will have implications for the permeability and hence subsequent transport in these materials.

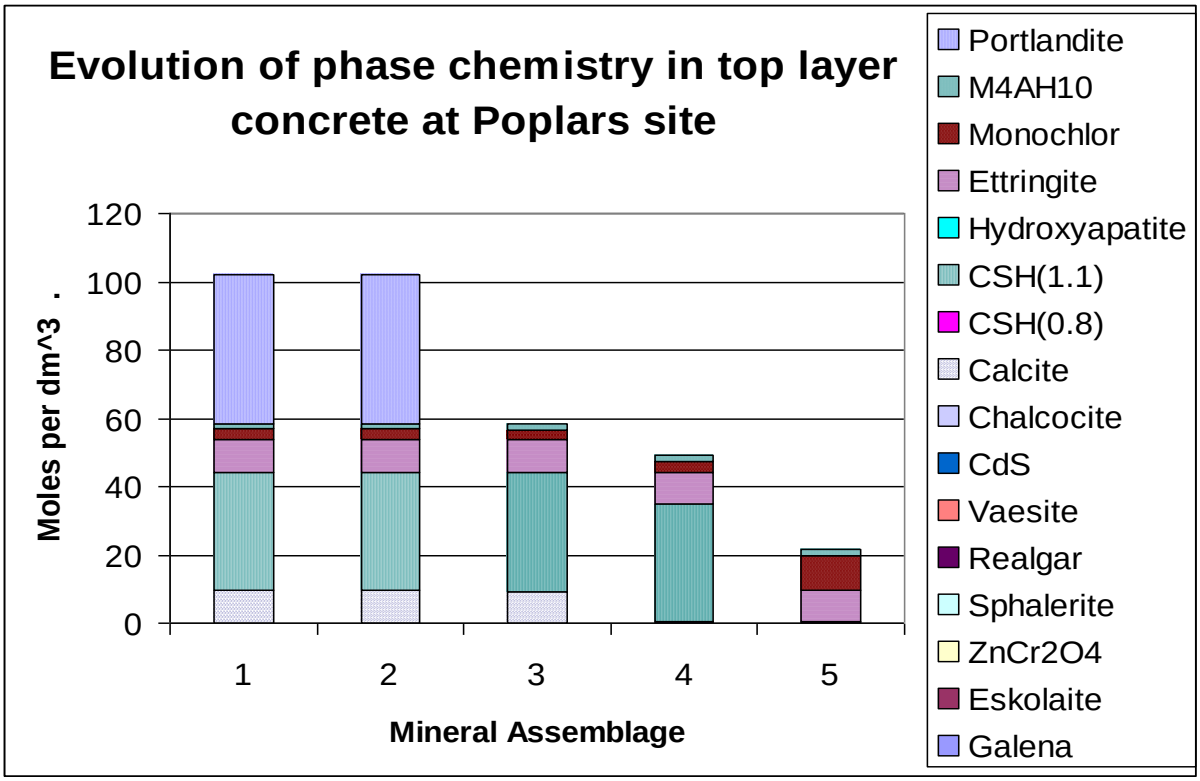

Figure 11.12 *Evolution of the binder phase chemistry is determined bay a relatively small number of phases which dissolve sequentially. This sacrificial action maintains the alkalinity of the local chemical environment and establishes a sequence of stable mineral assemblages.*

In the later stages of evolution, the solution pH falls from above 12 to around 10, with significant changes in speciation and implications for ion mobility. Nonetheless, coupled chemical transport calculations show that a period in excess of 1,300 years is necessary even to dissolve the portlandite fraction of the solid. The subsequent transition from phase assemblage 3 to assemblage 4, does not result in a massive release of the metal fraction, as there remains a considerable quantity of CSH gel, maintaining the alkaline reserve. Once this phase also dissolves, there remains only one third of the original solid (!) yet the alkalinity of the system is predicted to exceed pH 9.7, three orders of magnitude above the incoming leachate. Simulations of material behaviour over time scales of millions of years are to say the least, highly speculative, but it is important to appreciate the design theory underlying this approach is sound. Engineering sufficient alkaline reserve to influence the local chemical environment, even when two thirds of the starting material has been dissolved, ensures the reactive barrier will remain effective long into the future.

	Order of stable mineral assemblage Moles per dm3 of pore solution					
Phase	**1st**	**2nd**	**3rd**	**4th**	**5th**	
Galena	5.00E-06	1.00E-05	1.50E-05	2.00E-05	2.50E-05	PbS
Eskolaite				3.07E-05	3.84E-05	Cr2O3
ZnCr2O4	7.67E-06	1.53E-05	2.30E-05			
Sphalerite	3.23E-03	6.45E-03	1.15E-04	1.53E-04	1.91E-04	ZnS
Realgar			9.68E-03	1.29E-02	1.62E-02	AsS
Vaesite	3.83E-05	7.66E-05				NiS2
CdS	9.50E-07	1.90E-06	2.85E-06	3.80E-06	4.75E-06	
Chalcocite	9.04E-06	1.81E-05	2.71E-05	3.62E-05	4.52E-05	Cu2S
Calcite	9.50E+00	9.44E+00	9.33E+00			CaCO3
CSH(0.8)			8.63E-02	3.89E-01	3.88E-01	Ca0.8SiO5H4.4
CSH(1.1)	3.48E+01	3.48E+01	3.47E+01	3.44E+01		Ca1.1SiO7H7.8
Hydroxylapatite	2.47E-04	4.94E-04	7.42E-04	9.89E-04	1.24E-03	Ca5(OH)(PO4)3
Ettringite	9.50E+00	9.50E+00	9.50E+00	9.47E+00	9.44E+00	Ca6Al2(SO4)3(OH)12 :20H2O
Monochlor	3.06E+00	3.06E+00	3.06E+00	3.09E+00	9.98E+00	Ca4Al2O6Cl2:10H2O
M4AH10	1.67E+00	1.67E+00	1.67E+00	1.67E+00	1.67E+00	Mg4Al2O7:10H2O
Portlandite	4.36E+01	4.35E+01				

Table 11.5 *Predicted phase quantities available to interact with 1dm3 of pore solution during the evolution of the barrier proposed for the Poplars site.*

The solution chemistry is shown in figure 11.13 and is expected to remain relatively constant for some thousands of years.

Considering the release of toxic transition metals, many remain under the control of a solubility-limiting phase and are predicted to remain so for a period in excess of a thousand years. Consequently, their release from the base of the barrier layer is constant, governed by dissolution of that phase into the eluting leachate. The driving force for metal release is the flow rate, as the very robust chemistry limits the concentration of these elements in any body of leachate. A simplified simulation considering only mercury, allows an interesting comparison with the conservative model predictions shown earlier in this chapter (compare figures 11.6 and 11.17).

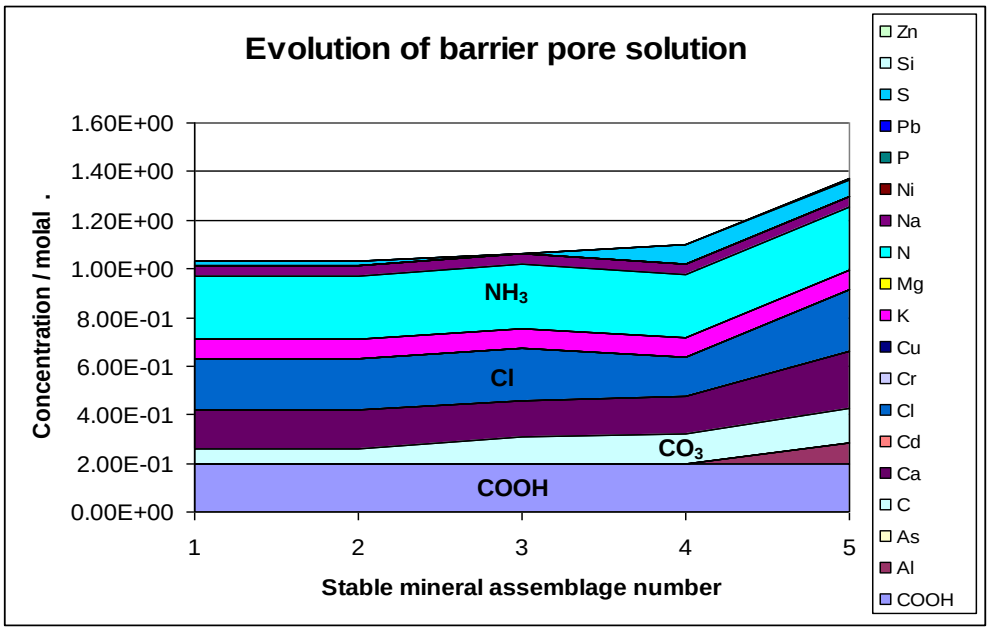

Figure 11.13 *Evolution of the pore solution chemistry as the mineral hydrate assemblages evolve through reaction with the eluting leachate.*

	Concentration in pore solution of each mineral assemblage / molal				
Analyte	**1st**	**2nd**	**3rd**	**4rth**	**5th**
COOH	1.98E-01	1.98E-01	1.98E-01	1.95E-01	1.95E-01
Al	1.68E-07	1.68E-07	8.65E-04	1.11E-03	8.69E-02
As	1.76E-05	1.76E-05	1.47E-07	5.64E-11	7.99E-12
C	6.10E-02	6.10E-02	1.09E-01	1.25E-01	1.44E-01
Ca	1.64E-01	1.64E-01	1.48E-01	1.57E-01	2.33E-01
Cd	1.83E-22	1.83E-22	3.68E-20	8.01E-23	5.60E-22
Cl	2.06E-01	2.06E-01	2.20E-01	1.62E-01	2.55E-01
Cr	2.89E-13	2.89E-13	2.93E-15	6.54E-14	2.91E-14
Cu	2.79E-19	2.79E-19	3.60E-17	5.05E-19	3.17E-18
K	8.04E-02	8.04E-02	8.04E-02	7.91E-02	7.94E-02
Mg	4.09E-07	4.09E-07	3.35E-06	3.07E-06	1.49E-06
N	2.62E-01	2.62E-01	2.62E-01	2.58E-01	2.58E-01
Na	4.38E-02	4.38E-02	4.38E-02	4.31E-02	4.33E-02
Ni	2.90E-14	2.90E-14	4.80E-15	8.48E-19	3.77E-18
P	1.80E-10	1.80E-10	7.88E-10	7.64E-10	8.63E-10
Pb	2.36E-17	2.36E-17	4.98E-18	4.80E-21	3.07E-21
S	1.93E-02	1.93E-02	1.62E-04	8.21E-02	7.17E-02
Si	3.79E-06	3.79E-06	6.56E-04	6.35E-04	1.08E-03
Zn	1.91E-14	1.91E-14	5.56E-15	9.40E-18	6.05E-17

Table 11.6 *Predicted concentration of element present in the simulated pore solutions shown above*

Attention can now be focused on the clay underlying the concrete. The Poplars site is covered with Pleistocene drift (boulder clay) described variously as sandy to chocolate brown. The excavations due to former coal workings have disturbed the natural sediments in many areas, such that a layer of made ground underlies both existing and proposed future landfill cell locations. The vadose zone, extends from ground level down to at least 11 metres, where the maximum predicted height of the groundwater may rise during rebound. This is estimated not to exceed 117m AOD. As a consequence, the proposal is to construct a simple containment

system, comprising a single layer of concrete (300mm) overlying a compacted clay layer (0.5m). The clay will be constructed of locally won sediments, devoid of large boulders and, where possible, appreciable gravel contents.

The clay mineralogy is not dominated by clay minerals, but typical of glacial till. To allow thermodynamic modelling of the clay using PHREEQC, a similar treatment was made to estimate the mineral quantities likely to be at equilibrium with each litre of pore solution. As is typical of fine grained sediments, the porosity is comparatively high at 40%, yet typically the permeability remains low, owing to the cohesive nature of the particles. This paradox is due to the geometry of the clay platelets occluding much of the unconnected microporosity, which accounts for the low bulk density of dry clay sediments. For the purposes of these calculations, the mineralogy is assumed to be as follows:

Phase	Volume fraction of rock	Volume /cm^3	cm^3 of solid	Grams of solid	Moles of solid
	per cubic metre of sediment		Per dm^{-3} of pore solution		
Montmorillonite	0.0927964	92796.43	231.991071	579.979232	1.55542119
Quartz	0.1167083	116708.3	291.770711	773.305642	12.8703445
Illite	0.1406008	140600.8	351.501995	966.632053	2.5179226
Chlorite	0.0393215	39321.51	98.3037791	289.989616	0.52175457
Albite	0.0445265	44526.52	111.3163	289.989616	1.11438883
Calcite	0.0198686	19868.61	49.6715128	115.995846	1.1589247
Kaolinite	0.1461779	146177.9	365.444631	966.632053	3.74430975
Porosity	0.4	400000	1000		

Table 11.7 *Predicted concentration of element present in the simulated pore solutions shown above*

In order to make in initial estimate of the probable pore solution chemistry of the compacted clay, it is assumed that the clay will be at equilibrium with local surface water. Three local water course (Wash Brook, Kingswood Lake and Newlands Brook) are each relatively rich in dissolved minerals; principally sodium, magnesium and calcium chloride, sulphate and

(presumably) hydrogen carbonate. The influence of these dissolved ions is relatively slight in comparison with the effect of equilibration with the minerals.

The following simplified water chemistry was assumed to be typical for the area, representing the mean composition of the three watercourses:

Analyte	Concentration mg/litre	Molality
Cl	78	2.200e-003
SO4	162	1.687e-003
Ca	92	2.296e-003
Mg	27	1.111e-003
Na	34	1.479e-003
K	5.6	1.432e-004
C (by difference)	Not reported	2.980e-003
pH	7.6	

Table 11.8 *Assumed local surface water chemistry at the Poplars site (Courtesy Biffa UK Plc)*

Equilibration of the surface water with the clay minerals, results in the following predicted phase equilibria:

Mineral	Initial quantity / moles	Final quantity / moles
Albite	1.110e+000	9.867e-001
Calcite	1.150e+000	1.035e+000
Clinochlore-14A	5.200e-001	4.732e-001
Illite	2.520e+000	2.520e+000
Kaolinite	3.740e+000	3.255e+000
Montmor-Ca	1.550e+000	2.261e+000
Quartz	1.287e+001	1.151e+001

Table 11.9 *Absolute quantities of mineral phases at equilibrium with local surface water, expressed as moles of phases equilibrated with one litre of common pore solution.*

The solution at equilibrium with the clay mineral assemblage is as shown below:

Element	Concentration / M
Al	1.100e-007
C	1.172e-001
Ca	1.948e-005
Cl	2.185e-003
K	2.100e-004
Mg	5.093e-004
Na	1.239e-001
S	1.675e-003
Si	1.088e-004
pH	8.415

Table 11.10 *Absolute quantities of mineral phases at equilibrium with local surface water, expressed as moles of phases equilibrated with one litre of common pore solution.*

At this stage, both the cementitious binder and the clay minerals are at predicted equilibrium with their pore solutions. The clay mineral solution is slightly over saturated with respect to dolomite and substituted (Na & Mg) montmorillonites, but as disequilibria are common in geological systems, no adjustment was made at this stage. The next stage is to simulate reactive transport between the concrete and clay dominated regions.

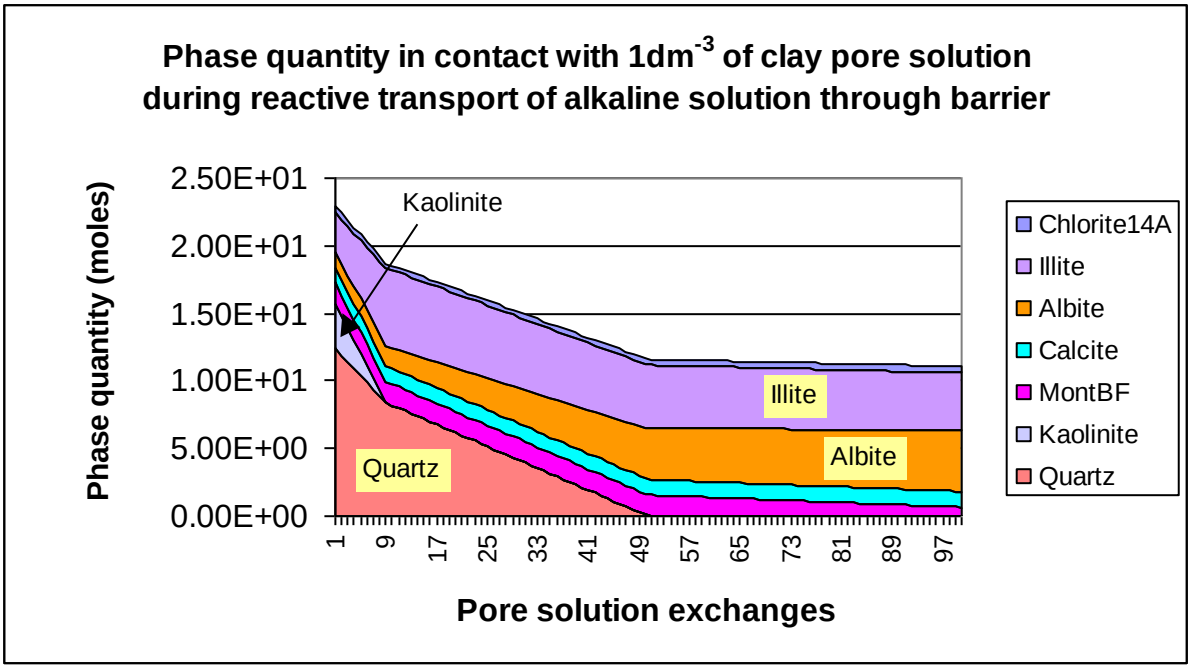

Figure 11.14 *Absolute quantities of mineral phases at equilibrium with local surface water, expressed as moles of phases equilibrated with one litre of common pore solution.*

Figure 11.14 shows the consequence of allowing alkaline, cement-conditioned pore solution to react with the clay minerals. Whilst the figure looks dramatic, centuries of construction in clay foundations demonstrates that these reactions do not rapidly react equilibrium. The sequence is well established, dissolution of quartz, raises the activity of silica in the pore solution, whilst neutralising the pH if the incoming liquid. Illitisation follows, as the silicate in solution and that liberated from the dissolving kaolinite react to precipitate more illite.

In terms of solution chemistry, figure 11.15 shows that the alkaline reserve originates from selective dissolution of portlandite in the upper layer, allowing a well-buffered, high pH solution to enter the clay.

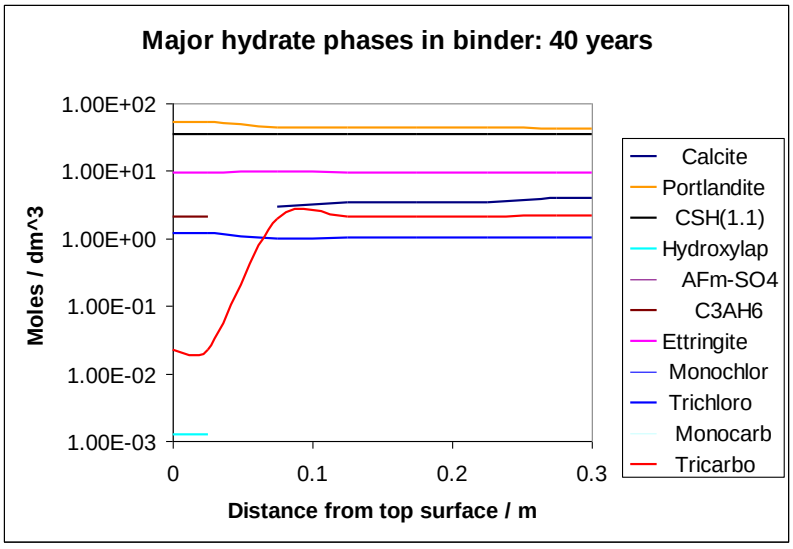

Figure 11.15 *Absolute quantities of mineral phases present in the binder component*

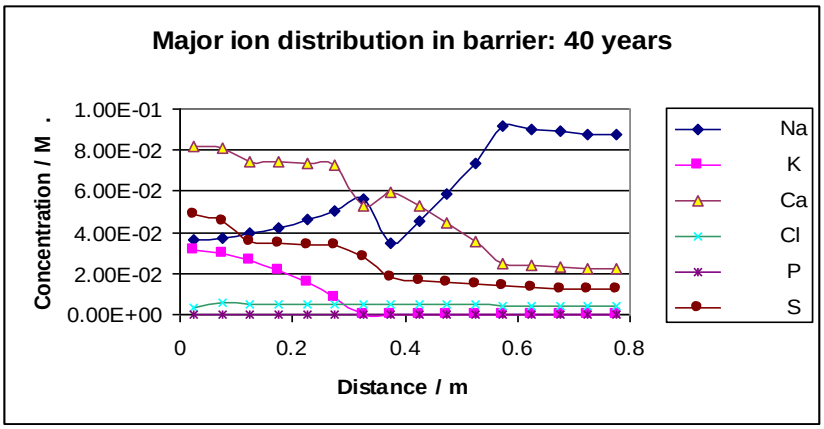

Figure 11.16 *Concentrations of major ions around the cement-clay interface*

At the interface between the mortar and clay (0.3m below the surface) the calcium liberated from portlandite dissolution is rapidly consumed and is predicted to precipitate in the clay. As Illite has a considerably higher molar volume than the quartz it replaces, the process is self-limiting and the system is not expected to approach equilibrium for a very long time.

The implications of these reactions for pollutant transport are predicted to be negligible. The extremely low concentrations of transition metals, which remain mobile in the cement pore solution, are well below the phase boundaries of likely solubility limiting phases. Even in the increasingly alkaline interface zone, no transition metal slats are predicted to form. The value of the clay layer in terms of safe performance of the barrier is simply increasing the path length through which mobile species travel before they leave the engineered system, as compacted clays are inherently low permeability media. The final figure shows the cumulative total of mercury eluted through the barrier per square metre of liner. Mercury is highly insoluble under reducing, alkaline conditions; its equilibrium solubility in these solutions predicted to be 4.33e-42 molal; well below the detection limit of any analytical technique.

Although the predicted concentration is meaninglessly low, comparison with figure 11.7 serves well to illustrate the value of an active, sacrificial barrier. Partitioning of elements into the solid phase is readily achievable through relatively simple engineering.

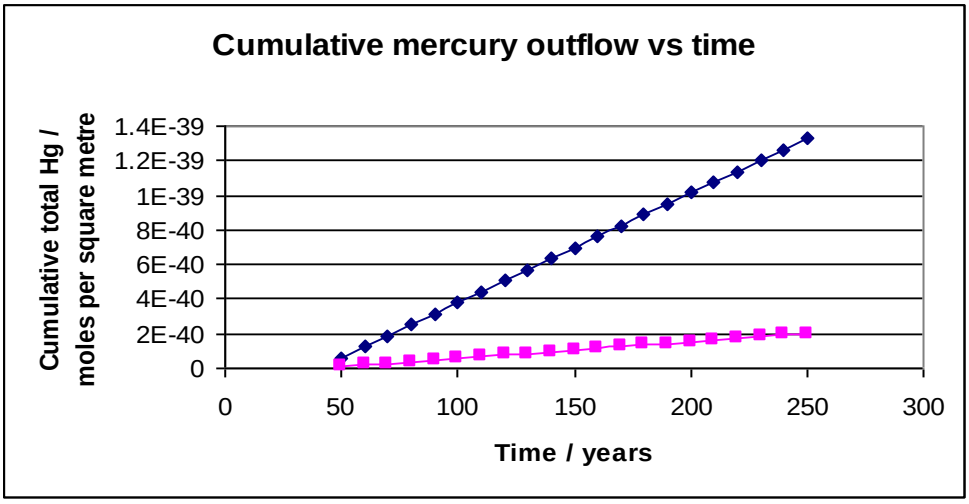

Figure 11.17 *Cumulative mercury output predicted when this element is under the solubility control of cinnabar. Diamond legend represents a single 0.3m concrete liner, whilst the square legend, shows the output for a concrete liner underlain by a 0.5m layer of engineered clay*

PART 3 A 3-LAYER BARRIER

12 INTRODUCTION

This part of the document has been written to demonstrate the performance of the 3-layer barrier concept. It is not written for a specific site and therefore the materials for the barrier have not been chosen on the basis of local availability in any particular area. One reason for presenting this analysis is that the site-specific study for the Poplars site showed that a single layer barrier was best suited to that site but the majority of the research has been based on 3 layers.

12.1 General Description

The design follows the basis system described in chapter 1 of this document. The base is 300mm of concrete, 500mm clay is placed on it and then a top layer of 200mm of concrete.

12.2 Mix design

Characteristics of the candidate mixes intended for the Poplars site are given in table 2.7 of the chapter 2 of this document.

13 TRANSPORT MODELLING

13.1 Results from the CU model

The results are given in table 13.1 below.

Table 13.1: Break through time and Steady state rate of toxic elements for 3 layer barrier using mixes 2 and 3 in table 2.7.

Elements	Assumed concentration above the barrier (mg/l)	Break through time (Years)	Break through time percentiles		Rate at 160 years (mg/m^2/year)	Rate percentiles	
			10th	90th		10th	90th
As	454	136.4	73.7	155	12.6	0.0	25.1
Pb	395	91.9	43.3	134	11.5	2.5	21.8
Zn	400	123.5	46.2	154	11.9	0.0	22.1
Hg	600	147.7	93.1	154	3.4	0.0	33.1
Mg	194	18.0	9.1	40.4	5.8	2.7	10.7
Cr	392	30.7	16.2	63.5	11.8	5.5	21.7
Al	400	67.0	33.7	139	12.0	3.9	22.1
Cu	415	150.7	74.8	155	0.5	0.0	20.8
Sr	427	29.1	15.8	59.3	12.8	6.0	23.6

PART 4 A VERTICAL BARRIER

14 INTRODUCTION

The ability to build vertical barriers is seen as one of the great strengths of the novel barrier system. We are confident that novel barriers of this type will offer the potential to develop steep-sided quarries for waste disposal. The design has been developed on a generic basis and is not site-specific.

14.1 General Description

The barrier is simply a 3-layer system turned upright. Vertical concrete walls have been built for thousands of years starting with the Romans who actually used basically similar mixes to the pozzolanic ones in this work. The concrete parts of the barrier can therefore be built using a range of conventional technologies. The problem is the compacted clay interlayer and for this a pourable mix would be used. This could be an "artificial clay" made with, for example, slag and waste gypsum or it could be a bentonite mix similar to those used in cut-off walls. The construction method for the whole barrier would be chosen by the contractor but some sort of tie between the two concrete layers would inevitably be required to contain the pressure when the clay is poured. Steel would not be permitted for the ties as it would corrode and form pathways for leachate migration. Glass fibre or polymer composite ties would be used.

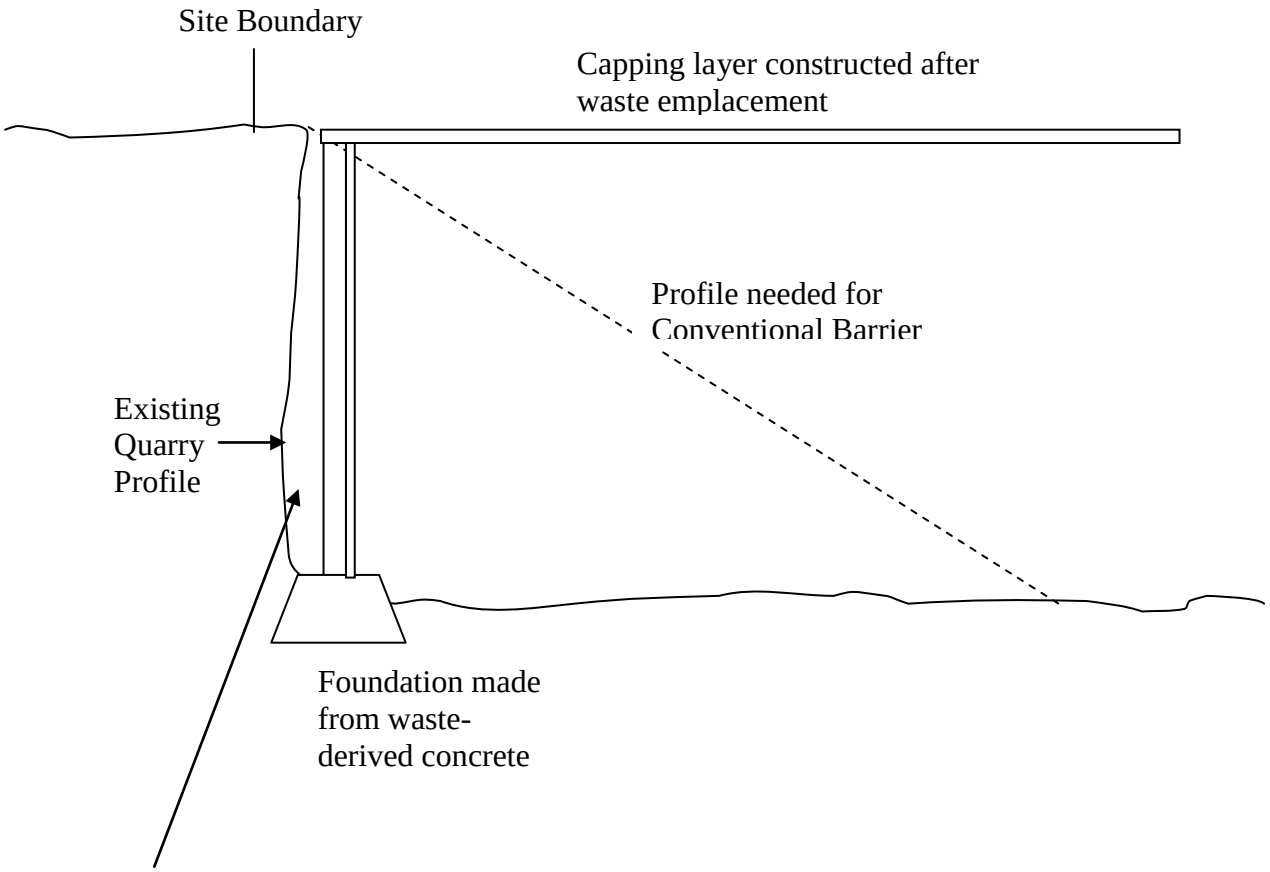

Multi-layer barrier. Waste-derived concrete poured against existing quarry face and in inner layer and "pourable artificial clay" (also waste-derived) placed between the layers of concrete.

14.2 Mix design

The same mix designed used for the horizontal barrier are used for the analysis in this section and the characteristics of the these mixes are given in table 2.7 of the chapter 2 of this document.

15 TRANSPORT MODELLING

15.1 Results from the CU model

The results are presented in table 15.1

Table 15.1: Break through time and Steady state rate of toxic elements for 3 layer vertical barrier using mixes 2 and 3 in table 2.7.

Elements	Assumed concentration above the barrier (mg/l)	Break through time (Years)	Break through time percentiles		Rate at 160 years ($mg/m^2/year$)	Rate percentiles	
			10th	90th		10th	90th
As	454	154.7	140	156	7E-6	0.0	8.96
Pb	395	126.8	78	145	2.9	0.0	9.90
Zn	400	153.0	92	155	2.4E-3	0.0	10.0
Hg	600	153.6	147	155	7.3E-6	0.0	2.53
Mg	194	35.5	18	80	2.9	1.4	5.36
Cr	392	60.9	32	119	5.9	2.6	10.8
Al	400	130.5	67	153	5.7	0.0	11.1
Cu	415	155.0	139	156	7.2E-11	0.0	7.10
Sr	427	57.9	32	115	6.4	2.9	11.8

References:

1. Claisse P A and Unsworth H P. "The Engineering of a Cementitious Barrier". "Engineering Geology of Waste Disposal" Geological Society Engineering Geology Special Publication No.11, pp.267-272. 1995.

2. Anon. Technical Literature on Hoek Cell and drainage platens, Robertson Geologging, Conwy, Gwynedd, LL31 9PX, 1994.

3. ASTM C1202. “Electrical indication of concrete’s ability to resist chloride ion penetration”.1997.

4 Harris A W, Atkinson A, Nickerson A K and Everitt N M. "Mass transfer in water saturated concretes" Nirex Safety Studies report NSS/R125. 1988 UK Nirex Ltd. Didcot Oxon.

5 UK Nirex 1993, Report No 525, Scientific Update p.25. United Kingdom Nirex Ltd. Harwell, Didcot, OXON, UK.

6 Atkinson A and Claisse P A. "The use of cement in a repository for the disposal of spent fuel” Harwell report AERE R 13479 1989

7 Claisse PA, Ganjian E, Atkinson A and Tyrer M. “Concrete without calcium or silica” 10th. British Cement Association Annual Conference on Higher Education and The Concrete Communication Conference, University of Birmingham, pp. 117-123, June 29-30, 2000.